NASA CONTRACTOR
REPORT

NASA CR-137619

*AVAILABLE TO THE PUBLIC*

# TEST EVALUATION OF POTENTIAL HEATSHIELD CONTAMINATION OF AN OUTER PLANET PROBE'S GAS SAMPLING SYSTEM

by W. C. KESSLER

*Prepared by*

MCDONNELL DOUGLAS ASTRONAUTICS COMPANY -EAST
St. Louis, Missouri 63166 (314) 232-0232
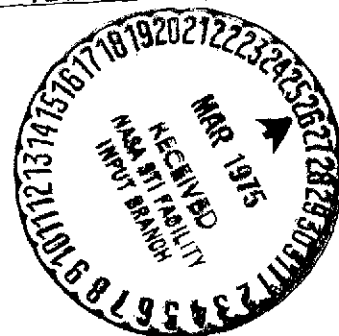
# TEST EVALUATION OF POTENTIAL HEATSHIELD CONTAMINATION OF AN OUTER PLANET PROBE'S GAS SAMPLING SYSTEM

## by W. C. KESSLER

*by*

MCDONNELL DOUGLAS ASTRONAUTICS COMPANY -EAST
St. Louis, Missouri

for

AMES RESEARCH CENTER

NATIONAL AERONAUTICS AND SPACE ADMINISTRATION

# TABLE OF CONTENTS

## TABLE OF CONTENTS (CONT.)

## LIST OF PAGES

TITLE, ii - vi

1 - 96

# LIST OF FIGURES

## LIST OF FIGURES

# LIST OF FIGURES

# INTRODUCTION

The National Aeronautics and Space Administration proposes to explore the atmospheres of the outer planets in the 1980's using instrumented atmospheric entry probes. The first generation probes will obtain in situ measurements of pressure, temperature and aerodynamic deceleration during descent for the purpose of determining the atmospheric structure. An onboard mass spectrometer and/or gas chromatograph will define the atmospheric composition and hence the mean molecular weight of the atmosphere. The direct, accurate identification of the chemical compounds present in the atmosphere, and measurement of their relative abundance and isotropic ratios, can elucidate the chemical history of the outer planets from the time of their formation from the primordial solar nebula.

Mission feasibility studies have shown that a retained heatshield concept for the Outer Planet Probe can result in a lower system weight and higher mission reliability than the jettisoned heatshield concept (References 1, 2, and 3). The onboard science instruments which are affected by the concept are those which are deployed through the heatshield (i.e., pressure sensor, temperature sensor, visible - IR detector, nephelometer and gas sampling instruments). The deployment process is a mechanical design consideration whose concept may be demonstrated to be acceptable by simple mechanical tests. Once successfully deployed, only the data measured by the atmospheric gas analysis system could be affected by the retained heatshield concept. Due to the retention of the charred heatshield, there is a potential source of atmospheric sample contamination by outgassing products. Although the amount of mass leaving the heatshield is small and has an outward momentum which is orders of magnitude lower than that of the on-coming stream, the complexity of the local flow field precludes a simple conclusion that contamination does not exist. The shadowgraph pictures shown in Figure 1 indicate the nature of the flow disturbance created by the deployed inlet sampling tube.

The deployed sampling tube is used to extract and deliver atmospheric gas samples to the gas analyzer. These chemical composition experiments are performed in the troposphere, where the atmosphere is homogeneous. In this region,

# PLANETARY PROBE FLOW FIELD

$M = 0.91$
$Re_D = 1.59 \times 10^6$
$\alpha = 14^0$
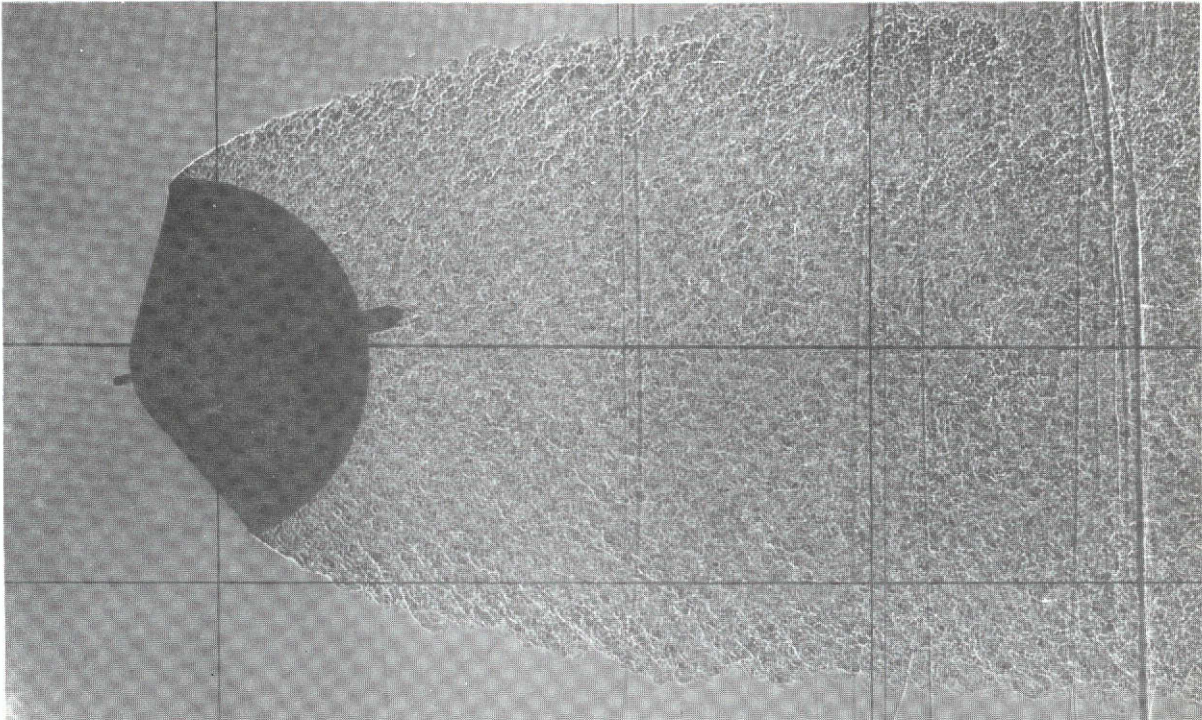


$M = 1.28$
$Re_D = 2.22 \times 10^6$
$\alpha = 17^0$
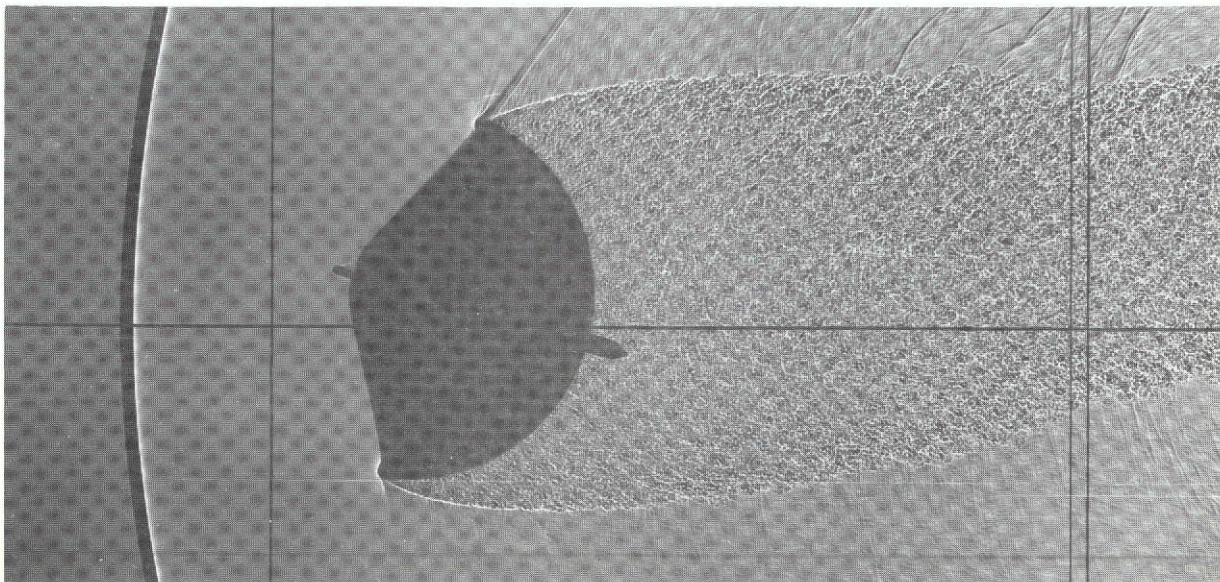


FIGURE 1

convective forces tend to raise atmospheric trace species to their conden-
sation levels thereby precipitating clouds. Water, methane, and ammonia ices,
as well as solution clouds have been included in the model atmospheres of the
outer planets (References 4-6). To ensure the detection of such atmospheric
trace species it is necessary to use a gas sampling system capable of accu-
rately detecting[+] abundances at the 40-50 parts per million (ppm) level in a
species mass range from 16-18 g/g-mole. Figure 2 provides a summary of the
trace species abundances expected in the atmospheres of Jupiter, Saturn and
Uranus.

## ATMOSPHERIC TRACE SPECIES

| PLANET (MODEL ATMOSPHERE*) | TRACE SPECIES (MOLECULAR WEIGHT) | | | | |
|---|---|---|---|---|---|
| | $H_2O$ (18) | $CH_4$ (16) | $NH_3$ (17) | Ne (20.2) | OTHERS |
| SATURN (WARM) (NOMINAL) (COOL) | 330[++] 1050 3670 | 200 630 2221 | 50 150 530 | 40 130 470 | 50 190 650 |
| URANUS (WARM) (NOMINAL) (COOL) | 330 1000 3000 | $1 \times 10^4$ $3 \times 10^4$ $9 \times 10^4$ | 50 150 450 | 40 130 390 | 60 190 570 |
| JUPITER (WARM) (NOMINAL) (COOL) | 480 1020 2400 | 280 620 1450 | 70 150 350 | 60 130 310 | 80 160 380 |

[++]NUMBERS ARE TRACE SPECIES ABUNDANCES IN PARTS PER MILLION (PPM)

*ATMOSPHERIC MODELS AND PPM LEVELS TAKEN FROM REFERENCES 4, 5 AND 6

FIGURE 2

+ It is clear that abundance measurements at the 40-50 ppm level are required,
however, the accuracy to which the isotropic abundances must be measured is
still open to question.

The peak entry heat pulse has been traversed when the sampling tube is deployed and atmospheric sampling acquisition initiated. However, the internal heatshield temperature is still sufficiently high to cause decomposition of the resin and outgassing at the surface. Some of the outgassing products (methane and water vapor) will be in a species mass range of 16-18 g/g-mole and will be indistinguishable from the trace species in the atmosphere. Since some of the heatshield outgassing products and the atmospheric trace species are in the same mass range, it is necessary to determine the amount, if any, of "contamination" introduced in the extracted atmospheric gas sample by heatshield outgassing products.

This report documents the results of a parametric experimental program which was conducted to determine the level of contamination, due to heatshield outgassing, at the worst case trajectory conditions for atmospheric entry at the outer planets.

TEST DEFINITION

A schematic of the local flow field in the vicinity of the probe stagna-
tion region and atmospheric sampling tube is shown by Figure 3. For flight
conditions at the outer planets, the free stream gas is composed primarily of
hydrogen and helium (References 4, 5, and 6) and the gas injected into the
viscous layer contains constituents from the charred heatshield. The complex-
ity of the flow field in the inlet region precludes the possibility of
numerically calculating the quantity of outgassing products which are ingested
by the sampling tube. Full-scale testing of potential contamination at
planetary flight conditions is also clearly beyond current capabilities. The
approach taken in this study is to define an experimental program which scales
the key flight flow field features to the flow in an earth based test facility
in such a manner that the measured contamination data are directly relatable
to contaminant levels at flight conditions. This approach requires the
determination of the worst case flight conditions for potential contamination,
the specification of scaling parameters which relate the flight conditions to
test conditions, and a demonstration that the scaling parameters are applicable.
The following paragraphs review these topics and define the ground facility
test conditions for the flight simulation of potential contamination.

Worst Case Flight Conditions - Before the scaling parameters (relating
the planetary flight conditions to test) can be defined, the flight conditions
must be specified. The objective is to determine the single, worst case
planetary entry environment for sample contamination; that is, to define the
flight entry trajectory conditions which result in the highest potential for
atmospheric sample contamination. Figure 4 illustrates the ablator mass
flow rate and the reference altitude time histories for a typical outer
planet mission (shallow entry into the warm model atmosphere of Saturn). For
all the outer planet missions, the atmospheric sampling tube is deployed
through the heatshield on command at a preselected deceleration level. The
deployment always occurs after the peak heat pulse has been traversed and the
probe has been decelerated to a subsonic Mach number. The chemical composition
experiments are initiated at sampling tube deployment and continue for the

## SCHEMATIC DIAGRAM OF INLET FLOW FIELD
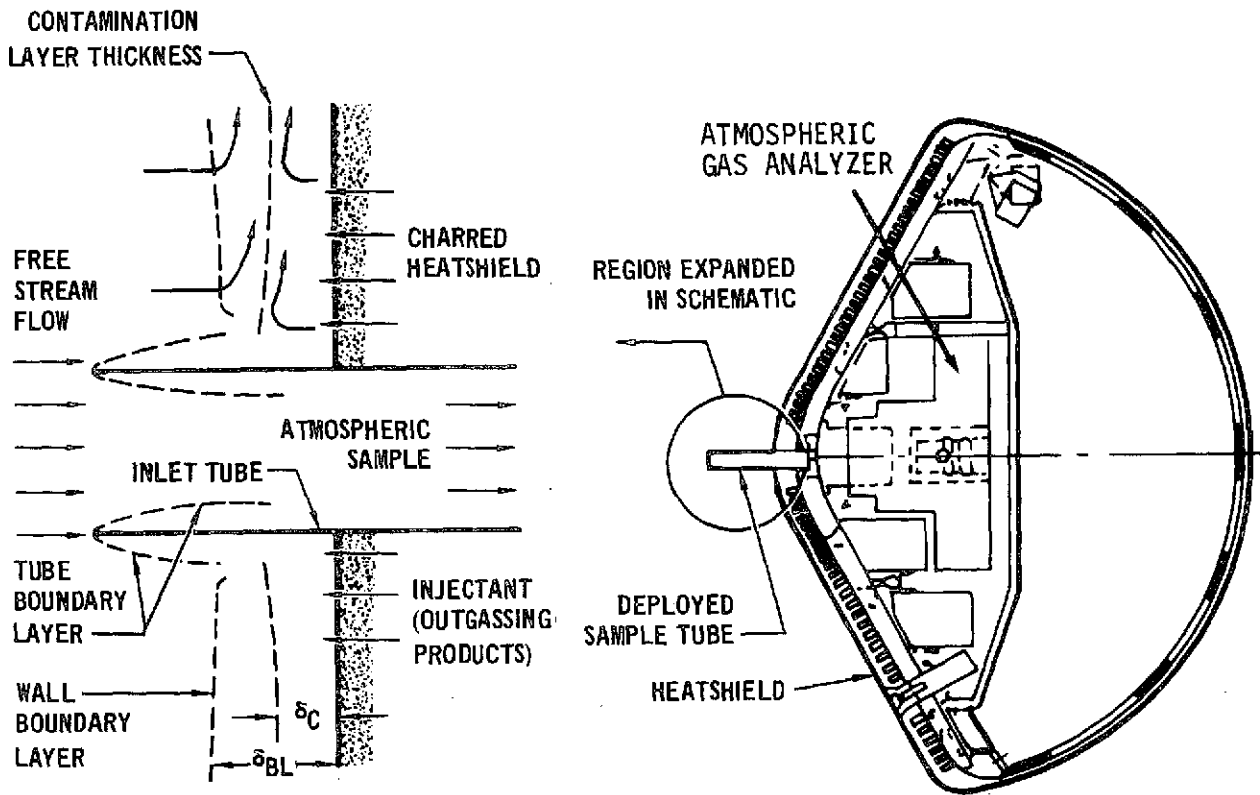


FIGURE 3

duration of the mission (15-60 minutes, depending on the planet and entry conditions). Figure 4 illustrates the rapid decrease in ablator mass flow rate with increasing trajectory time after deployment. The decreasing flow rate results in a decreasing potential for sample contamination due to outgassing. A summary of flight conditions at deployment is provided by Figure 5.

The primary parameters which affect the potential for contamination of the atmospheric sample are the: 1) ratio of injected gas to freestream gas momentum, 2) the molecular diffusion due to local concentration gradients and 3) the thickness of the viscous layer. In general, the lowest Reynolds number ($Re_D$) results in the thickest boundary layer, the lowest Schmidt number (Sc) results in the greatest ratio of contamination layer to boundary layer thickness, and the highest momentum ratio parameter ($I_i/I_\infty$) results in the largest contaminant gas penetration into the flow. Based on the data summarized by Figure 5, the "worst case" flight conditions for contamina-

## DESCENT TRAJECTORY TIME HISTORIES
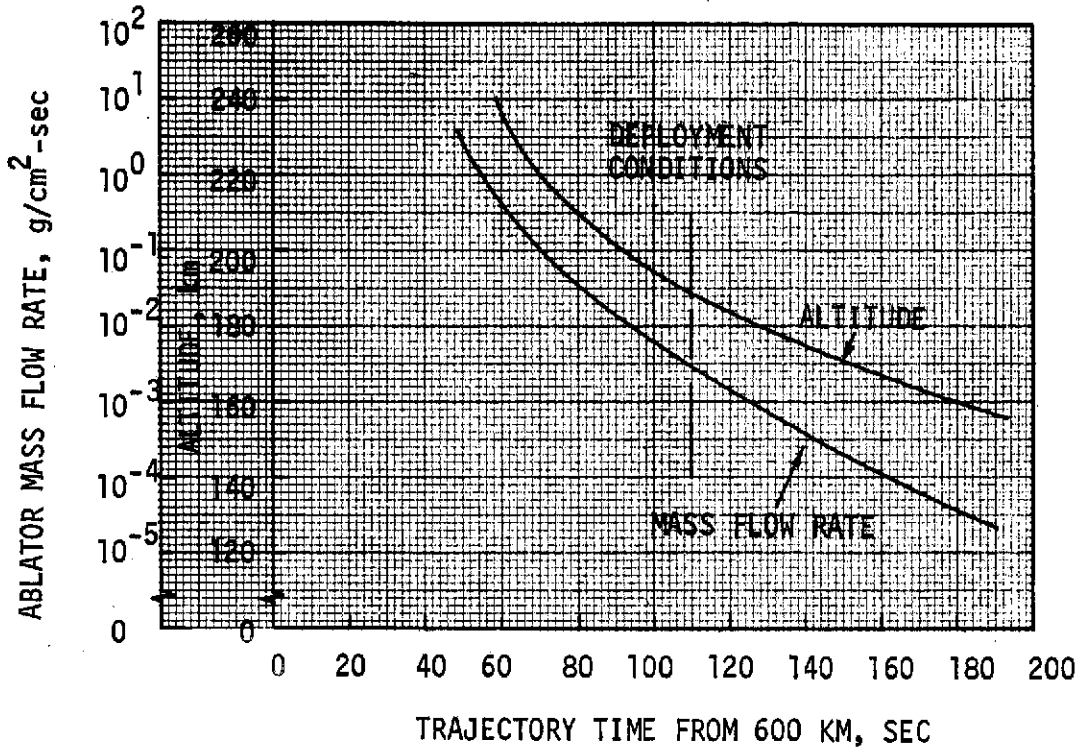


FIGURE 4

## INSTRUMENT DEPLOYMENT CONDITIONS

| PLANET | ATMOSPHERE (MODEL/FLT PATH ANGLE) | ALTITUDE[+] (km) | M | $P_\infty$ (n/cm²) | $T_\infty$ (°K) | $Re_D$ (X10⁶) | $I_i/I_\infty$ (X10⁻⁹) | Sc |
|---|---|---|---|---|---|---|---|---|
| SATURN | WARM/-15° | 187.2 | 0.90 | 0.306 | 88.5 | 1.223 | 174 | 1.33 |
|  | NOMINAL/-30° | 90.4 | 0.78 | 0.716 | 77.0 | 3.093 | 46 | 1.33 |
|  | COOL/-40° | 44.8 | 0.53 | 1.216 | 72.0 | 27.163 | 5 | 1.31 |
| URANUS | WARM/-30° | 87.4 | 1.00 | 0.286 | 63.4 | 2.389 | 114 | 1.33 |
|  | NOMINAL/-40° | 80.6 | 0.89 | 0.511 | 57.7 | 3.578 | 60 | 1.30 |
|  | COOL/-50° | 52.3 | 0.58 | 0.864 | 47.0 | 5.379 | 46 | 1.22 |
| JUPITER | NOMINAL/-7.5° | 47.8 | 0.98 | 0.861 | 113.0 | 2.618 | 20 | 1.33 |

+ ATMOSPHERIC ENCOUNTER CONDITIONS, TRAJECTORY TIME HISTORIES AND INSTRUMENT DEPLOYMENT PARAMETERS WERE OBTAINED FROM REFERENCES 1, 2 AND 3.

$$1 \text{ n/cm}^2 = 9.8692 \times 10^{-2} \text{ atm}$$

FIGURE 5

tion occur at instrument deployment for the shallow entry into the Saturn warm model atmosphere. These conditions result in the thickest viscous layer and a contaminant layer of nearly equal thickness. Furthermore, the momentum ratio is appreciably higher than for any other flight conditions. In conclusion, the deployment conditions for entry into the Saturn warm atmosphere are the worst case conditions (for outgassing contamination of the atmospheric samples) encountered for outer planet entries. These worst case conditions are cross-hatched for emphasis on Figure 5.

Scaling Requirements - The procedure used in determining the parameters which scale the worst case flight conditions to test conditions is illustrated by Figure 6. The calculated descent trajectories, atmospheric models and specified ablator characteristics are used to calculate the flight forebody boundary layer characteristics. These calculations ignore, by necessity, the presence of the sampling tube (i.e., a "clean" configuration calculation). The candidate scaling parameters are used to determine the tunnel test conditions and, for these conditions, forebody boundary layer solutions are calculated for comparison with the flight results. The proper scaling parameters are selected based upon the criterion that the contaminant gas mass fraction at the boundary layer edge is matched for flight and test conditions. The study resulted in the selection of the Mach number, Reynolds number and the ratio of injectant gas to free stream momentum as the scaling parameters.

Boundary Layer Calculations - Boundary layer calculations were made for the spherical nose region of the planetary probe at the worst case flight and scaled test conditions. Parameters considered in defining the scaling parameters included velocity, temperature and mass fraction profiles, as well as such surface distributions as the momentum Reynolds number. The boundary layer computations, including the effect of wall mass injection, were carried out with the computer program described in Reference 7. The following subsections summarize the results obtained from the flight and test boundary layer calculations.

(a) Flight - The free stream conditions for the flight boundary layer calculations were obtained from the descent trajectory results for a shallow probe entry into the warm model atmosphere of Saturn. Boundary layer edge properties were determined by an isentropic expansion of stagnation properties to a hemispherical Newtonian pressure distribution. The free stream gas com-

## TEST CONDITION DEFINITION: FLOW DIAGRAM

```
┌──────────────────────────┐        ┌──────────────────────────────┐
│ • DESCENT TRAJECTORY      │───────▶│ LOCAL FREE STREAM CONDITIONS │
│ • MODEL ATMOSPHERES       │        │ MACH NUMBER                  │
└──────────────────────────┘        │ REYNOLDS NUMBER              │
                                     └──────────────────────────────┘
                                                     │
┌──────────────────────────┐        ┌──────────────────────────────┐
│ • ABLATOR CHARACTERISTICS │───────▶│ ABLATOR OUTGASSING RATE      │
└──────────────────────────┘        │ INJECTANT MOLECULAR WEIGHT   │
                                     │ WALL TEMPERATURE             │
                                     └──────────────────────────────┘
                                                     │
                                     ┌──────────────────────────────┐
                                     │ FLIGHT BOUNDARY LAYER        │
                                     │ PROPERTIES                   │
                                     └──────────────────────────────┘
                                                     │
                                            DEFINE   ▼
                                     ┌──────────────────────────────┐
                                     │ SCALING PARAMETERS           │
                                     │ M, Re, µᵢ/µ∞, ṁᵢ Vᵢ/ṁ∞ V∞    │
                                     └──────────────────────────────┘
                                                     │
┌──────────────────────────┐        ┌──────────────────────────────┐
│ NO                        │        │ M  }─▶ TEST FACILITY         │
│ CONSIDER OTHER SCALING    │        │ Re                           │
│ PARAMETERS                │        │ µᵢ/µ∞  }   INJECTANT GAS      │
│                           │        │        ─▶ PROPERTIES AND     │
│                           │        │ ṁᵢVᵢ/ṁ∞V∞ }  MODEL DESIGN    │
└──────────────────────────┘        └──────────────────────────────┘
            ▲                                        │
┌───────────┐ ┌──────────────────┐ ┌────────────────────────────────┐
│ YES        │ │ DID FLIGHT AND   │ │ DETERMINE BOUNDARY             │
│ SET DESIGN │◀│ TEST CONTAMINANT │◀│ LAYER PROPERTIES FOR TEST      │
│ CONDUCT    │ │ PENETRATION      │ │                                │
│ TEST       │ │ SCALE?           │ │                                │
└───────────┘ └──────────────────┘ └────────────────────────────────┘
```

FIGURE 6

position consisted of a mixture of hydrogen and helium and the single char layer outgassing product was specified as methane. For carbon phenolic heatshields (baseline proposed by References 1, 2 and 3), the primary products of ablation are methane, hydrogen, carbon monoxide and water vapor. Chain cracking products such as $C_2H_6$ and $C_7H_8$ will also be present as will traces of the halogens. The abundance of these products of ablation are temperature dependent and are not well defined at the relatively low wall temperatures (810°K) associated with the deployment conditions. At the low surface temperatures, it is expected that the long chain, high molecular weight cracking products would predominate the outgassing mixture. Such high molecular weight products could be detected in the atmospheric gas sample and hence are not considered as contaminants. In the spirit of defining worst case flight conditions, it is assumed that the outgassing products are formed by cracking the carbon chain within the char layer where the in depth temperatures (at deployment) are greater than 1600°K. For

these temperatures, the primary product of ablation formed within the char layer will be methane. Figure 7 illustrates the results of a calculation for an equilibrium mixture of the freestream gases and the products formed within the char layer. For the ablation mass fractions of interest the primary outgassing products are methane ($CH_4$), carbon monoxide (CO) and water vapor ($H_2O$). The most severe condition for contamination of the ingested atmospheric gas sample occurs when methane is the primary outgassing product. Thus, for the flight boundary layer calculations, methane was used as the single chemical species injected into the flow.

The state of the boundary layer (laminar, transitional or turbulent) may be determined from the local value of the Reynolds number based on momentum thickness ($Re_\theta$). Transition data for the geometrically similar Apollo reentry vehicle are presented by Figure 8 (reported in Reference 8). The ratio of injectant to free stream mass flow (B') is in the 0-3 range on the figure and indicates that transition from laminar to turbulent flow occurs at Reynolds numbers based on momentum thickness ($Re_\theta$) between 150 and 200. There is a possibility that the extended sampling tube may trip the boundary layer locally to result in a strip of turbulent flow (Figure 1). For the angle of attack range of interest ($0°-10°$), this local tripping will have minimal effect on the potential contamination and hence has been ignored. Below $Re_\theta = 150$ the flow is laminar and above $Re_\theta = 200$ the flow is turbulent. Figure 9 illustrates the $Re_\theta$ distribution for the worst case deployment conditions. Since the calculated values of momentum thickness Reynolds number are all below 100 (to the hemisphere-cone juncture) it is concluded that the flight boundary layer flow is completely laminar in the region of interest. Figures 10 and 11 present the calculated results for the velocity and concentration profiles normal to the wall. These results are used in comparisons with the test condition results to determine the proper scaling parameters. Figure 12 summarizes the freestream and wall boundary conditions used in the flight calculations.

(b) <u>Test</u> - Before the wind tunnel boundary layer calculations can be performed, the scaling parameters must be applied to the flight conditions to define the tunnel test conditions, injectant gas and injectant mass flow rate. The scaled test program is constrained to be conducted in a wind tunnel which uses air as the test media. The flight values of Mach number and Reynolds

# ABLATION PRODUCTS AT WALL

## (Equilibrium Values)
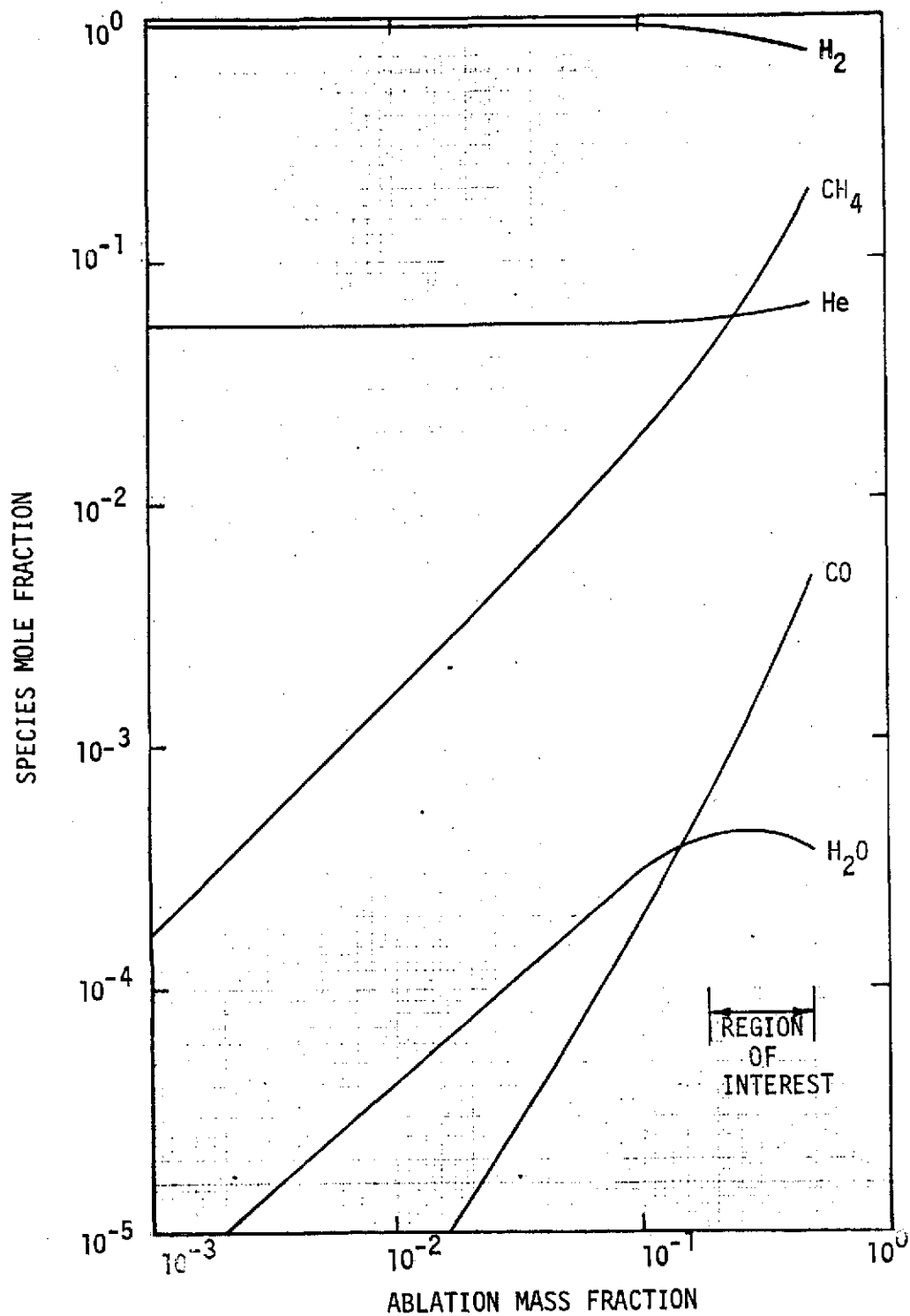


FIGURE 7

## BOUNDARY LAYER TRANSITION CRITERION
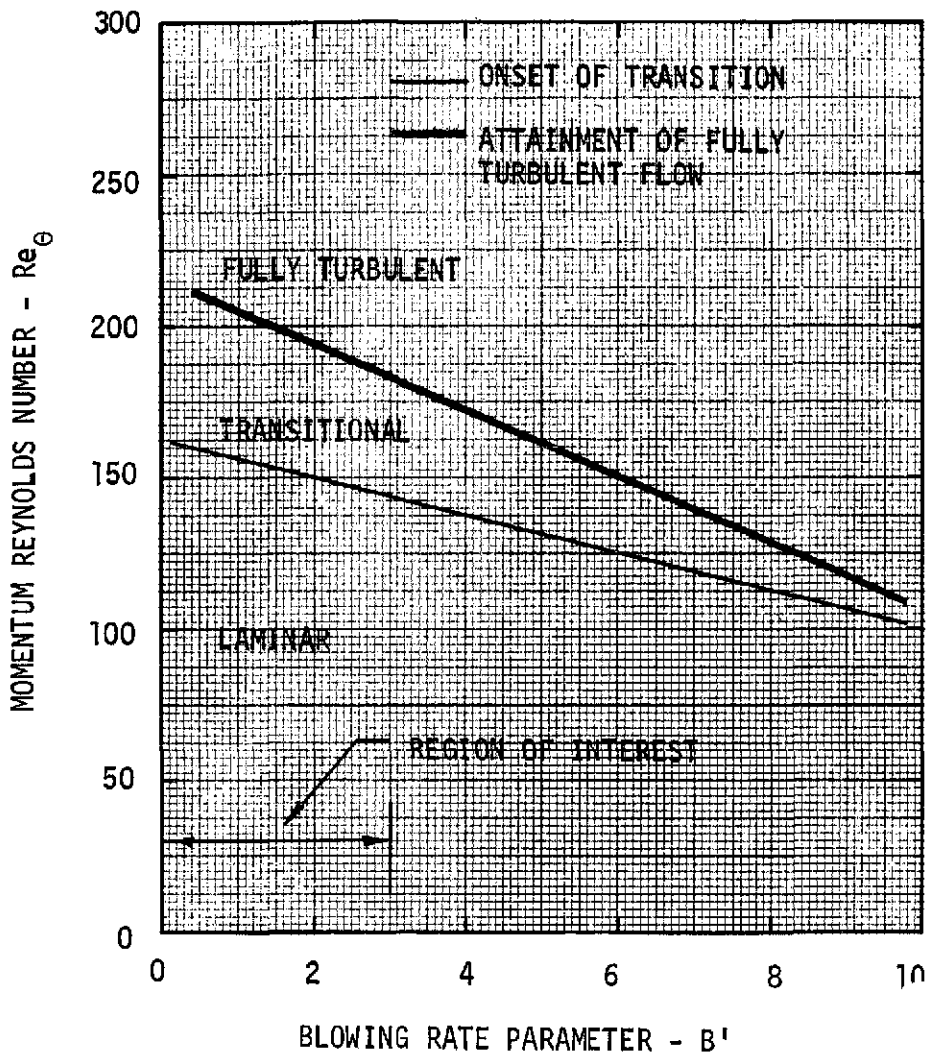


FIGURE 8

number are to be matched identically in the test to simulate the state of the flight boundary layer. The tests were conducted in the NASA/Ames Research Center's 2' x 2' Transonic Test Facility to match the flight Mach number and Reynolds number (Figure 12). A 10.16 cm (4 in) diameter model was tested

# FLIGHT: MOMENTUM REYNOLDS NUMBER DISTRIBUTION

$$M = 0.9$$
$$Re_D = 1.223 \times 10^6$$
$$\hat{m}_i = 2.93 \times 10^{-4} \text{ g/cm}^2\text{-sec}$$



NONDIMENSIONAL SURFACE DISTANCE - S*

MOMENTUM REYNOLDS NUMBER - $Re_\theta$

FIGURE 9

13
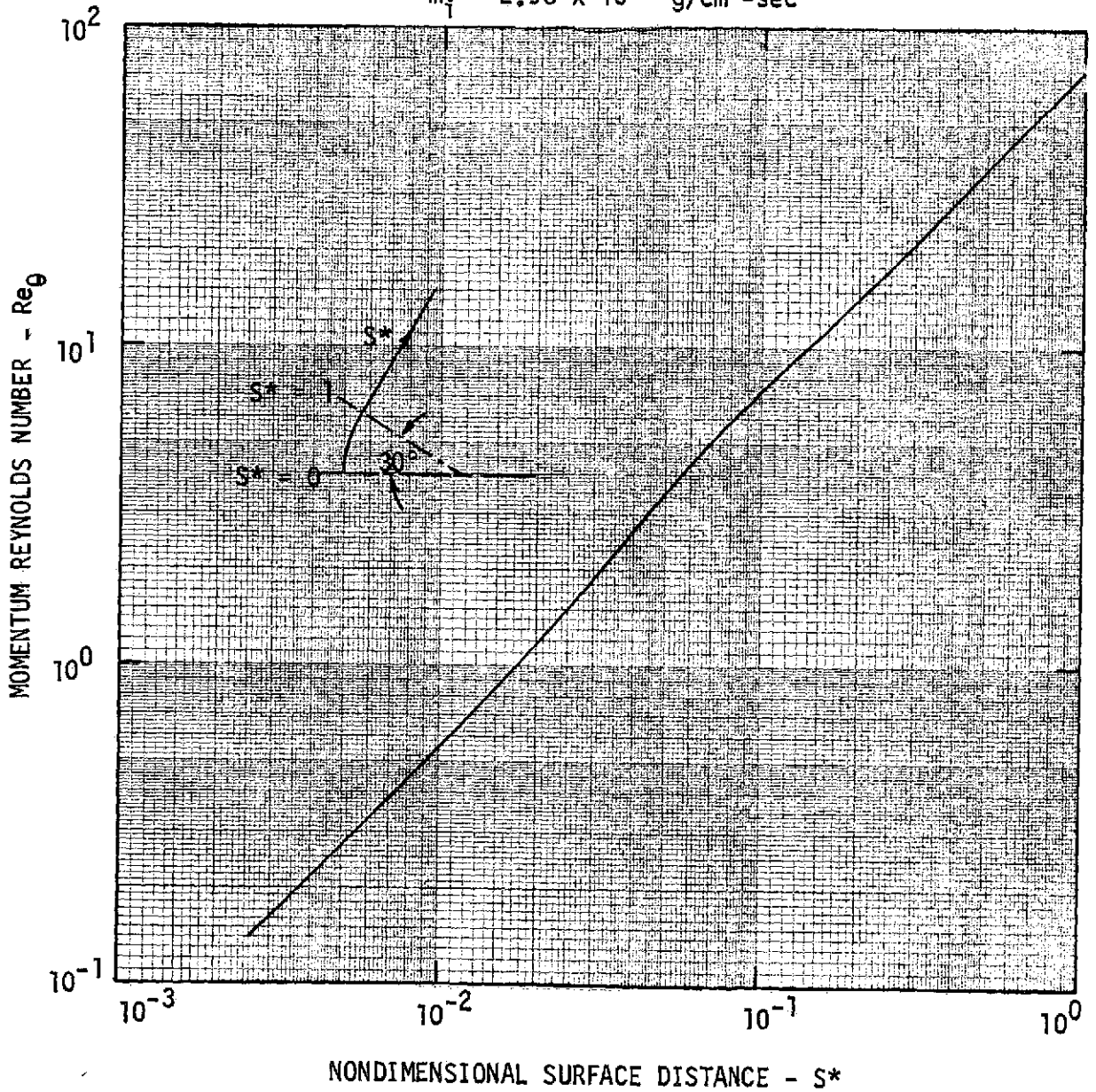
# FLIGHT: VELOCITY PROFILE NORMAL TO WALL

$$\delta = 3.0 \times 10^{-1} \text{ cm}$$

$$X_W = 2.4 \times 10^{-1}$$

$$S^* = 1.0$$

$$\dot{m}_i = 2.93 \times 10^{-4} \text{ g/cm}^2\text{-sec}$$
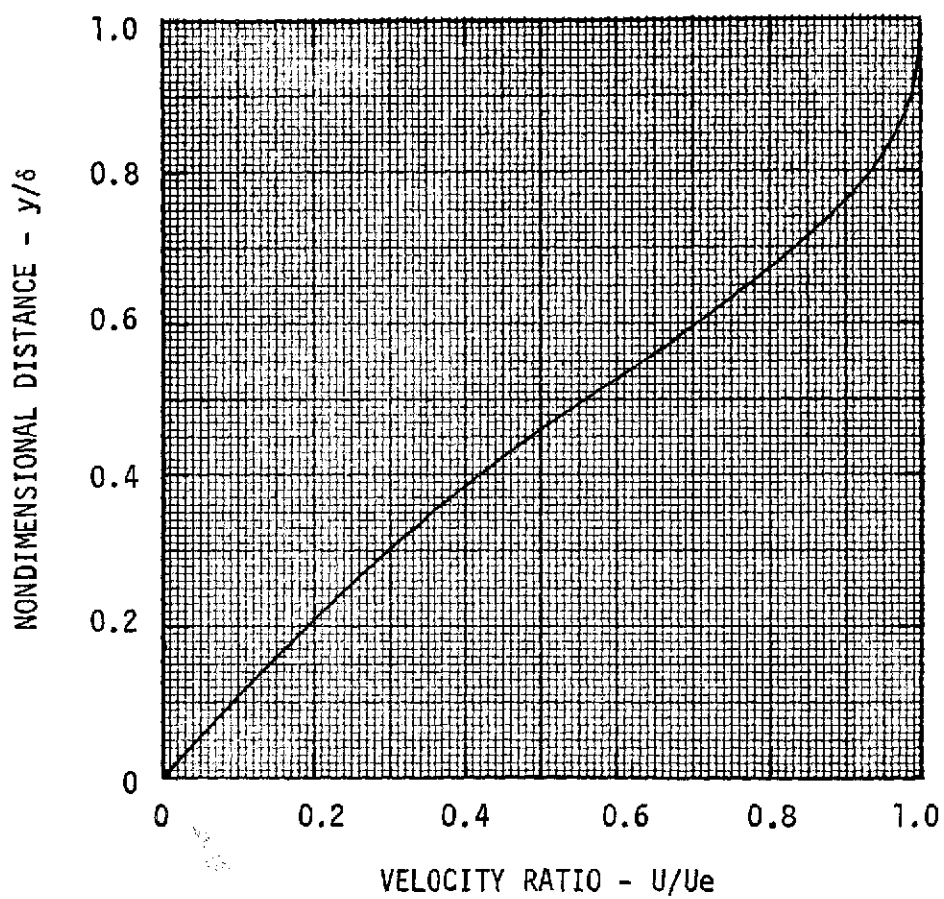


FIGURE 10

# FLIGHT: CONTAMINATION PROFILE NORMAL TO WALL

$$\delta = 3.0 \times 10^{-1} \text{ cm}$$
$$\chi_W = 2.4 \times 10^{-1}$$
$$S^* = 1.0$$
$$\overset{\bullet}{m}_i = 2.93 \times 10^{-4} \text{ g/cm}^2\text{-sec}$$



443 ppm

NONDIMENSIONAL DISTANCE – $y/\delta$

CONTAMINANT RATIO – $\chi/\chi_W$
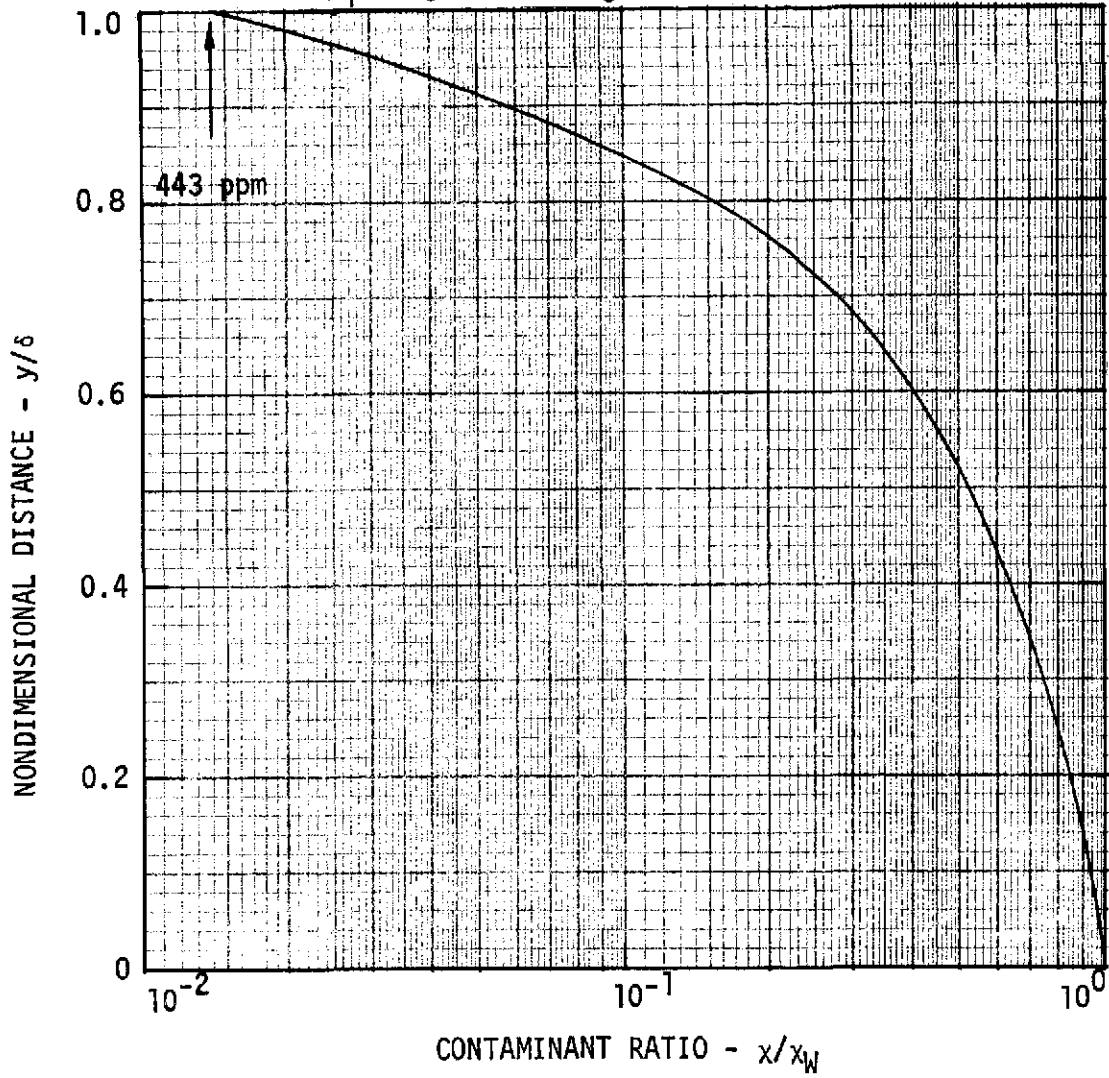
FIGURE 11

# FLIGHT BOUNDARY CONDITIONS
## (Worst Case)

FREE STREAM

$M_\infty = 0.9$

$Re_D = 1.223 \times 10^6$

$\rho_\infty = 8.87 \times 10^{-6}$ g/cm$^3$ (1.72 $\times$ 10$^{-5}$ slugs/ft$^3$)

$p_\infty = 3.06 \times 10^{-1}$ n/cm$^2$ (3.02 $\times$ 10$^{-2}$ atm)

$T_\infty = 88.47°$K (159.25°R)

$T_W = 810.8°$K (1459.4°R)

$\mu_\infty = 2.13$ g/g-mole

$x_{H_2} = 0.896$

$x_{He} = 0.104$

INJECTANT

METHANE (CH$_4$)

$\mu_i = 16.04$ g/g-mole

$\dot{m}_i = 2.93 \times 10^{-4}$ g/cm$^2$-sec (6.00 $\times$ 10$^{-4}$ lb$_m$/ft$^2$-sec)

FIGURE 12

at the following conditions (refer to Figure 13 for the facility test envelope):

$$M = 0.9$$
$$Re_D = 1.223 \times 10^6$$

## TRANSONIC TEST FACILITY OPERATION ENVELOPE
### (NASA/ARC 2 Ft x 2 Ft Transonic Tunnel)



| MACH RANGE: | 0.2 TO 1.4 |
| REYNOLDS NUMBER (x $10^6$/ft): | 0.5 TO 8.7 |
| TOTAL PRESSURE (psia): | 2.3 TO 44.1 |
| DYNAMIC PRESSURE (psf): | 60 TO 2175 |
| TOTAL TEMPERATURE ($^\circ$R): | 580 |
| RUN TIME: | CONTINUOUS |
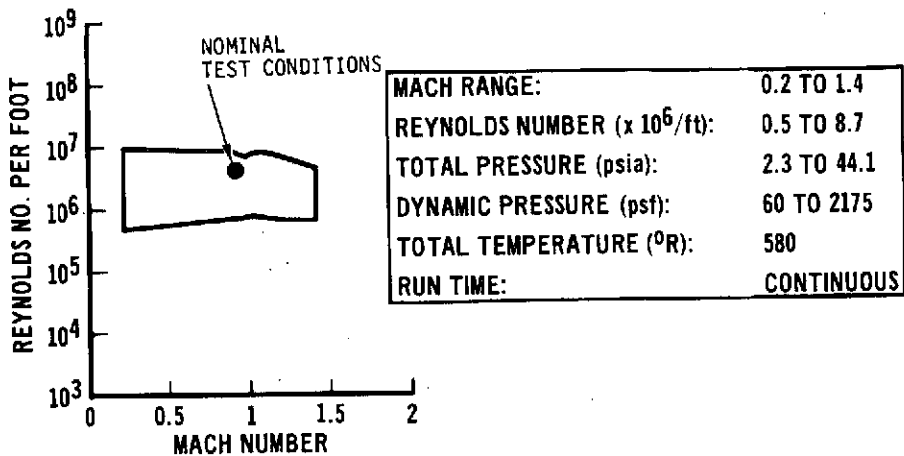
FIGURE 13

The criterion of matching the flight injected gas to freestream gas momentum ratio in the test program requires:

$$\left. \frac{\hat{m}_i V_i}{\hat{m}_\infty V_\infty} \right)_T = \left. \frac{\hat{m}_i V_i}{\hat{m}_\infty V_\infty} \right)_F \tag{1}$$

Using the ideal gas and mass flow equations in equation (1) results in:

$$\left[ \frac{P_T}{P_\infty} \cdot \frac{T_\infty}{T_T} \cdot \frac{\mu_i}{\mu_\infty} \cdot \sigma \cdot \left( \frac{V_i}{V_\infty} \right)^2 \right]_T = \left[ \hat{m}_i^2 \frac{R_o^2 T_W T_\infty}{P_T P_\infty \mu_i \mu_\infty V_\infty^2} \sigma \right]_F \tag{2}$$

The wall pressure and temperature were used to calculate the injectant density for Equation (2). The porosity, $\sigma$, of the carbon phenolic heat-shield (at deployment conditions) and the permeable forebody used in the test program are discussed in Appendix A. The remaining parameters, with the exception of the test injectant molecular weight ($\mu_i$) and velocity ($V_i$), are known from the trajectory conditions, tunnel scaled conditions or

17

ablator characteristics. Thus, equation (2) can be restated in terms of the unknown quantities ($\mu_i$ and $V_i$) and the flight heat shield outgassing mass flow rate per unit area:

$$(\mu_i V_i^2)_T = \text{Const. } (\dot{m}_i)^2{}_F$$

The calculated ablator mass loss rate in flight is $2.93 \times 10^{-4} \frac{g}{cm^2\text{-sec}}$ ($6 \times 10^{-4} \frac{lb_m}{ft^2\text{-sec}}$). Accurate predictions of the low pyrolysis mass flow rates are difficult since ablation prediction codes are developed and validated for the significantly higher flow rates associated with the peak heating environment. Thus, in this parametric study, off-nominal values of plus and minus factors of five on the "nominal" calculated mass flow rate are included due to prediction uncertainties. Figure 14 illustrates the relationship between the test molecular weight and injectant velocity for simulating the flight nominal and two off-nominal mass flow rates by matching the respective momentum ratios.

The injectant gas scaling parameters, relating flight and test results, investigated included matching the mass flow rate ratio and matching the momentum ratio. The momentum ratio parameter resulted in the requirement for the highest mass flow rate in the experiment. The higher injectant mass flow rate results in a higher potential for contamination. Figure 15 summarizes the freestream conditions for the test and the "nominal" injectant conditions used in the boundary layer calculations. For flight, the freestream gas molecular weight (2.13 g/g-mole) is specified by the atmospheric model and the injectant gas molecular weight (16 g/g-mole) is approximated from the outgassing products. Matching the flight ratio of molecular weights in the test requires an injectant gas with a molecular weight of 217.62 g/g-mole in a test media of air (28.97 g/g-mole). Freon C-318 ($\mu$ = 200 g/g-mole) was specified in the theoretical calculations along with methane ($\mu$ = 16 g/g-mole) to provide a range of injectant molecular weights for assessing the validity of the scaling parameters. However, Freon C-318 was not available at the time of testing and was replaced by Freon 114 ($\mu$=170.9 g/g-mole). Figure 14 shows that scaling can be achieved for a matched flight and test momentum ratio by injecting any molecular weight gas and adjusting its injectant velocity. Thus, methane and Freon 114 were selected as the injectant gases for the experiment based on past

# TUNNEL INJECTANT PARAMETERS FOR MATCHING FLIGHT MOMENTUM RATIO



INJECTANT VELOCITY, cm/sec

INJECTANT MOLECULAR WEIGHT, g/g-mole

FIGURE 14

19
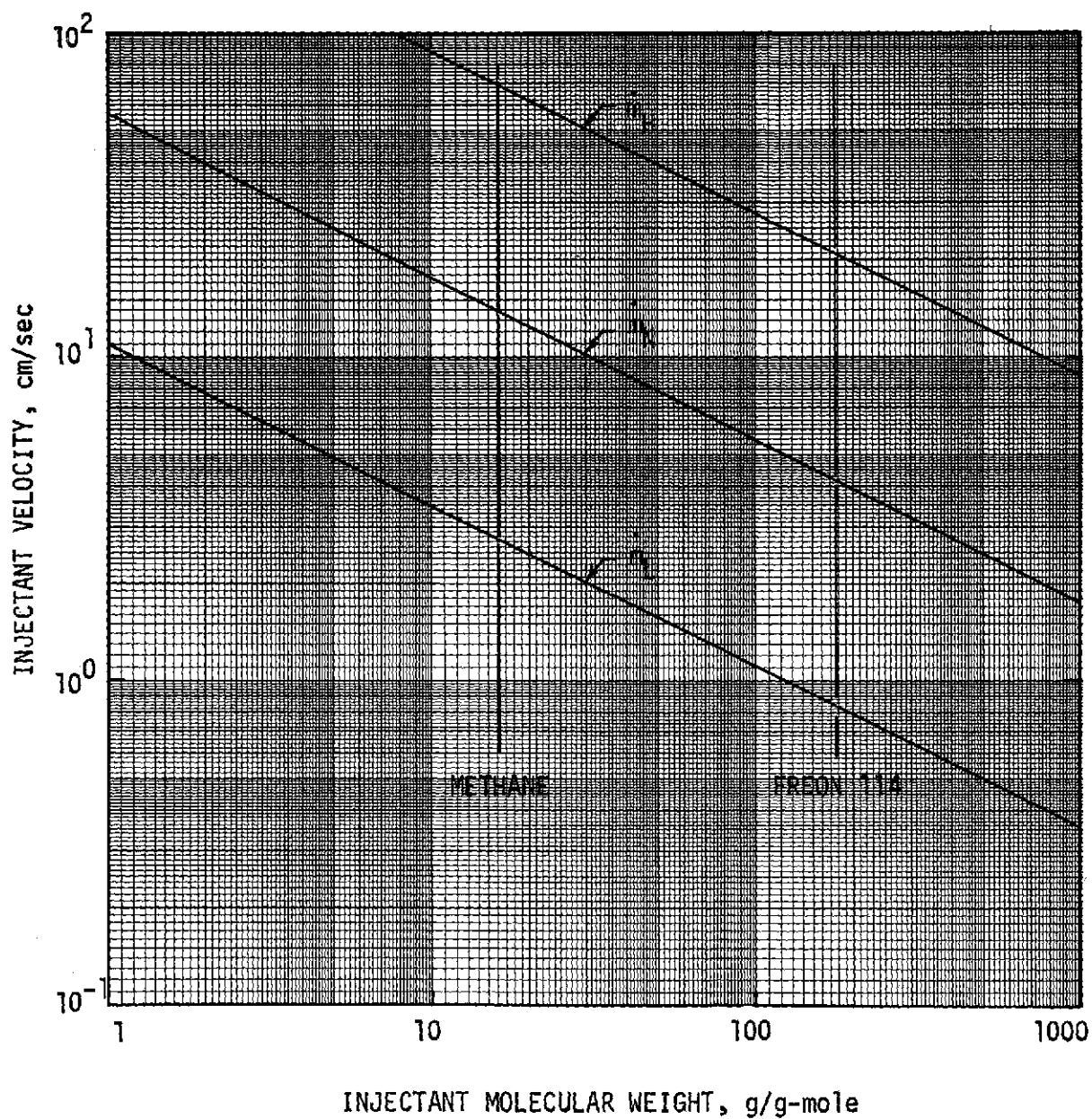
# TUNNEL BOUNDARY CONDITIONS
## (Simulates Flight Worst Case)

FREE STREAM

$M_\infty = 0.9$

$Re_D$   $1.223 \times 10^6$

$P_\infty = 4.904 \ n/cm^2 \ (0.484 \ atm)$

$T_\infty = 253.39°K \ (456.1°R)$

$T_w = 298.33°K \ (537.0°R)$

$\mu_\infty = 28.97 \ g/g\text{-mole}$

$x_{O_2} = 0.23455$

$x_{N_2} = 0.76545$


INJECTANT (LIGHT GAS)

  METHANE $(CH_4)$

  $\mu_i = 16.04 \ g/g\text{-mole}$

  $\dot{m}_i = 4.048 \times 10^{-1} \ g/sec$


INJECTANT (HEAVY GAS)

  FREON C-318 $(C_4F_8)$

  $\mu_i = 200.04 \ g/g\text{-mole}$

  $\dot{m}_i = 1.323 \ g/sec$


FIGURE 15

test experience and their availability. Furthermore, testing with two gases with significantly different molecular weights provides a larger data base and increases confidence in the general test results and conclusions.

Boundary layer calculations were made for the wind tunnel test conditions, using Freon C-318 and methane as the injectants to determine if the scaling criterion was achieved. Figures 16, 17 and 18 summarize the results for methane injection while Figures 19, 20 and 21 illustrate the Freon C-318 results. For both cases the flow over the nose cap is demonstrated to be laminar by the local values of $Re_\Theta$ (Figures 16 and 19). These distributions are in reasonable agreement with the flight results presented by Figure 9. Figure 22 presents the primary comparison of flight and test data. The criterion selected for determining if scaling from flight conditions to tunnel conditions is accomplished is the degree of matching in the amount of contaminate mass fraction at the boundary layer edge. The calculations demonstrate that the flight and Freon injection results for contaminant gas mass fraction at the boundary layer edge are matched. Methane injection in the test facility does not result in the same contaminant mass fraction at the boundary layer edge. The mismatch is not great, however, and it is concluded that both the light and heavy gas injectants can be used to simulate the flight contaminant. The wall Schmidt number calculations imply that, for all three cases, the contaminant layer thickness is approximately equal to the boundary layer thickness (at $Sc = 1$, $\delta = \delta_c$).

The results obtained from the boundary layer calculations indicate that the flight boundary layer state and contaminant mass fraction at the boundary layer edge can be duplicated in an earth based wind tunnel test by matching the flight values of Mach number, Reynolds number and ratio of injected gas to free stream momentum.

# TUNNEL (METHANE INJECTION): MOMENTUM REYNOLDS NUMBER DISTRIBUTION

$M = 0.9$

$Re_D = 1.223 \times 10^6$

$\hat{m}_i = 2.67 \times 10^{-4}$ g/cm$^2$-sec



NONDIMENSIONAL SURFACE DISTANCE – S*

MOMENTUM REYNOLDS NUMBER – Re$_\theta$
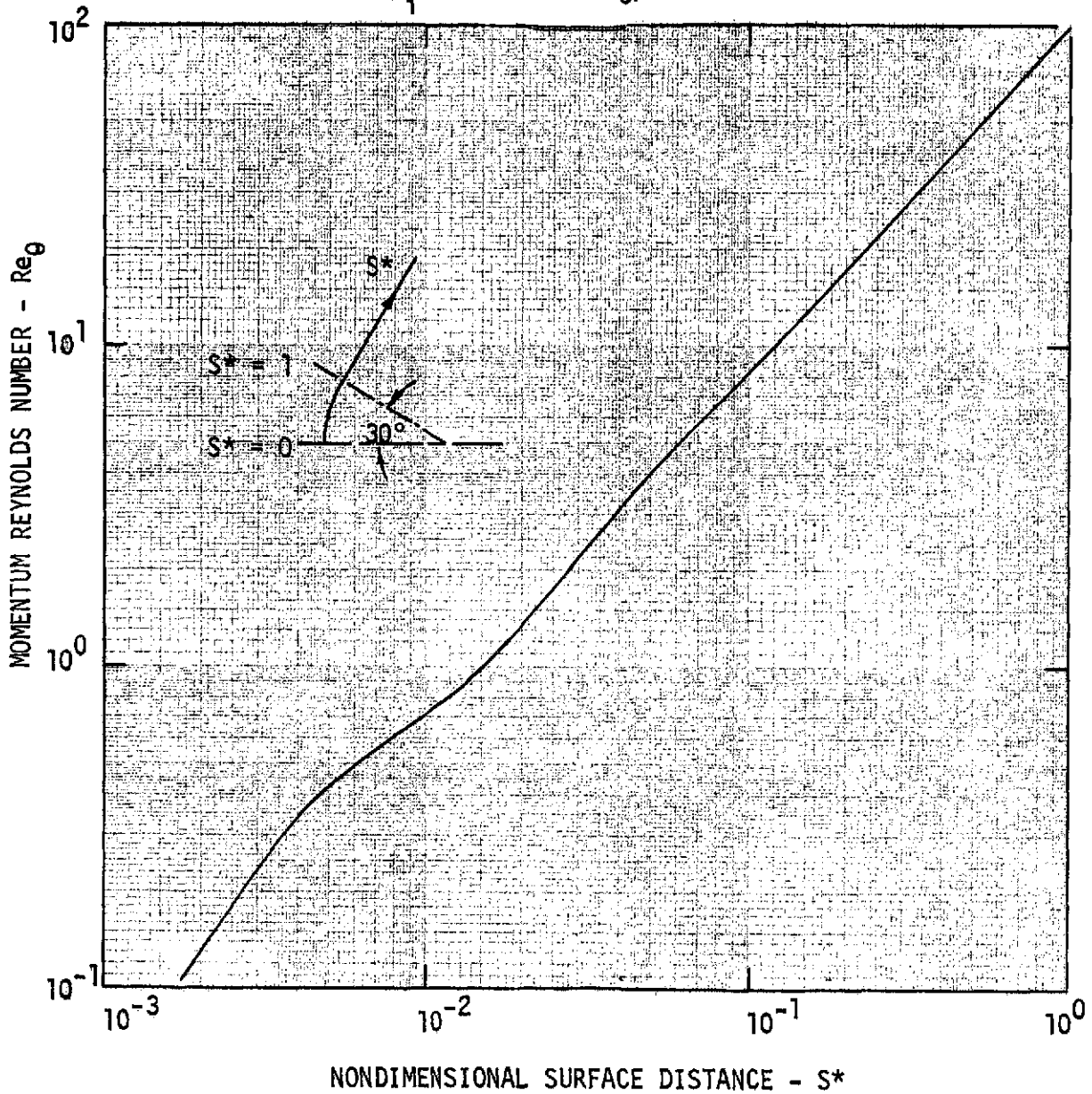
FIGURE 16

# TUNNEL (METHANE INJECTION): VELOCITY PROFILE NORMAL TO WALL

$$\delta = 1.43 \times 10^{-2} \ cm$$
$$x_W = 1.77 \times 10^{-1}$$
$$S^* = 1.0$$
$$\hat{\dot{m}}_i = 2.67 \times 10^{-4} \ g/cm^2\text{-sec}$$
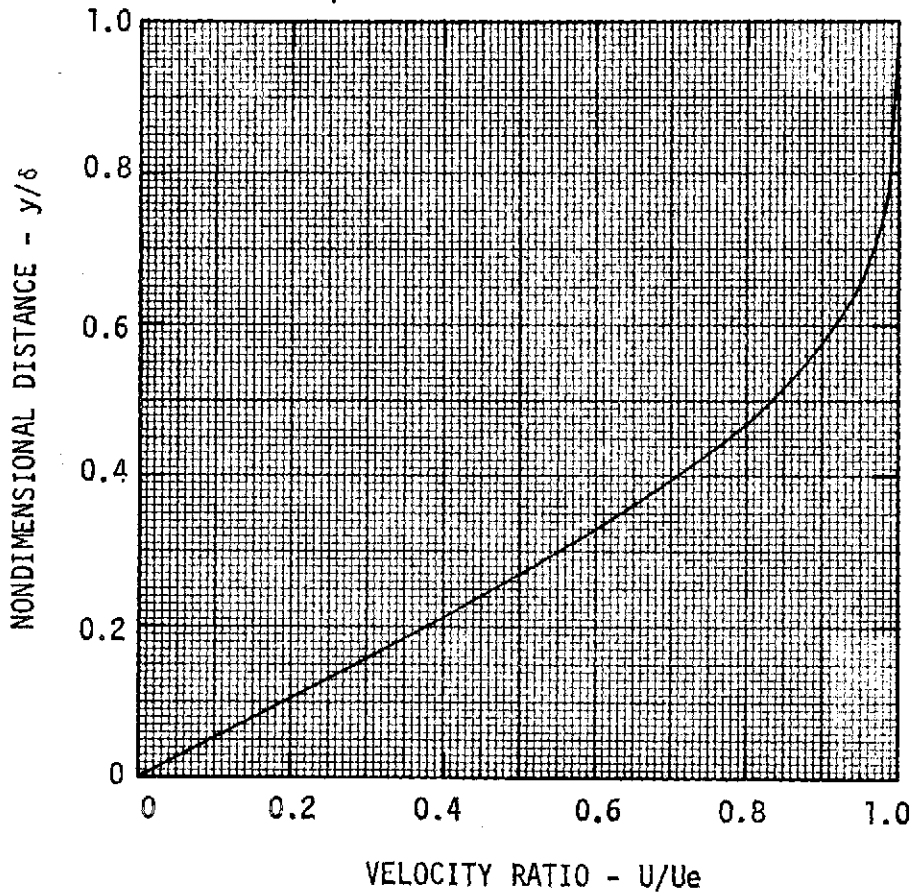


FIGURE 17

# TUNNEL (METHANE INJECTION): CONTAMINATION PROFILE
## NORMAL TO WALL

$$\delta = 1.43 \times 10^{-2} \text{ cm}$$
$$x_W = 1.77 \times 10^{-1}$$
$$S^* = 1.0$$
$$\hat{m}_1 = 2.67 \times 10^{-4} \text{ g/cm}^2\text{-sec}$$
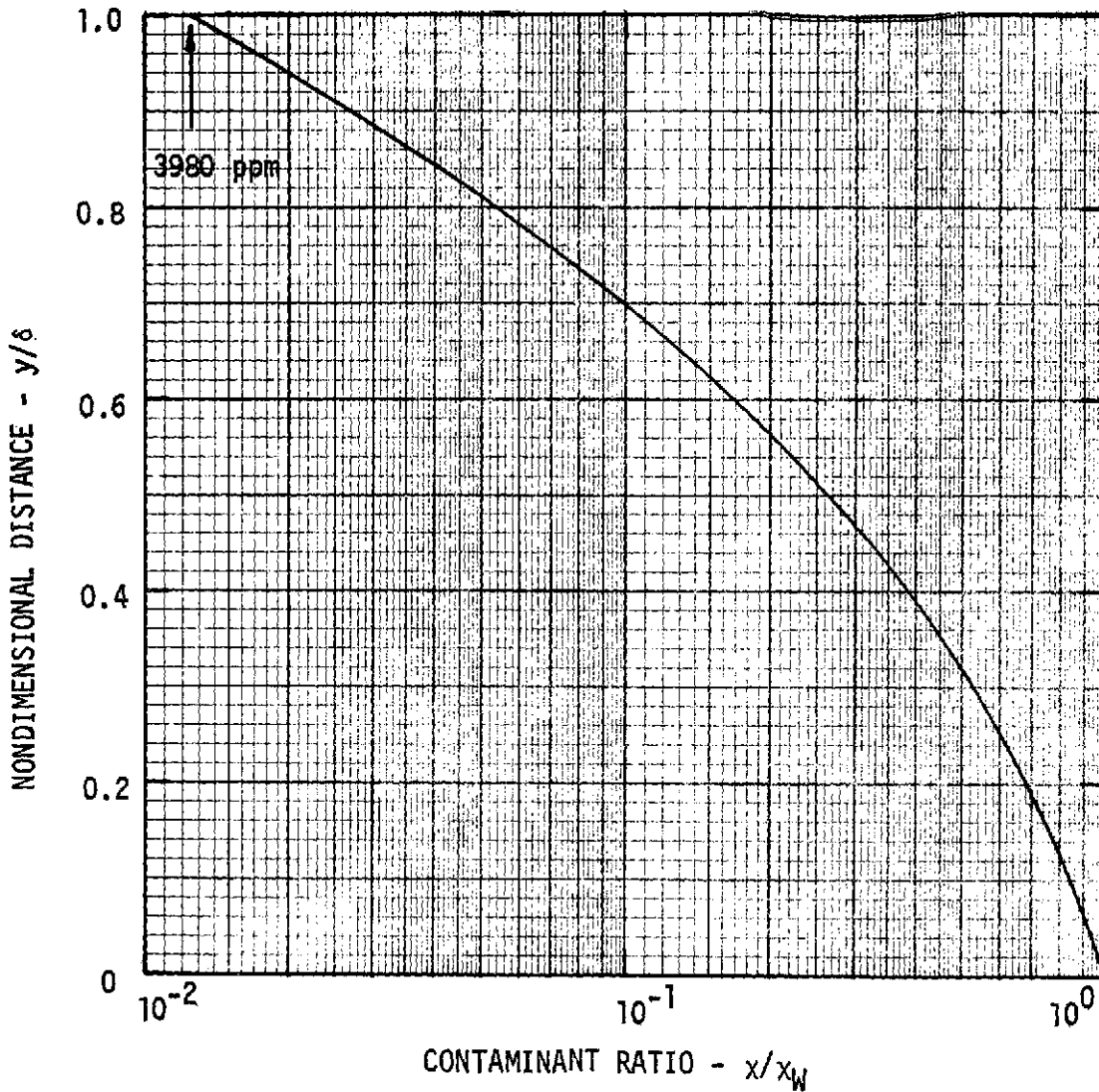


FIGURE 18

# TUNNEL (FREON C-318 INJECTION): MOMENTUM REYNOLDS NUMBER DISTRIBUTION

$$M = 0.9$$
$$Re_D = 1.223 \times 10^6$$
$$\hat{\dot{m}}_i = 9.44 \times 10^{-4} \ g/cm^2\text{-sec}$$



NONDIMENSIONAL SURFACE DISTANCE - S*
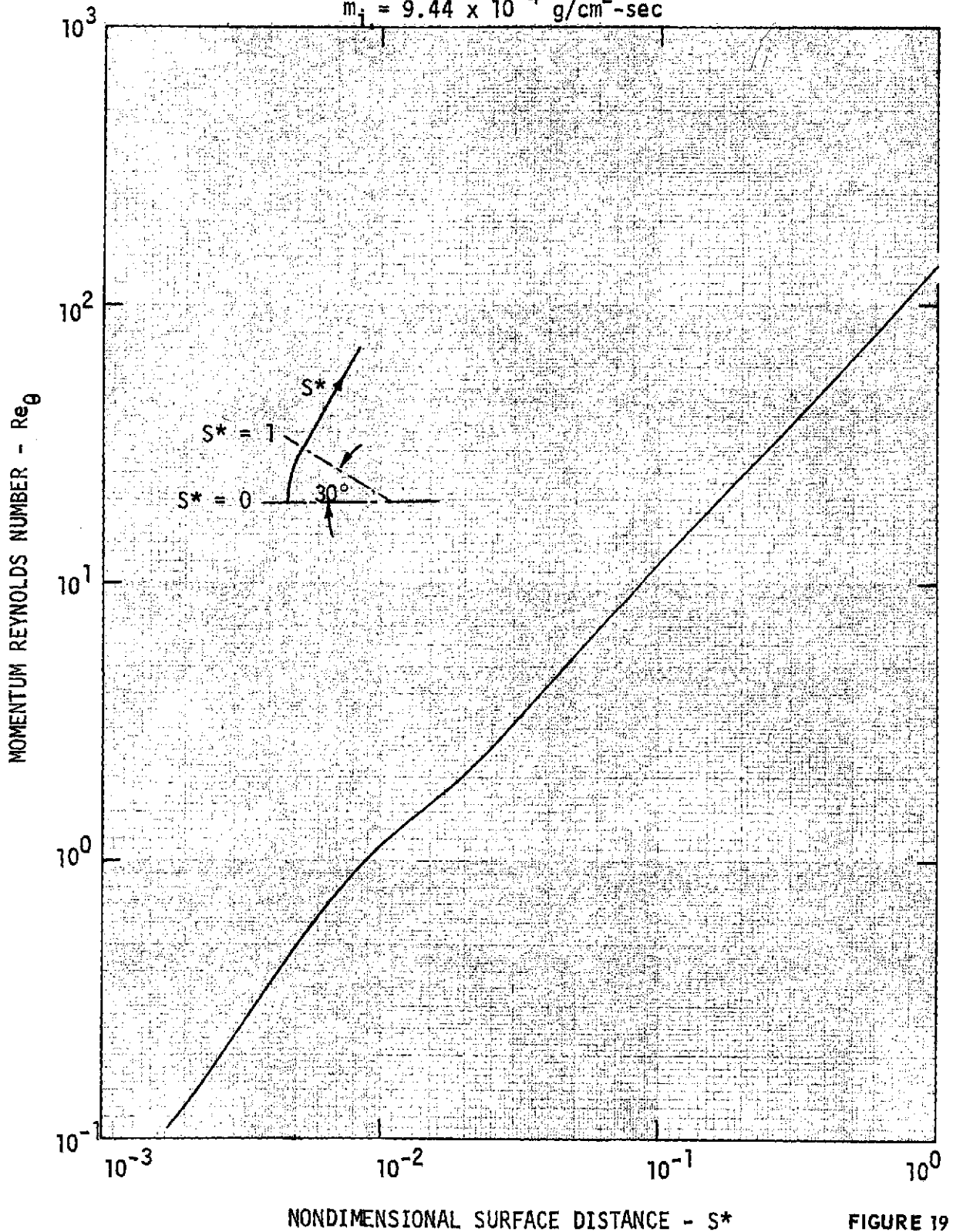
FIGURE 19

# TUNNEL (FREON C–318 INJECTION): VELOCITY PROFILE NORMAL TO WALL

$$\delta = 1.46 \times 10^{-2} \text{ cm}$$
$$\chi_W = 4.75 \times 10^{-1}$$
$$S^* = 1.0$$
$$\hat{m}_i = 9.44 \times 10^{-4} \text{ g/cm}^2\text{-sec}$$



NONDIMENSIONAL DISTANCE – y/δ

VELOCITY RATIO – U/Ue

FIGURE 20

# TUNNEL (FREON C–318 INJECTION): CONTAMINATION PROFILE
## NORMAL TO WALL

$$\delta = 1.46 \times 10^{-2} \text{ cm}$$
$$x_W = 4.75 \times 10^{-1}$$
$$S^* = 1.0$$
$$\hat{m}_i = 9.44 \times 10^{-4} \text{ g/cm}^2\text{-sec}$$
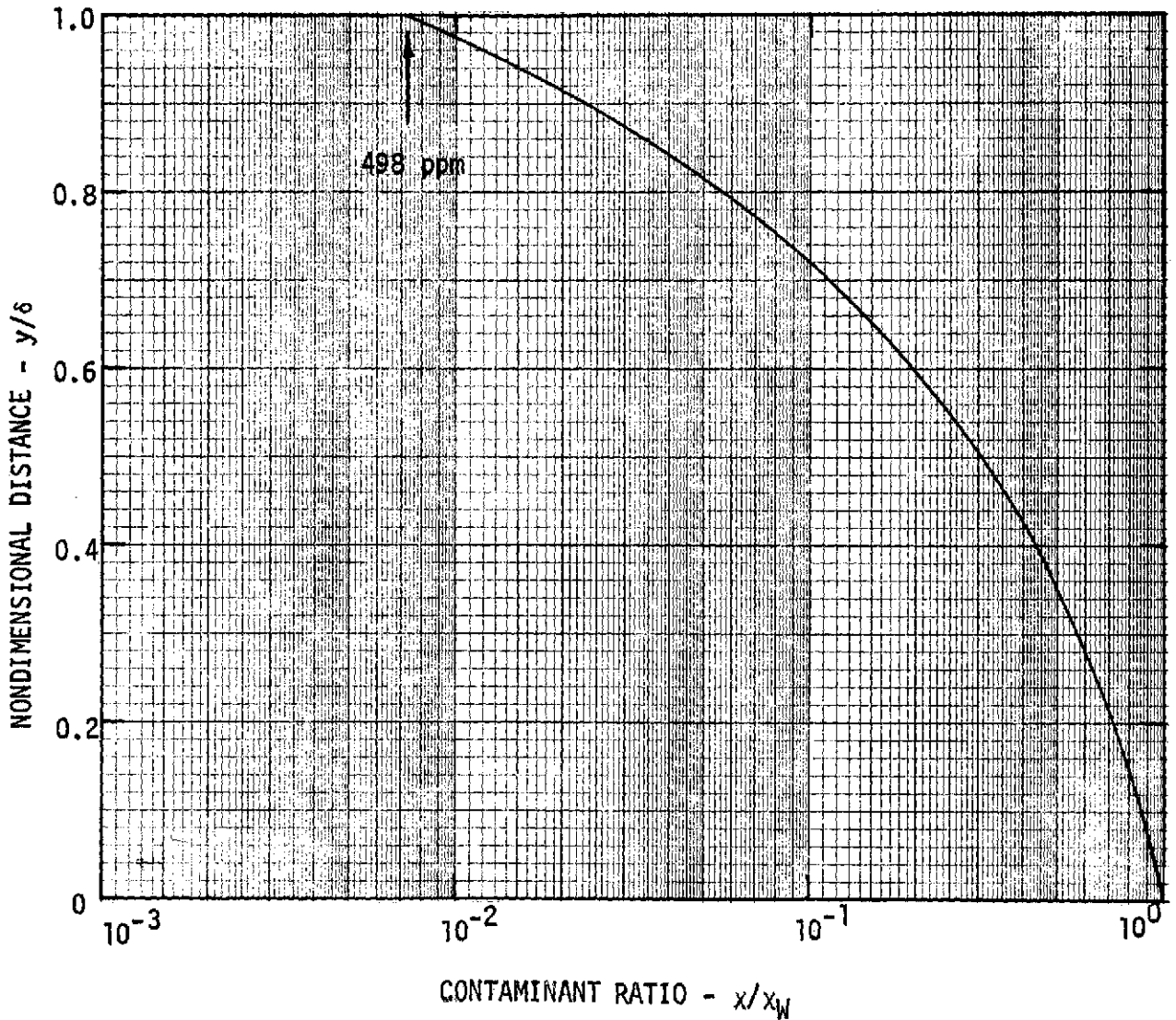


FIGURE 21

## BOUNDARY LAYER CHARACTERISTICS
### (Flight and Tunnel Comparison)

| | FLIGHT (METHANE) | TUNNEL (METHANE) | TUNNEL (FREON C-318) |
|---|---|---|---|
| MASS FRACTION (WALL) | $2.40 \times 10^{-1}$ | $1.77 \times 10^{-1}$ | $4.75 \times 10^{-1}$ |
| MOLE FRACTION (WALL) | $4.00 \times 10^{-2}$ | $2.79 \times 10^{-1}$ | $1.15 \times 10^{-1}$ |
| MASS FRACTION (B.L. EDGE[+]) | $3.35 \times 10^{-3}$ | $2.21 \times 10^{-3}$ | $3.44 \times 10^{-2}$ |
| MOLE FRACTION (B.L. EDGE) | $4.43 \times 10^{-4}$ | $3.98 \times 10^{-3}$ | $4.98 \times 10^{-4}$ |
| PPM (BOUNDARY LAYER EDGE) | 443 | 3980 | 498 |
| SCHMIDT NO. (WALL CONDS.) | 1.33 | 0.73 | 1.13 |
| $\hat{\dot{m}}_i$ (g/cm$^2$-sec) | $2.93 \times 10^{-4}$ | $2.67 \times 10^{-4}$ | $9.44 \times 10^{-4}$ |

[+]BOUNDARY LAYER EDGE TAKEN TO BE POSITION WHERE THE VELOCITY RATIO, $U/U_e$, IS 0.999.

FIGURE 22

# MODEL DESIGN

Figures 23-25 present the detailed assembly drawings used in fabrication of the test model. The basic configuration is a 60°, blunted half-angle cone with a hemispherical afterbody. The model is a 1/8.75 scale of the Outer Planet Probe designed under NASA/Ames Research Center contract NAS2-7328 (Reference 1).

The forebody is uniformily permeable and capable of providing the scaled mass flow rates at designated pressure differentials across the surface. The forebody was designed, and the model fabricated and assembled, by the Mott Metallurgical Corporation of Farmington, Connecticut. Mott used a sintering process in forebody fabrication to obtain the specified material permeability.

The hemispherical afterbody provides the hardpoints for attaching the plenum pressure measurement and injectant gas supply lines. These hardpoints consist of a 0.2175 cm (1/8 in) fitting for the pressure line and a 0.9525 cm (3/8 in) fitting for the gas supply line. The fitting and inlet size for the gas supply line were changed after the drawings were completed, due to mass flow rate considerations, and hence, the drawings do not reflect the correct dimensions for the gas supply fitting. A tapered stub, integral with the model afterbody, provides the interface between the model and the NASA/Ames Research Center's sting extension (ARC drawing A13197-C1) for the 0.75" Task Balance. A taper ratio of 5.208 cm/m (0.25 in/ft) is incorporated to match the ARC taper gage 300550. The integral tapered stub is fabricated complete with set screw flats for push-on and pull-off screws.

An adjustable length sampling tube, with a 0.211 cm (0.082 in) outside diameter and 0.0254 cm (0.010 in) wall thickness, can be extended in front of the model nose to simulate the flight gas sampling tube. A teflon O-ring type plug provides a leak seal around the tube at its interface with the permeable forebody. Plenum leaks are avoided at the aft wall by a standard O-ring seal. The knurled end of the sampling tube assembly screws into the hemispherical base to permit adjustment of the sampling tube length. A run of 0.203 cm (0.080 in) outside diameter stainless steel tubing extends through the integral tapered stub and provides the attachment point for continuing the sampling tube line to the contaminant gas measuring device.

POROUS NOSE ASSY

C5572-0108C

FIGURE 23

SECTION A-A

SECTION D-D
ROTATED 90° COUNTERCLOCKWISE

SECTION C-C

VIEW B
SCALE 2/1

SEE VIEW B

.156 +.005/-.000 DIA THRU
1/8 NPT DEPTH SHOWN
OPPOSITE SIDE
2 PLACES

#4-40 UNC-2B
.19 FULL THD DEPTH
ON .750 DIA B.C.
5 PLACES

.172 +.006/-.000 DIA THRU
C'BORE .313 +.002/-.000 DIA
DEPTH SHOWN - OPP SIDE
ON 3.437 DIA B.C.
6 PLACES

CONICAL
TAPER 5/8 PER FT
OR 3° INCL

MOTT METALLURGICAL CORPORATION
FARMINGTON INDUSTRIAL PARK
FARMINGTON, CONNECTICUT

| DRAWING SYMBOLS | STANDARD TOLERANCE |
|---|---|
| ⊿ FLATNESS & STRAIGHTNESS | FRACTIONAL ± 1/64 |
| ∠ ANGULARITY | .0   ± .020 |
| ⊥ PERPENDICULARITY | .00  ± .010 |
| ∥ PARALLELISM | .000 ± .005 |
| ⊕ CONCENTRICITY | .0000 ±.0005 |
| ⊕ TRUE POSITION | ANGLES ± 0° 30' |
| ○ ROUNDNESS | UNLESS OTHER-WISE SPECIFIED |
| USAI Y14 | |

BREAK SHARP EDGES & CORNERS
.005 TO .015 APPROXIMATE RADIUS

PART TO BE FREE OF BURRS & OILS

THIS DRAWING IS THE PROPERTY OF THE MOTT METALLURGICAL CORPORATION AND RETURNABLE UPON REQUEST. IT MUST NOT BE REPRODUCED OR THE INFORMATION CONTAINED HEREIN TRANSMITTED TO ANY UNAUTHORIZED PERSON, COMPANY OR ORGANIZATION WITHOUT WRITTEN CONSENT FROM THE MOTT METALLURGICAL CORPORATION.

TITLE
PLENUM BODY

DWG. NO.
C5572-0308D

FIGURE 24

31

# DRAWING NO. B5572-0708B: SENSOR TUBE
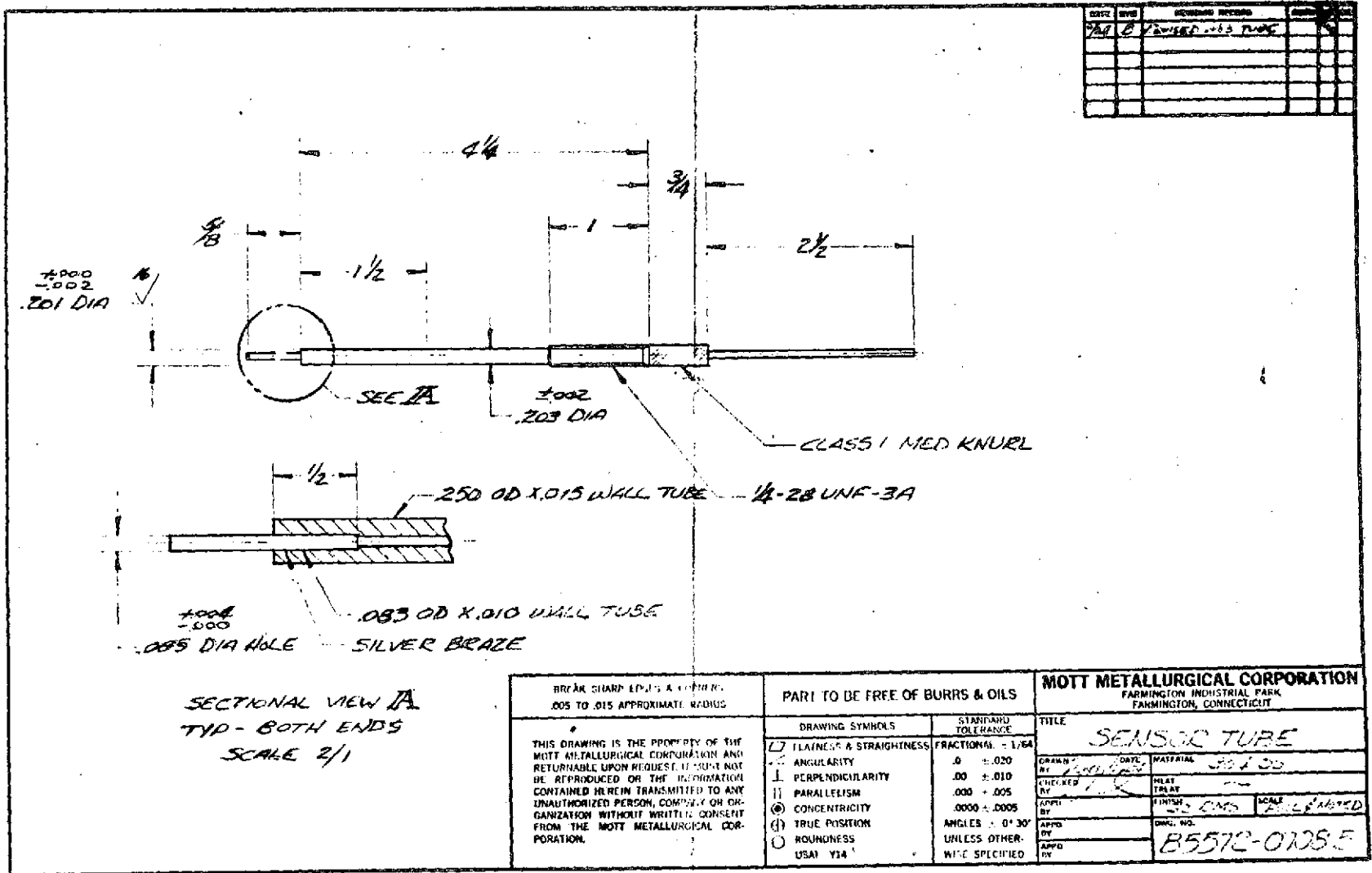


FIGURE 25

# TEST CONDITIONS

Tunnel Conditions - The nominal tunnel conditions were determined by the defined scaling parameters to simulate the worst case flight conditions for potential contamination of the ingested atmospheric samples. The conditions follow:

$$M = 0.90$$
$$Re_D = 1.223 \times 10^6$$
$$P_\infty = 4.904 \text{ n/cm}^2 \text{ (0.484 atm)}$$
$$T_\infty = 253.39°K \text{ (456.1°R)}$$
$$P_{T\infty} = 8.299 \text{ n/cm}^2 \text{ (0.819 atm)}$$
$$T_{T\infty} = 298.33°K \text{ (537.0°R)}$$
$$\mu_\infty = 28.97 \text{ g/g-mole}$$

An off-nominal test condition was included in the study to simulate a two order of magnitude decrease in flight ablator mass flow rate obtained by delaying the initial atmospheric sampling acquisition time by 75 seconds. These conditions were included to provide data for a trade study on the advisability of obtaining less atmospheric sample data at increased confidence in the sample cleanliness. The off-nominal test conditions follow:

$$M = 0.61$$
$$Re_D = 2.16 \times 10^6$$
$$P_{T\infty} = 18.54 \text{ n/cm}^2 (1.83 \text{ atm})$$
$$T_{T\infty} = 298.33°K \text{ (537.8°R)}$$

Injected Gas Conditions - The injected gas and its mass flow rate were determined from the worst case flight conditions and the defined scaling parameters. Figure 26 summarizes the calculated mass flow rates (low, nominal and high) for the two injectants used in the experiment. The nominal mass flow rate is multiplied or divided by a factor of five to obtain the off-nominal mass flow rates.

Model Conditions - The forebody of the model was designed to provide a specified range of mass flows for a designated range of pressure differentials across the porous forebody of the model. The model sampling tube length is adjustable to provide protrusion lengths from 0 to 0.76 cm (0-0.3 in). This length range on the 1/8.75 scale model corresponds to a range of 0 to 6.65 cm

# SUMMARY OF TEST INJECTANT PARAMETERS

o $M = 0.9$
o $Re_D = 1.223 \times 10^6$

|  | METHANE $(CH_4)$ | FREON 114 $(CClF_2-CClF_2)$ |
|---|---|---|
| MOLECULAR WEIGHT (g/g-mole) | 16.0 | 170.9 |
| $\dot{m}_L$ (g/sec) | $8.097 \times 10^{-2}$ | $2.646 \times 10^{-1}$ |
| $\dot{m}_N$ (g/sec) | $4.048 \times 10^{-1}$ | 1.323 |
| $\dot{m}_H$ (g/sec) | 2.024 | 6.616 |

**FIGURE 26**

(0 to 2.63 in) on the full scale flight configuration. Reference 1 indicates that the nominal sampling tube length in flight is 5.08 cm (2.0 in). Model angle of attack was also a variable considered in the test program.

Summary of Test Conditions - Figure 27 summarizes the tunnel, injected gas and configuration parameters considered in the test program.

# TUNNEL TEST CONDITIONS



## TEST PARAMETERS

$$M = 0.9$$
$$Re_D = 1.223 \times 10^6 \Big\} *$$
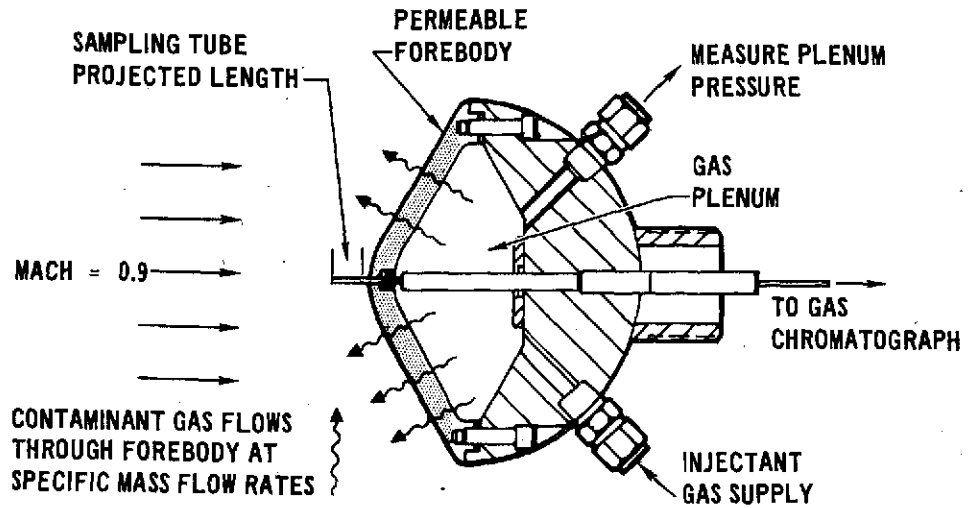
|  | FREON 114 | METHANE |
|---|---|---|
| ANGLE OF ATTACK (deg) | 0 - 10 | 0 - 5 |
| SAMPLING TUBE LENGTH (cm) | 0 - 0.76 | 0 - 0.51 |
| INJECTANT MASS FLOW RATE (g/sec) | 0.26 - 6.62 | 0.08 - 2.02 |

* TEST DATA OBTAINED AT TWO OFF-NOMINAL FREE STREAM CONDITIONS

   1.  $M = 0.90$, $Re_D = 0.3 \times 10^6$ (THICKER BOUNDARY LAYER)

   2.  $M = 0.61$, $Re_D = 2.16 \times 10^6$ (DESIGN DEPLOYMENT + 75 SECONDS)

FIGURE 27

# EXPERIMENT

Test Facility - The experiment was conducted in the 2' x 2' Transonic Wind Tunnel at the NASA/Ames Research Center, Moffett Field, California. This facility is a continuous flow, single return, closed loop, variable density wind tunnel. The test section is 2 feet wide by 2 feet deep and 5 feet long and is slotted to permit transonic testing. The flow envelope includes a Mach number range of 0.2 to 1.4, Reynolds numbers from $0.5 \times 10^6$ to $8.7 \times 10^6$ per foot at a corresponding total pressure variation of 2.3 psia to 44.1 psia and a total temperature value of approximately 560°R (Figure 13).

Test Set-up - Figure 28 provides a schematic of the test set-up. The model was sting supported in the center of the test section at a designated test angle of attack. The plenum pressure was measured in real time by a digital read-out manometer located near the adjusting valves for the injectant mass flow. This arrangement provided the capability of continual valve adjustment to maintain a constant plenum pressure within the model and hence, to maintain a constant injectant mass flow rate during the test measurement.

The methane or Freon 114 injectant gas was delivered to the model plenum by a 0.9525 cm (3/8 in) copper tube. The mass flow rate for the methane experiments was controlled by adjusting the pressure differential across an on-line flow meter. Experiments with the heavy gas were complicated by the high boiling point (3.8°C) of Freon 114 and line pressure losses. Four Freon bottles, connected to a common manifold, were immersed in a water bath to provide a large boil-off area which increased the effective bottle pressure. Line losses were minimized by eliminating the flow meter and by using 0.9525 cm (3/8 in) copper tubing and fittings instead of the original baseline values of 0.635 cm (1/4 in) Note that the change in fitting sizes are not shown on the model design drawings (Figures 23-25). Both injectant set-up arrangements required mass flow calibrations for the range of designated pressure differentials used in the experiment. The calibration techniques and resulting calibration curves are discussed in the section of this report entitled Test Results.

# TUNNEL AND EXPERIMENTAL SET-UP

1/16 IN. STEEL TUBING

TUNNEL WALL

BACKGROUND PROBE

1/4 IN. COPPER TUBING

GAS PLENUM

MODEL
SAMPLING TUBE

FLOW

1/16 IN. STEEL
TUBING

PERMEABLE
FOREBODY

3/8 IN. COPPER TUBING

TUNNEL WALL

CONTROL ROOM WALL

CARLE 100
ULTRA MICRO BEAD
THERMISTOR DETECTORS

GAS
DETECTOR/
ALARM

MANOMETER
(PLENUM
PRESSURE
READOUT)

FREON
114

COMMON
MANIFOLD

3

4

6

5

GAS CHROMATOGRAPH
(BACKGROUND)

GAS CHROMATOGRAPH
(MODEL)

1

H P 7100 BM
STRIP CHART
RECORDER

2

FLOW
METER

FLOW METER
PRESSURE
GAGE

PUMP

(1 FT$^3$/MIN)

PUMP

HOT WATER BATH

PRESSURE
GAGE

FREON

SCALE

TABLE

METHANE GAS SUPPLY

FREON
CALIBRATION
SET-UP

FIGURE 28

38

Since the test facility was of the continuous flow closed loop variety, it was necessary to measure the contaminant gas concentration in the model sampling tube and in the free stream. These contamination level measurements were designated as the model and background values, respectively. The numerical difference in the two values is the absolute sample contamination level due to the injection of the contaminant, or trace, gas. Figure 28 illustrates the dual sampling probes and gas chromatograph systems used in obtaining the two contamination measurements. The background probe and the sampling tube were designed to have identical inlet dimensions. The steel tube lines, which carried the ingested samples from the background probe and the sampling tube to the detector system, were of identical cross-section and length to ensure that the flow rate through each sampling line was the same. This procedure simplified the data acquisition by eliminating line lag corrections. Figure 29 illustrates the tunnel arrangement of the sting mounted model and the wall mounted background probe. The photograph of Figure 30 shows the details of the background probe and the fully extended model sampling tube.

The abundance of the contaminant gas contained in the gas samples was detected by a dual gas chromatograph set-up. The contamination detection set-up is schematically illustrated by Figure 28 and is partially shown by the photograph in Figure 31. A Carle 100 Ultramicrobead Thermistor Detector with a bridge circuit was used as the contaminant gas detector system. Carle Model 2014 crossover gas sampling valves with twin sampling loops were used in the system due to their demonstrated simplicity of operation in the 10 millitorr to 12 atmosphere pressure range. The NASA/Ames Research Center's Life Detection Systems Branch (LPD) custom built the gas chromotograph (G.C.) from standard Carle instrument components. The housing for the G.C. was draft tight and contained the twin valves and detectors in a side-by-side arrangement. The packed separation columns for the Freon experiments were wrapped with heat-tape and maintained at 80°C during testing. The methane columns were not heated during the experiments. The gas samples were drawn through the sampling lines by two $2.832 \times 10^4$ cm$^3$/min (1 ft$^3$/min) pumps. Once the sample was trapped, it was separated in the column and analyzed by the thermistor detector. The absolute concentration of contaminant (Freon 114

# STING MOUNTED MODEL AND BACKGROUND PROBE IN TUNNEL



INJECTANT SUPPLY LINE

POROUS FOREBODY

BACKGROUND SAMPLING TUBE

PLENUM PRESSURE LINE
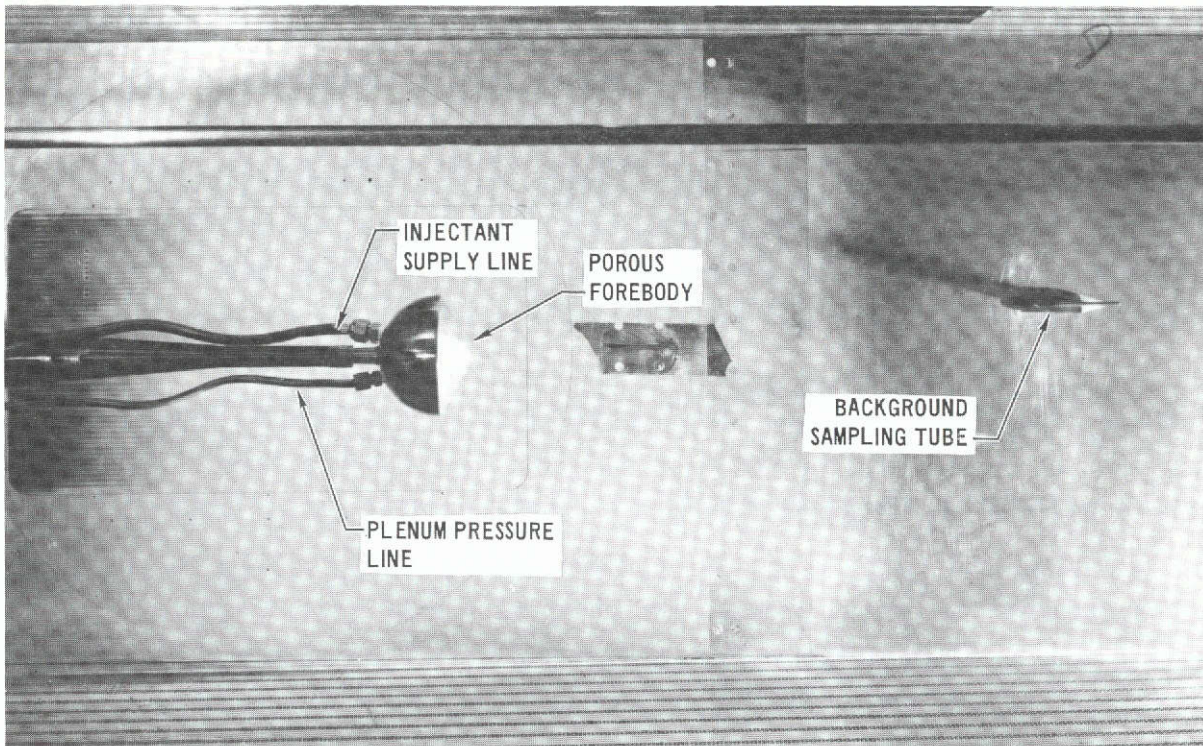
FIGURE 29

or methane) contained in the sample was determined directly, in volumetric parts per million (ppm), from the amplitude of the chromatogram traced out on the Hewlett Packard 7100 BM strip chart recorder.

Test Sequence - The following sequence was followed in obtaining the experimental data (refer to Figure 28):

1.  Set model angle of attack and sampling tube length. Check lines for leaks if model changes were made. Bring tunnel up to specified run conditions.

2.  Open valves 1 and 2 on the background and sampling tube lines. This pumps samples through the lines.

3.  Open combination of valves 3, 4, 5 and 6 until the digital read-out of the manometer indicates that the specified pressure differential has been attained. This sets the mass flow rate of contaminant gas through the permeable model forebody. Fine valving adjustments during the test are required to maintain a constant pressure read-out.

## MODEL AND BACKGROUND PROBE



DEPLOYED
SAMPLING TUBE

SCALE MODEL

BACKGROUND SAMPLING PROBE
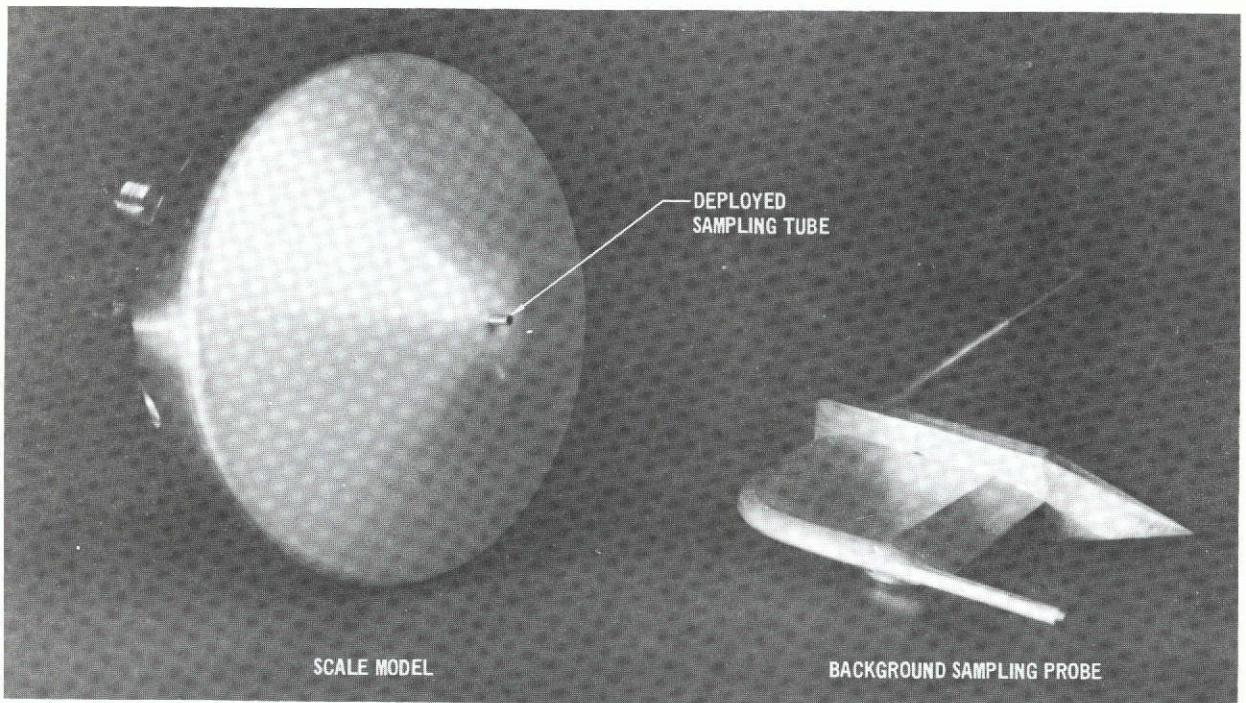
FIGURE 30

4. Two minutes after the injectant mass flow rate has stabilized (constant pressure differential), valves 1 and 2 are closed to trap a column of gas in each sampling line at the tunnel total pressure.

5. After 30 seconds, the samples are simultaneously injected into the respective channels of the gas chromatograph by activating the gas sampling valves.

6. The contaminant gas flow is terminated by closing valves 3, 4, 5 and 6. Valves 1 and 2 are opened to permit flow in the sampling lines.

7. Approximately 5 minutes is required from the time the samples enter the gas chromatograph to the time when both chromatograms are traced by the recorder.

8. Tunnel is purged if contaminant level of background exceeds 300 ppm. If contaminant level of background is less than 300 ppm, return to step 3 with a new mass flow rate.

# METHANE SAMPLING SYSTEM SET-UP
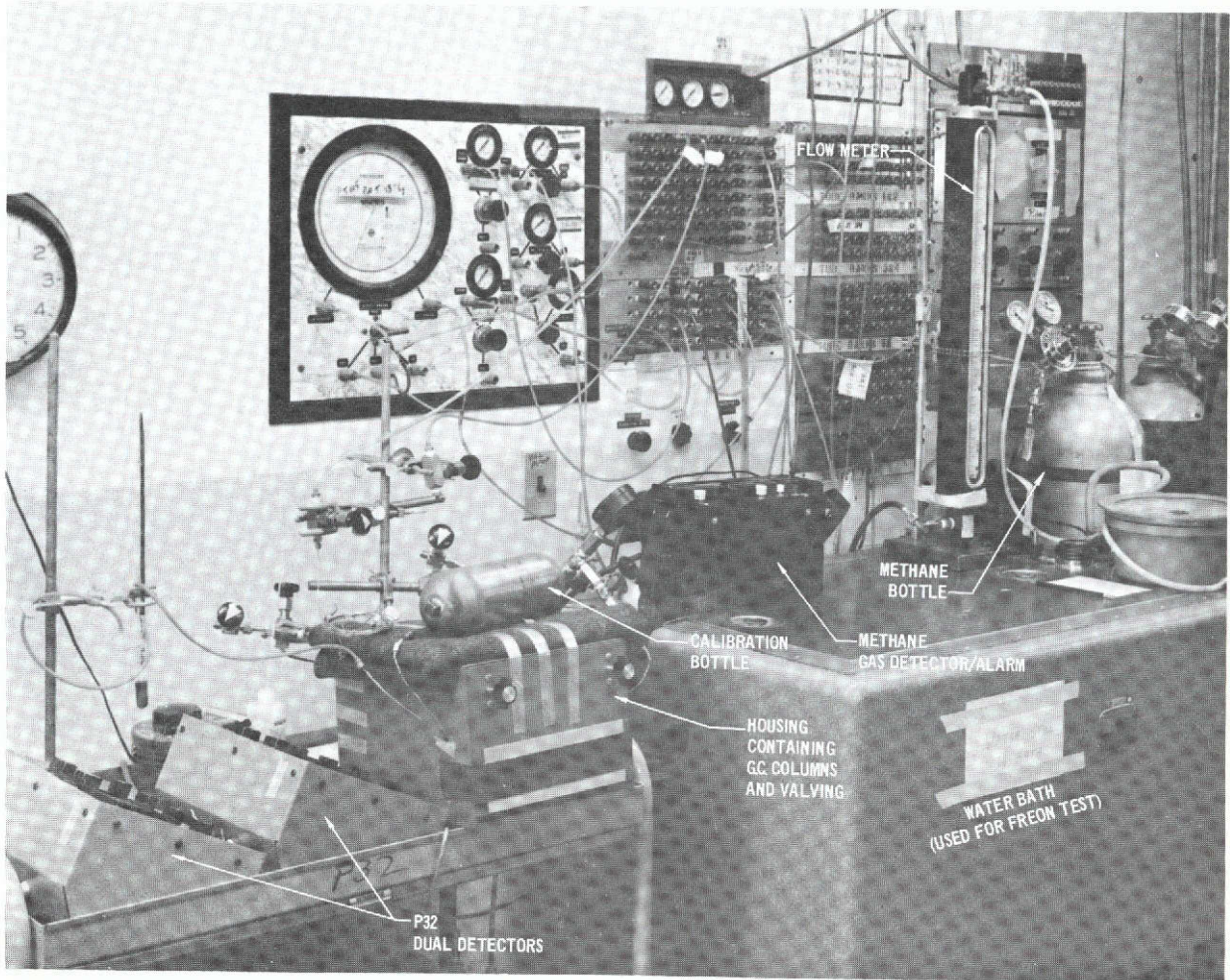


FIGURE 31

# TEST RESULTS

Freon 114 Injection - Figure 32 provides a table summarizing the test
conditions and the resulting contamination levels for the Freon 114 test series.
Experimental uncertainties (due to random measurement errors) associated with
the absolute contaminant level are included in the summary table and are
discussed in detail in Appendix B. The mass flow rates indicated in the table
were determined from a dynamic calibration of the model obtained while the
tunnel was operating at the nominal test conditions ($M = 0.9$ and $Re_D = 1.223$
$\times 10^6$). In the calibration, a single Freon 114 bottle, wrapped with heat-tape,
was placed on a measurement scale and the valve adjusted until a constant
pressure differential (constant mass flow rate) was attained at the manometer.
When steady conditions were reached, the total weight of the system was noted
and a stop watch was started. The Freon 114 mass flow rate was determined at
various pressure differentials by measuring the mass loss of gas in a known
time interval. Figure 33 presents the resulting calibration curve and also
notes the low, nominal and high mass flow rates which simulate the range of
worst case flight outgassing rates. Note that the model plenum pressure is
always less than the tunnel total pressure (Figure 32) for the case of no
mass injection. This is because the model surface pressure decreases from
the tunnel stagnation value at the nose to a 60° cone value over the model flanks.

The experimental results obtained at the nominal tunnel conditions (worst
case flight conditions) are presented by Figures 34, 35 and 36. These data
were obtained for sampling tube lengths of 0.508, 0.635 and 0.762 cm, respect-
ively. Figure 37 presents the nominal Reynolds number data obtained for the
0.508 cm sampling tube at 5° and 10° angles of attack. All of these data
points were obtained by calculating the difference between the measured
contaminant levels at the model sampling tube and at the background probe.
Each of these measurements contained systematic and random errors due to
experimental uncertainties. The magnitude of these uncertainties is
discussed in Appendix B and is represented as an error band on each of the
data points of Figures 34, 35, 36 and 37. The open symbol data points on
these figures indicate that the measured contaminant levels cannot be
distinguished from a zero measurement since the magnitude of the data point

## DATA SUMMARY: FREON 114

| RUN NO. | L cm(in.) | α DEG | TUNNEL CONDITION + | $P_{PL_{O_2}}$ n/cm² | $P_{PL}$ n/cm² | ΔP n/cm² | MODEL (SAMPLING TUBE) CALIBR. FACTOR | ATTENU-ATION | TRACE AMPLITUDE cm | BACKGROUND CALIBR. FACTOR | ATTENU-ATION | TRACE AMPLITUDE cm | ΔPPM | ΔPPM MAX | ΔPPM MIN | $\dot{m}_I$ g/sec | $\frac{100\,\Delta PPM}{PPM}\,x_{BP}$ |
|---|---|---|---|---|---|---|---|---|---|---|---|---|---|---|---|---|---|
| 100-108 | POOR DATA OBTAINED DUE TO LINE LEAKS AND CALIBRATION DRIFT | | | | | | | | | | | | | | | | |
| 109 | 0 | 0 | NOM | 7.04 | 7.79 | 0.75 | 39.33 | 1 | 2.65 | 20.43 | 1 | 5.0 | 2.4 | 15.04 | -9.76 | 0.65 | 1.92 |
| 110 | 0 | 0 | NOM | 7.04 | 8.84 | 1.80 | 39.33 | 1 | 10.95 | 20.43 | 1 | 11.15 | 247.4 | 291.97 | 203.88 | 1.85 | 88.95 |
| 111 | 0 | 0 | NOM | 7.13 | 8.30 | 1.17 | 39.33 | 2 | 4.1 | 20.43 | 2 | 7.75 | 7.12 | 45.84 | -30.82 | 1.15 | 1.84 |
| TUNNEL PURGED | | | | | | | | | | | | | | | | | |
| 112 | .508(.2) | 0 | NOM | 7.08 | 8.13 | 1.05 | 39.33 | 1 | 2.8 | 20.43 | 1 | 5.85 | -11.5 | 2.2 | -24.83 | 1.01 | -7.88 |
| 113 | .508(.2) | 0 | NOM | 7.15 | 9.11 | 1.96 | 39.33 | TRACE NOT READABLE | | | | | | | | | 2.19 | |
| 114 | .508(.2) | 0 | NOM | 7.15 | 9.24 | 2.09 | 39.33 | 2 | 6.0 | 20.43 | 2 | 10.35 | 60.21 | 115.38 | 6.18 | 2.19 | 11.66 |
| TUNNEL PURGED | | | | | | | | | | | | | | | | | |
| 115 | .508(.2) | 0 | NOM | 7.04 | 8.74 | 1.70 | 39.33 | 1 | 4.45 | 20.43 | 1 | 8.35 | 5.40 | 26.37 | -15.13 | 1.75 | 2.59 |
| 116 | .508(.2) | 0 | NOM | 7.15 | 8.60 | 1.45 | 39.33 | 1 | 7.1 | 20.43 | 1 | 12.9 | 19.15 | 52.27 | -13.33 | 1.44 | 5.95 |
| 117 | .508(.2) | 0 | NOM | 7.18 | 8.57 | 1.39 | 39.33 | TRACE NOT READABLE | | | | | | | | | | |
| 118 | .508(.2) | 0 | NOM | 7.14 | 10.53 | 3.39 | 39.33 | 5 | 3.12 | 20.43 | 5 | 5.8 | 25.71 | 99.01 | -46.10 | 3.72 | 3.55 |
| TUNNEL PURGED | | | | | | | | | | | | | | | | | |
| 119 | .508(.2) | 0 | NOM | 7.08 | 8.36 | 1.28 | 39.33 | 1 | 4.1 | 20.43 | 1 | 7.55 | 8.55 | 27.74 | -10.28 | 1.27 | 4.54 |
| 120 | .508(.2) | 0 | NOM | 7.11 | 8.97 | 1.86 | 39.33 | 1 | 7.98 | 20.43 | 2 | 6.95 | 36.68 | 73.47 | -.66 | 1.92 | 10.58 |
| 121 | .508(.2) | 0 | NOM | 7.11 | 9.31 | 2.20 | 39.33 | 2 | 5.9 | 20.43 | 2 | 10.15 | 60.21 | 114.41 | -7.10 | 2.32 | 11.89 |
| TUNNEL PURGED | | | | | | | | | | | | | | | | | |
| 122 | .508(.2) | 0 | NOM | 7.04 | 9.58 | 2.54 | 39.33 | 2 | 3.0 | 20.43 | 2 | 4.9 | 43.62 | 70.80 | 17.01 | 2.71 | 17.84 |
| 123 | .508(.2) | 0 | NOM | 7.08 | 9.92 | 2.84 | 39.33 | 2 | 5.85 | 20.43 | 2 | 10.35 | 45.44 | 99.63 | -7.63 | 3.06 | 8.80 |
| 124 | .508(.2) | 0 | NOM | 7.08 | 11.21 | 4.13 | 39.33 | 5 | 3.6 | 20.43 | 5 | 7.2 | -33.83 | 52.89 | -118.34 | 4.67 | -3.74 |
| TUNNEL PURGED | | | | | | | | | | | | | | | | | |
| 125 | .762(.3) | 0 | NOM | 7.11 | 8.13 | 1.02 | 39.33 | 1 | 2.2 | 20.43 | 1 | 4.6 | -9.09 | 1.63 | -19.60 | 0.96 | -7.92 |
| 126 | .762(.3) | 0 | NOM | 7.08 | 8.47 | 1.39 | 39.33 | 1 | 4.25 | 20.43 | 1 | 8.65 | -11.67 | 8.85 | -31.79 | 1.39 | -5.40 |
| 127 | .762(.3) | 0 | NOM | 7.15 | 9.58 | 2.43 | 39.33 | 2 | 4.0 | 20.43 | 2 | 7.9 | -9.94 | 28.34 | -47.45 | 2.58 | -2.52 |
| 128 | .762(.3) | 0 | NOM | 7.15 | 11.18 | 4.03 | 39.33 | 5 | 2.85 | 20.43 | 5 | 5.45 | 4.55 | 72.07 | -61.61 | 4.52 | 0.67 |
| TUNNEL PURGED | | | | | | | | | | | | | | | | | |
| 129 | .762(.3) | 0 | NOM | 7.08 | 8.47 | 1.39 | 39.33 | 1 | 3.65 | 20.43 | 1 | 7.25 | -5.57 | 11.93 | -22.72 | 1.39 | -3.08 |
| 130 | .762(.3) | 0 | NOM | 7.11 | 9.24 | 2.13 | 39.33 | 1 | 7.3 | 20.43 | 2 | 6.38 | 32.22 | 65.91 | -.78 | 2.25 | 10.12 |
| TUNNEL PURGED | | | | | | | | | | | | | | | | | |
| 131 | .762(.3) | 0 | NOM | 7.04 | 10.84 | 3.80 | 39.33 | 1 | 6.1 | 20.43 | 1 | 11.4 | 8.55 | 37.26 | -19.57 | 4.23 | 3.01 |
| 132 | .762(.3) | 0 | NOM | 7.14 | 12.29 | 5.15 | 39.33 | 1 | 14.55 | 20.43 | 2 | 13.9 | 5.24 | 74.17 | -62.29 | 6.15 | 0.76 |
| TUNNEL PURGED | | | | | | | | | | | | | | | | | |
| 133 | .635(.25) | 0 | NOM | 7.18 | 9.21 | 2.03 | 39.33 | TRACE NOT READABLE | | | | | | | | | | |
| 134 | .635(.25) | 0 | NOM | 7.18 | 8.50 | 1.32 | 39.33 | TRACE NOT READABLE | | | | | | | | | | |
| 135 | .635(.25) | 0 | NOM | 7.25 | 9.89 | 2.64 | 39.33 | 1 | 10.0 | 20.43 | 2 | 8.95 | 33.66 | 80.13 | -11.85 | 2.82 | 7.54 |
| TUNNEL PURGED | | | | | | | | | | | | | | | | | |
| 136 | .635(.25) | 0 | NOM | 7.18 | 9.18 | 2.00 | 39.33 | TRACE NOT READABLE | | | | | | | | | | |
| 137 | .635(.25) | 0 | NOM | 7.18 | 10.26 | 3.08 | 39.33 | 1 | 8.5 | 20.43 | 2 | 7.7 | 24.01 | 63.65 | -14.82 | 3.35 | 6.25 |
| 138 | .635(.25) | 0 | NOM | 7.25 | 10.87 | 3.62 | 39.33 | 2 | 6.55 | 20.43 | 2 | 12.5 | 5.46 | 67.49 | -55.33 | 4.00 | 0.87 |
| TUNNEL PURGED | | | | | | | | | | | | | | | | | |
| 139 | .635(.25) | 0 | NOM | 7.18 | 9.48 | 2.30 | 39.33 | 1 | 3.9 | 20.43 | 1 | 8.1 | -14.74 | 4.22 | -33.33 | 2.44 | -7.30 |
| TUNNEL PURGED | | | | | | | | | | | | | | | | | |
| 140 | .508(.2) | 10 | NOM | 7.01 | 9.14 | 2.13 | 39.33 | 1 | 5.65 | 20.43 | 1 | 11.0 | -3.1 | 23.9 | -29.4 | 2.25 | -1.13 |
| 141 | .508(.2) | 10 | NOM | 7.08 | 10.67 | 3.59 | 39.33 | 1 | 10.6 | 20.43 | 2 | 10.6 | -19.8 | 31.2 | -69.6 | 3.98 | -3.74 |
| TUNNEL PURGED | | | | | | | | | | | | | | | | | |
| 142 | .508(.2) | 10 | NOM | 7.08 | 8.13 | 1.05 | 39.33 | TRACE NOT READABLE | | | | | | | | | 1.01 | |
| 143 | .508(.2) | 10 | NOM | 7.08 | 9.96 | 2.88 | 39.33 | 1 | 4.2 | 20.43 | 1 | 8.35 | -6.6 | 13.5 | -26.3 | 3.11 | -3.17 |
| TUNNEL PURGED | | | | | | | | | | | | | | | | | |
| 144 | .508(.2) | 5 | NOM | 7.01 | 9.04 | 2.03 | 39.33 | 1 | 2.3 | 20.43 | 1 | 4.75 | -7.9 | 3.3 | -18.9 | 2.12 | -6.67 |
| 145 | .508(.2) | 5 | NOM | 7.04 | 8.40 | 1.36 | 39.33 | 1 | 4.4 | 20.43 | 1 | 8.7 | -5.6 | 15.5 | -26.2 | 1.35 | -2.58 |
| 146 | .508(.2) | 5 | NOM | 7.08 | 9.79 | 2.71 | 39.33 | 2 | 3.9 | 20.43 | 2 | 7.85 | -17.1 | 20.5 | -53.9 | 2.90 | -4.37 |
| TUNNEL PURGED | | | | | | | | | | | | | | | | | |
| 147 | .762(.3) | 0 | NOM | 7.04 | 9.18 | 2.14 | 39.33 | TRACE NOT READABLE | | | | | | | | | 5.05 | |
| 148 | .762(.3) | 0 | NOM | 7.11 | 11.51 | 4.40 | 39.33 | 2 | 5.55 | 20.43 | 5 | 4.3 | -3.7 | 49.1 | -55.4 | 5.05 | -0.69 |
| 149 | .762(.3) | 0 | NOM | 7.11 | 9.24 | 2.13 | 39.33 | 2 | 7.9 | 20.43 | 5 | 5.9 | 22.87 | 96.5 | -50.6 | 2.25 | 3.70 |
| TUNNEL PURGED | | | | | | | | | | | | | | | | | |
| 150 | .508(.2) | 0 | A | 16.86 | 18.22 | 1.36 | 39.33 | 1 | 3.2 | 20.43 | 1 | 6.35 | -2.15 | 4.79 | -8.91 | 1.35 | -3.03 |
| 151 | .508(.2) | 0 | A | 16.76 | 17.44 | 0.68 | 39.33 | 1 | 5.7 | 20.43 | 1 | 10.8 | 2.5 | 14.03 | -10.01 | 0.61 | 2.07 |
| TUNNEL PURGED | | | | | | | | | | | | | | | | | |
| 162 | | | | (DYNAMIC CALIBRATION OF $\dot{m}_I$ vs ΔP) | | | | | | | | | | | | | | |
| TUNNEL PURGED | | | | | | | | | | | | | | | | | |
| 153 | .762(.3) | 0 | NOM | 6.98 | 9.11 | 2.13 | | TRACE NOT READABLE | | | | | | | | | 2.25 | |
| 154 | .762(.3) | 0 | NOM | 6.98 | 8.67 | 1.69 | 39.33 | 1 | 4.4 | 20.43 | 1 | 8.8 | -8.4 | 12.7 | -29.1 | 1.75 | -3.82 |
| 155 | .762(.3) | 0 | NOM | 6.98 | 9.11 | 2.13 | 39.33 | 2 | 3.65 | 20.43 | 2 | 6.7 | 16.0 | 50.1 | -17.4 | 2.25 | 4.79 |
| TUNNEL PURGED | | | | | | | | | | | | | | | | | |
| 156-165 | .762(.3) | 0 | NOM | (DYNAMIC CALIBRATION OF $\dot{m}_I$ vs ΔP) | | | | | | | | | | | | | | |

1 n/cm² = 9.8692 x 10⁻² ATM

### +TUNNEL CONDITION NOMENCLATURE

| CONDITION | M | $Re_D$ | $P_T$ n/cm² (atm) | $T_T$ °K (°R) |
|---|---|---|---|---|
| NOMINAL | 0.90 | 1.223 x 10⁶ | 8.299 (0.819) | 298.3 (537.0) |
| A | 0.61 | 2.160 x 10⁶ | 18.54 (1.83) | 298.8 (537.8) |
| B | 0.90 | 0.307 x 10⁶ | 2.04 (0.201) | 288.5 (519.2) |

FIGURE 32

MASS FLOW RATE CALIBRATION: FREON 114
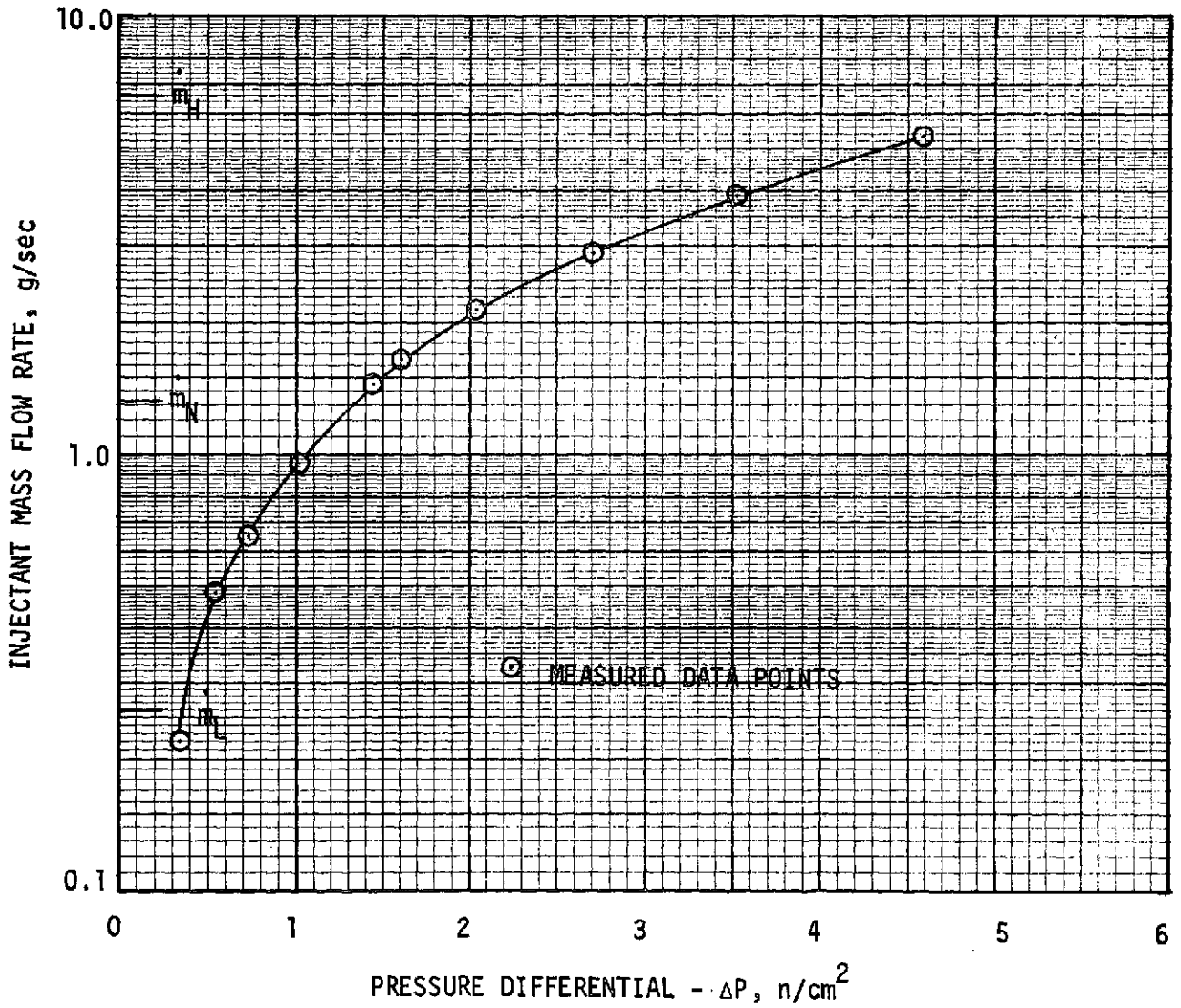


FIGURE 33

FREON 114 DATA

$M = 0.90$
$Re_D = 1.223 \times 10^6$
$L = 0.508$ cm (0.20 in)
$\alpha = 0°$
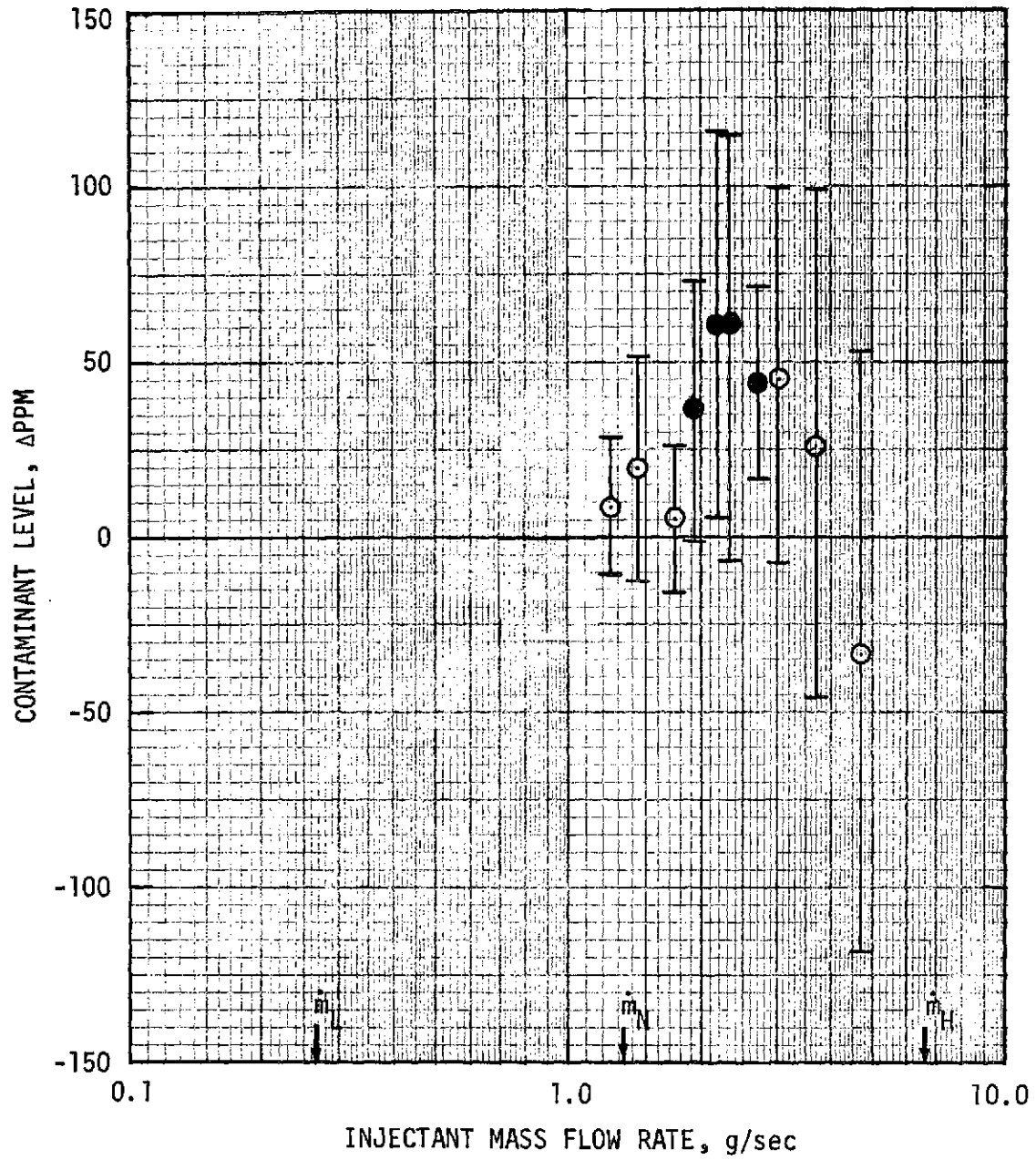
FIGURE 34

FREON 114 DATA

M     = 0.90
$Re_D$  = 1.223 x $10^6$
L     = 0.635 cm (0.25 in)
$\alpha$     = 0°
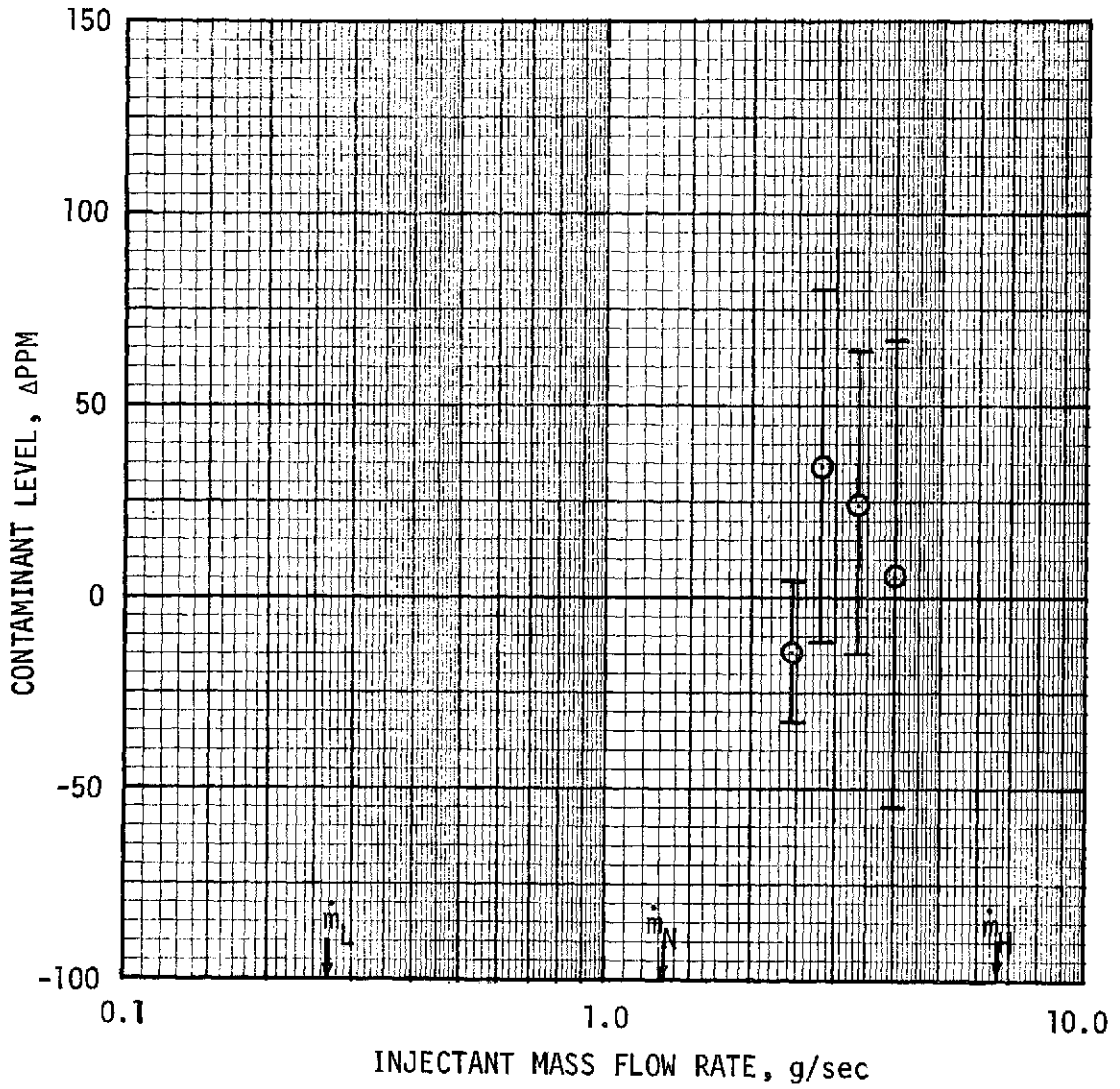
FIGURE 35

FREON 114 DATA

M = 0.90
$Re_D$ = 1.223 x $10^6$
L = 0.762 cm (0.30 in)
α = 0°
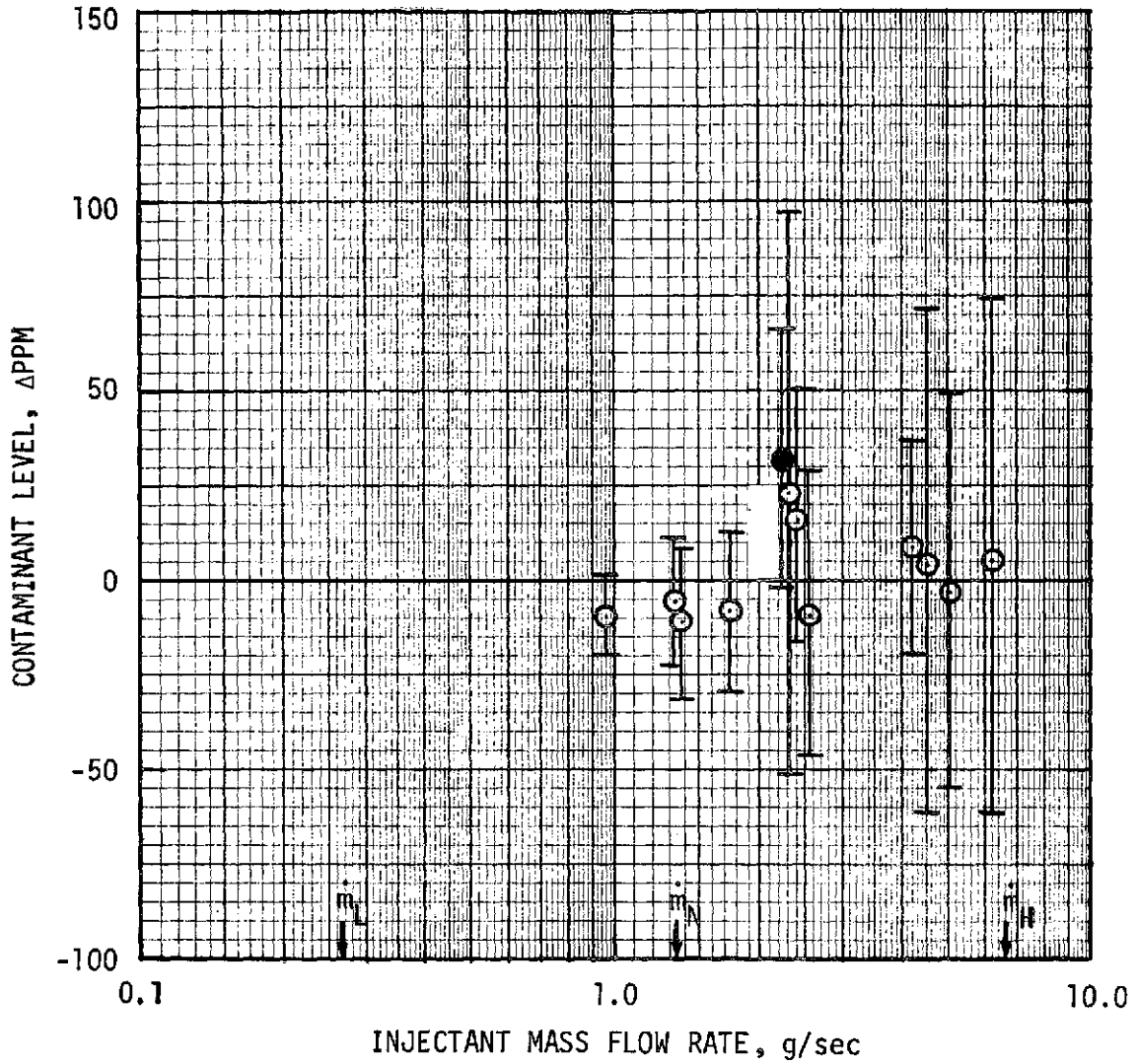
FIGURE 36

# FREON 114 DATA

## (ANGLE OF ATTACK SUMMARY)

$$M = 0.90$$
$$Re_D = 1.223 \times 10^6$$
$$L = 0.508 \text{ cm } (0.20 \text{ in.})$$
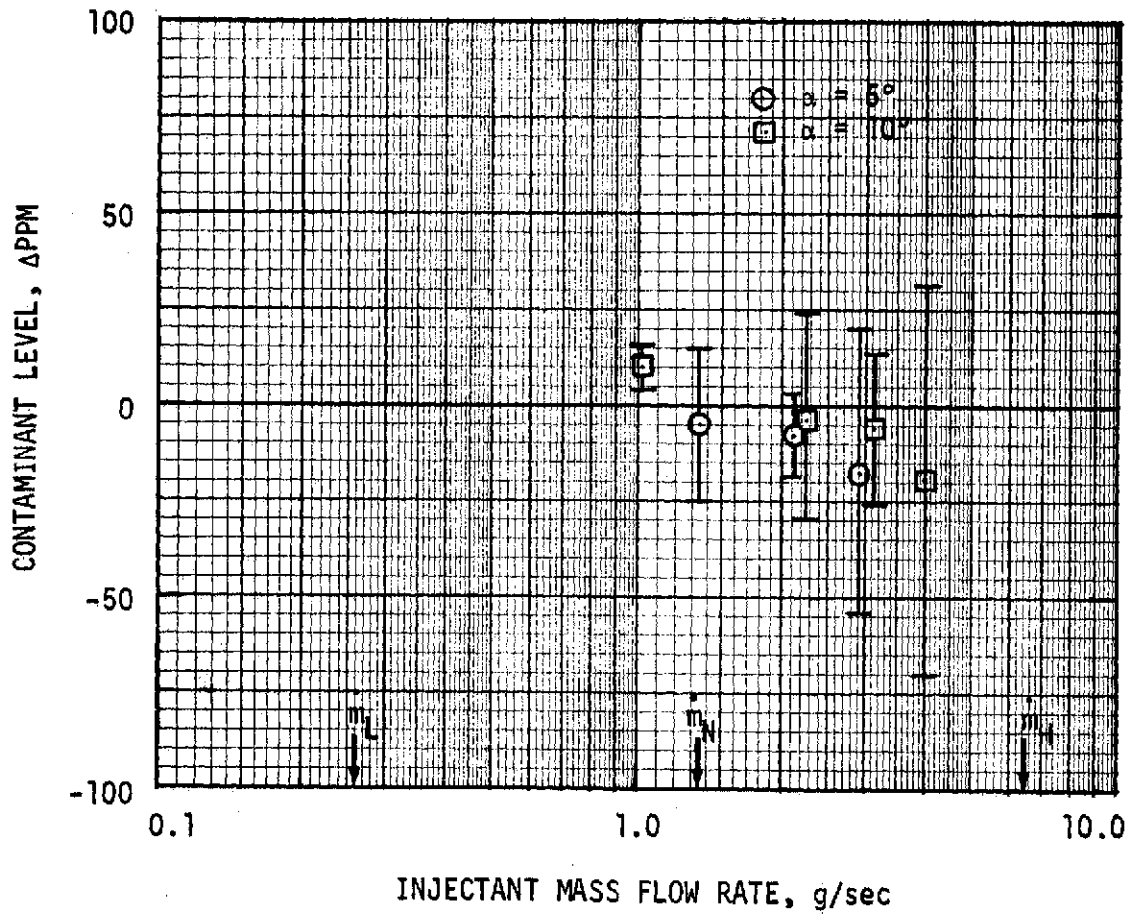


FIGURE 37

is within the uncertainty of the experiment. The solid symbol data points denote contaminant measurements greater than the experimental uncertainty and hence, signify contamination of the gas sample.

The error analysis for Freon 114 shows that values of the differential parts per million ($\Delta$PPM) that are less than or equal to 9.9% of the background contaminant level ($PPM_{BP}$) cannot be distinguished from a zero contaminant level. The complete set of Freon 114 data is summarized by Figure 38 to indicate the level of contamination observed in the experiment. The 34 data points were obtained at two different tunnel conditions using combinations of three angles of attack and three sampling tube lengths. Twenty-nine (29) of the points predict zero contamination within the calculated accuracy of the experiment ($\Delta$PPM/$PPM_{BP} \leq 0.099$) while five (5) data points indicate contamination. Of the five contamination points, only one measurement predicts contamination by an amount of more than 2% over the experimental accuracy value of 9.9%. The trend of the data is clearly to indicate a zero contaminant level within the accuracy of the experiment. The actual value of the uncertainty in the data is dependent upon the background contamination level but is approximately represented by ±50 ppm.

The potential for contamination of the gas sample decreases after instrument deployment in flight due to the rapidly decreasing ablator mass flow rate. Figure 39 presents the results obtained from the off-nominal test condition which corresponds to a time delay of 75 seconds in initiating the flight atmospheric sampling experiment. At this trajectory point the ablator outgassing rate has been reduced two orders of magnitude from its value at deployment. The experiment mass flow rates for outgassing simulation at the off-nominal conditions are substantially reduced ($\dot{m}_H = 0.6$g/sec) from the nominal test conditions and the measured contaminate level in this range is zero, within the accuracy of the data (±15 ppm).

The nominal test condition measurements, using Freon 114 as an injectant indicate that the contamination level is 0±50 ppm. However, since atmospheric trace species abundances may be as low as 40-50 ppm, it is necessary to improve the accuracy of the experiment to increase confidence in the actual contaminant level measurement. The methane test series results show a marked improvement in measurement sensitivity.

# FREON 114 DATA:   ERROR ANALYSIS SUMMARY

⊙ L = 0.508 cm (BASELINE DESIGN)
◊ L = 0.762 cm
◗ L = 0.635 cm
△ L = 0.508 cm, α = 10°
□ L = 0.508 cm, α = 5°
◑ L = 0.508 cm, TUNNEL COND. A

FIGURE 38

51
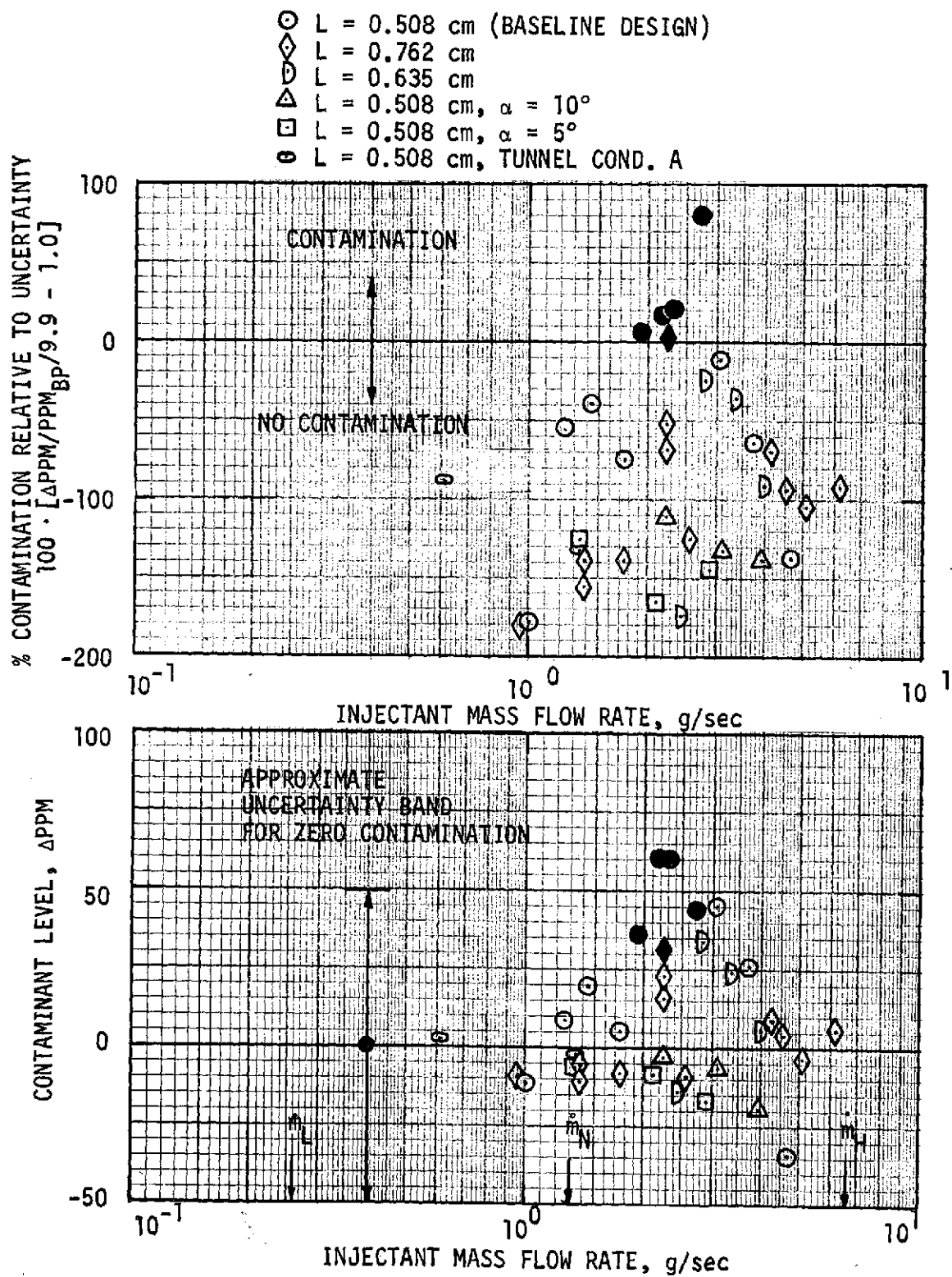
FREON 114 DATA:   OFF NOMINAL CONDITIONS

$$M = 0.61$$
$$Re_D = 2.16 \times 10^6$$
$$L = 0.508 \text{ cm } (0.20 \text{ in})$$
$$\alpha = 0°$$
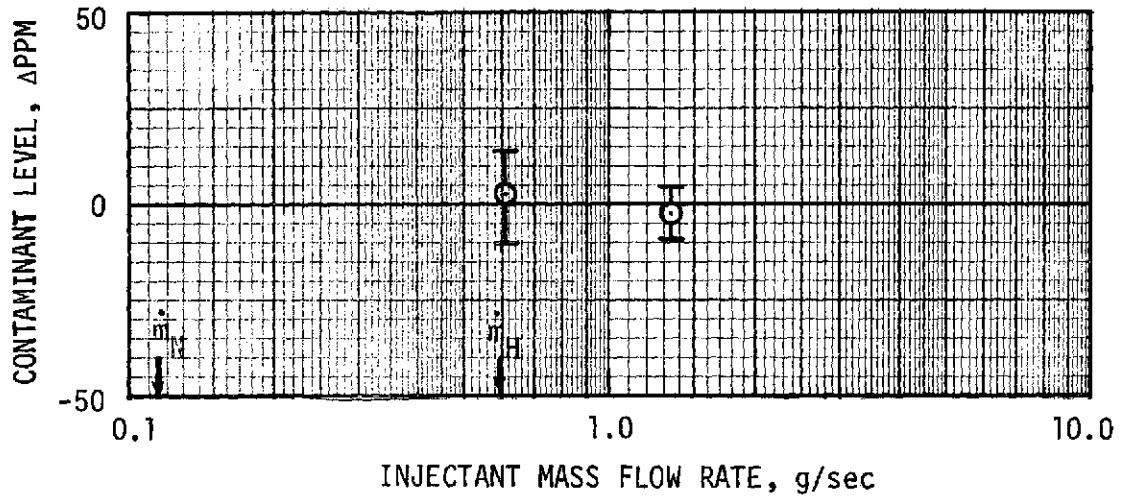


FIGURE 39

Methane Injection - The methane experiments provide data for a low molecular weight injectant at an improved experimental accuracy in comparison with the Freon 114 results.

Figure 40 summarizes the model parameters, tunnel conditions, injectant conditions and contaminate measurements and levels (including uncertainties) for the series of methane tests. As in the Freon 114 test series, a calibration relating the actual mass flow rate and the applied pressure differential was obtained. The resulting calibration curve is presented by Figure 41. The mass flow calibration data was obtained at ambient (static) conditions and then numerically corrected for tunnel condition effects. The pressure differentials and mass flow rates which simulate the flight low, nominal and high outgassing rates are indicated on the calibration curve for reference.

The contaminant data obtained at the start of the methane test series were affected by a calibration factor (not to be confused with the mass flow calibration) drift on both detector channels of the twin loop gas chromatograph. The Freon 114 test results did not indicate an appreciable calibration drift during the 40 hour test series and therefore, the calibration drift in the methane tests was not anticipated (results summarized by Appendix C). The drift was attributed to the combined effect of operating the thermistors at a low current to maximize system sensitivity and to the local temperature excursions in the wind tunnel control room. Increasing the thermistor current and minimizing local temperature plunges were incorporated to control the drift. However, some drifting still occurred and an accurate time history of each of the gas chromatograph channel's calibration factor was obtained during the remainder of the test series. This experimental procedure resulted in an accurate determination of the calibration factors associated with each test measurement.

The results of the methane experiments are presented in terms of:
(a) zero angle of attack test results,(b) angle of attack and off-nominal test results and (c) accuracy of test measurements.

(a) Methane: Zero Angle of Attack Results - Figures 42-46 graphically present the contamination level measurements for different sampling tube lengths. When the sampling tube length is zero (Figure 42), significant contamination occurs even at the lowest mass injection rates. Such high

## DATA SUMMARY: METHANE

| RUN NO. | L cm(in.) | α DEG | TUNNEL CONDITION | $P_{PL_0}$ n/cm² | $P_{PL}$ n/cm² | ΔP n/cm² | MODEL (SAMPLING TUBE) CALIBR. FACTOR | ATTENUATION | TRACE AMPLITUDE cm | BACKGROUND CALIBR. FACTOR | ATTENUATION | TRACE AMPLITUDE cm | ΔPPM | ΔPPM MAX | ΔPPM MIN | $\dot{m}_1$ g/sec | 100 ΔPPM / PPM BP |
|---|---|---|---|---|---|---|---|---|---|---|---|---|---|---|---|---|---|
| 166 | .762(.3) | 0 | NOM* | 6.94 | 7.96 | 1.02 | | | | | | | | | | 0.12 | |
| 167 | .762(.3) | 0 | NOM | 7.01 | 9.72 | 2.71 | | | | | | | | | | 0.27 | |
| 168 | .762(.3) | 0 | NOM | 7.01 | 11.07 | 4.06 | | | | | | | | | | 0.43 | |
| TUNNEL PURGED | | | | | | | | | | | | | | | | | |
| 169 | .762(.3) | 0 | NOM | 6.91 | 12.73 | 5.82 | | | | | | | | | | 0.70 | |
| 170 | .762(.3) | 0 | NOM | 6.94 | 12.39 | 5.45 | LARGE UNCERTAINTY IN CALIBRATION FACTORS DUE TO DRIFT | | | | | | | | | 0.63 | |
| TUNNEL PURGED | | | | | | | | | | | | | | | | | |
| 171 | .762(.3) | 0 | NOM | 6.90 | 16.22 | 9.32 | | | | | | | | | | 1.45 | |
| TUNNEL PURGED | | | | | | | | | | | | | | | | | |
| 172 | .762(.3) | 0 | NOM | 6.93 | 11.57 | 4.64 | | | | | | | | | | 0.52 | |
| 173 | .762(.3) | 0 | NOM | 6.97 | 12.06 | 5.09 | | | | | | | | | | | |
| TUNNEL PURGED | | | | | | | | | | | | | | | | | |
| 174 | .508(.2) | 0 | NOM | 7.01 | 10.53 | 3.52 | 5.31 | 10 | 4.45 | 6.40 | 10 | 3.55 | 11.10 | 23.88 | -1.71 | 0.36 | 4.00 |
| 175 | .508(.2) | 0 | NOM | 7.00 | 12.43 | 5.43 | 5.31 | 10 | 11.15 | 6.40 | 10 | 9.25 | -.085 | 21.65 | -21.51 | 0.63 | -0.01 |
| TUNNEL PURGED | | | | | | | | | | | | | | | | | |
| 176 | .508(.2) | 0 | NOM | 7.00 | 12.43 | 5.43 | 5.31 | 5 | 14.3 | 6.40 | 5 | 11.55 | 12.28 | 24.98 | -0.44 | 0.63 | 2.72 |
| 177 | .508(.2) | 0 | NOM | 7.03 | 9.07 | 2.04 | 5.31 | TRACE NOT READABLE | | | | | | | | 0.21 | |
| TUNNEL PURGED | | | | | | | | | | | | | | | | | |
| 178 | .508(.2) | 0 | NOM | 7.00 | 13.11 | 6.11 | 5.31 | TRACE NOT READABLE | | | | | - | - | - | 0.75 | |
| TUNNEL PURGED | | | | | | | | | | | | | | | | | |
| 179 | .508(.2) | 0 | NOM | 6.97 | 14.79 | 7.82 | 5.31 | TRACE NOT READABLE | | | | | - | - | - | 1.10 | |
| TUNNEL PURGED | | | | | | | | | | | | | | | | | |
| 180 | .508(.2) | 0 | NOM | 6.91 | 16.75 | 9.84 | 5.1 | 5 | 22.7 | 6.22 | 5 | 18.42 | 7.30 | 24.79 | -10.20 | 1.60 | 1.04 |
| TUNNEL PURGED | | | | | | | | | | | | | | | | | |
| 181 | .508(.2) | 0 | NOM | 6.93 | 8.98 | 2.05 | 5.1 | 2 | 14.70 | 6.22 | 2 | 12.15 | -1.48 | 3.59 | -6.52 | 0.21 | -0.80 |
| 182 | .508(.2) | 0 | NOM | 6.93 | 15.18 | 8.25 | 5.1 | 10 | 11.35 | 6.22 | 10 | 9.2 | 8.06 | 29.0 | -12.89 | 1.20 | 1.15 |
| 183-214 | DATA OBTAINED UNUSABLE DUE TO LINE LEAKS AND CALIBRATION DRIFT | | | | | | | | | | | | | | | | |
| TUNNEL PURGED | | | | | | | | | | | | | | | | | |
| 215 | .127(.05) | 0 | NOM | 7.11 | 8.80 | 1.69 | 8.35 | 2 | 4.0 | 8.77 | 2 | 4.05 | -5.1 | -.83 | -9.5 | 0.18 | -5.88 |
| 216 | .127(.05) | 0 | NOM | 7.10 | 10.50 | 3.40 | 8.49 | 2 | 4.12 | 8.90 | 2 | 10.2 | -8.2 | -.34 | -15.9 | 0.35 | -3.70 |
| 217 | .127(.05) | 0 | NOM | 7.15 | 12.19 | 5.04 | 8.59 | 5 | 11.80 | 8.97 | 5 | 11.35 | -2.7 | 9.3 | -14.6 | 0.59 | -0.43 |
| 218 | .127(.05) | 0 | NOM | 7.15 | 13.88 | 6.73 | 8.68 | 10 | 8.90 | 9.05 | 10 | 8.60 | -7.1 | 16.5 | -30.6 | 0.92 | -0.75 |
| TUNNEL PURGED | | | | | | | | | | | | | | | | | |
| 219 | .127(.05) | 0 | NOM | 7.20 | 16.97 | 9.77 | 9.28 | 10 | 5.73 | 9.45 | 5 | 10.94 | 18.0 | 36.5 | -.27 | 1.62 | 2.85 |
| TUNNEL PURGED | | | | | | | | | | | | | | | | | |
| 220 | 0 | 0 | NOM | 7.19 | 13.89 | 6.70 | 9.23 | 20 | 8.47 | 9.31 | 20 | 2.94 | 239.3 | 1286.9 | 1191.3 | 0.89 | 185.41 |
| TUNNEL PURGED | | | | | | | | | | | | | | | | | |
| 221 | 0 | 0 | NOM | 7.19 | 9.97 | 2.78 | 9.24 | 5 | 7.75 | 9.27 | 5 | 4.50 | 162.3 | 194.3 | 170.4 | 0.30 | 71.58 |
| 222 | 0 | 0 | NOM | 7.26 | 8.62 | 1.36 | 9.25 | 5 | 6.63 | 9.29 | 5 | 6.50 | 5.7 | 17.8 | -6.3 | 0.14 | 1.55 |
| 223 | 0 | 0 | NOM | 7.29 | 11.37 | 4.08 | 9.28 | 10 | 8.28 | 9.30 | 10 | 5.40 | 324.6 | 348.8 | 300.4 | 0.45 | 52.94 |
| TUNNEL PURGED | | | | | | | | | | | | | | | | | |
| 224 | .064(.025) | 0 | NOM | 7.23 | 9.94 | 2.71 | 9.39 | 5 | 4.19 | 9.42 | 5 | 4.05 | 7.2 | 19.3 | -4.6 | 0.28 | 3.09 |
| 225 | .064(.025) | 0 | NOM | 7.26 | 11.33 | 4.07 | 9.40 | 5 | 9.17 | 9.44 | 5 | 8.87 | 15.0 | 27.6 | 2.5 | 0.44 | 2.93 |
| 226 | .064(.025) | 0 | NOM | 7.26 | 12.68 | 5.42 | 9.40 | 10 | 8.38 | 9.45 | 10 | 8.25 | 9.9 | 34.8 | -15.0 | 0.62 | 1.04 |
| TUNNEL PURGED | | | | | | | | | | | | | | | | | |
| 227 | .064(.025) | 0 | NOM | 7.22 | 13.98 | 6.76 | 9.49 | 10 | 3.62 | 9.60 | 5 | 6.75 | 23.8 | 42.1 | 5.6 | 0.88 | 6.02 |
| 228 | .064(.025) | 0 | NOM | 7.26 | 10.69 | 3.43 | 9.52 | 10 | 5.77 | 9.64 | 5 | 11.27 | 7.4 | 26.2 | -11.3 | 0.35 | 1.12 |
| TUNNEL PURGED | | | | | | | | | | | | | | | | | |
| 229 | .064(.025) | 0 | B* | 1.74 | 3.15 | 1.41 | 9.72 | 2 | 1.50 | 9.84 | 2 | 1.44 | 4.4 | 23.9 | -15.4 | 0.06 | 3.12 |
| 230 | .064(.025) | 0 | B | 1.74 | 4.84 | 3.10 | 9.75 | 2 | 3.39 | 9.86 | 2 | 3.24 | 11.0 | 31.3 | -8.9 | 0.15 | 3.46 |
| 231 | .064(.025) | 0 | B | 1.74 | 6.51 | 4.77 | 9.77 | 2 | 7.20 | 9.89 | 2 | 7.05 | 6.5 | 27.3 | -14.9 | 0.28 | 0.94 |
| TUNNEL PURGED | | | | | | | | | | | | | | | | | |
| 232 | .064(.025) | 0 | B | 1.74 | 10.64 | 8.90 | 9.80 | 2 | 11.00 | 9.89 | 2 | 10.50 | 39.3 | 61.2 | 17.4 | 0.83 | 3.83 |
| TUNNEL PURGED | | | | | | | | | | | | | | | | | |
| 233 | .0254(.01) | 0 | NOM | 7.21 | 9.92 | 2.71 | 9.74 | 2 | 6.40 | 9.74 | 2 | 6.15 | 6.0 | 11.0 | 0.89 | 0.29 | 3.39 |
| 234 | .0254(.01) | 0 | NOM | 7.21 | 10.94 | 3.73 | 9.73 | 2 | 14.36 | 9.72 | 2 | 13.90 | 11.2 | 16.7 | 5.9 | 0.37 | 3.39 |
| 235 | .0254(.01) | 0 | NOM | 7.20 | 12.48 | 5.28 | 9.73 | 5 | 10.38 | 9.70 | 5 | 10.00 | 24.4 | 37.4 | 11.3 | 0.59 | 4.12 |
| TUNNEL PURGED | | | | | | | | | | | | | | | | | |
| 236 | .0254(.01) | 0 | NOM | 7.17 | 9.20 | 2.03 | 9.70 | 2 | 6.57 | 9.66 | 2 | 6.38 | 5.1 | 10.1 | 0.09 | 0.21 | 3.39 |
| 237 | .0254(.01) | 0 | NOM | 7.20 | 11.60 | 4.40 | 9.69 | 5 | 6.30 | 9.72 | 2 | 15.0 | 19.1 | 28.2 | 10.2 | 0.46 | 5.40 |
| 238 | .0254(.01) | 0 | NOM | 7.23 | 14.68 | 7.45 | TRACE NOT READABLE | | | | | | | | | 1.00 | |
| TUNNEL PURGED | | | | | | | | | | | | | | | | | |
| 239 | .0254(.01) | 0 | B | 1.73 | 6.43 | 4.70 | 6.57 | 2 | 4.32 | 7.39 | 2 | 3.52 | 23.4 | 37.8 | 8.9 | 0.27 | 9.04 |
| 240 | .0254(.01) | 0 | B | 1.74 | 10.50 | 8.76 | 6.80 | 5 | 9.60 | 7.58 | 5 | 8.08 | 100.5 | 139.3 | 61.2 | 0.82 | 6.60 |
| TUNNEL PURGED | | | | | | | | | | | | | | | | | |
| 241 | .0254(.01) | 0 | B | 1.72 | 8.64 | 6.92 | 7.66 | 5 | 3.90 | 8.20 | 2 | 7.92 | 97.1 | 125.4 | 68.2 | 0.54 | 15.03 |
| TUNNEL PURGED | | | | | | | | | | | | | | | | | |
| 242 | .0254(.01) | 0 | B | 1.71 | 12.92 | 11.21 | 8.37 | 5 | 10.40 | 8.63 | 5 | 8.84 | 267.7 | 313.9 | 221.5 | 1.25 | 14.11 |
| TUNNEL PURGED | | | | | | | | | | | | | | | | | |
| 243 | .0254(.01) | 5 | B | 1.72 | 8.67 | 6.95 | TRACE NOT READABLE | | | | | | | | | 0.53 | |
| 244 | .0254(.01) | 5 | B | 1.72 | 8.55 | 6.83 | 8.22 | 10 | 6.65 | 8.60 | 5 | 8.76 | 845.8 | 912.6 | 778.7 | 0.51 | 45.13 |
| TUNNEL PURGED | | | | | | | | | | | | | | | | | |
| 245 | .0254(.01) | 5 | B | 1.71 | 7.29 | 5.58 | 8.19 | 5 | 6.97 | 8.59 | 2 | 5.45 | 954.3 | 985.1 | 923.4 | 0.36 | 204.86 |
| TUNNEL PURGED | | | | | | | | | | | | | | | | | |
| 246 | .0254(.01) | 5 | B | 1.72 | 3.09 | 1.37 | 8.10 | 2 | 2.80 | 8.53 | 2 | 1.35 | 111.0 | 127.9 | 94.0 | 0.05 | 96.87 |
| 247 | .0254(.01) | 5 | B | 1.72 | 4.42 | 2.70 | 8.07 | 2 | 6.80 | 8.51 | 2 | 3.20 | 275.1 | 292.6 | 257.7 | 0.12 | 101.53 |
| 248 | .0254(.01) | 5 | B | 1.72 | 6.00 | 4.27 | 8.05 | 2 | 12.65 | 8.50 | 2 | 5.45 | 467.7 | 485.6 | 449.8 | 0.23 | 85.73 |
| TUNNEL PURGED | | | | | | | | | | | | | | | | | |
| 249 | .0254(.01) | 5 | NOM | 7.17 | 12.55 | 5.38 | 7.99 | 5 | 12.20 | 8.45 | 5 | 4.90 | 341.9 | 352.8 | 331.0 | 0.62 | 135.26 |
| TUNNEL PURGED | | | | | | | | | | | | | | | | | |
| 250 | .254(.10) | 5 | NOM | 7.12 | 9.97 | 2.85 | 8.02 | 2 | 4.5 | 8.45 | 2 | 4.25 | 0.44 | 4.6 | -3.8 | 0.29 | 0.50 |
| 251 | .254(.10) | 5 | NOM | 7.12 | 11.21 | 4.09 | 8.05 | 5 | 5.55 | 8.45 | 5 | 5.25 | 1.9 | 12.6 | -8.7 | 0.40 | 0.70 |
| 252 | .254(.10) | 5 | NOM | 7.11 | 14.16 | 7.05 | 8.08 | 5 | 13.30 | 8.47 | 5 | 12.59 | 5.0 | 16.5 | -6.3 | 0.91 | 0.77 |
| 253 | .254(.10) | 5 | NOM | 7.10 | 16.59 | 9.49 | 8.13 | 10 | 12.85 | 8.49 | 10 | 12.05 | 26.5 | 49.1 | 3.7 | 1.45 | 2.12 |

1 n/cm² = 9.8692 x 10⁻² atm

* defined on Figure 32

FIGURE 40

MASS FLOW RATE CALIBRATION:  METHANE
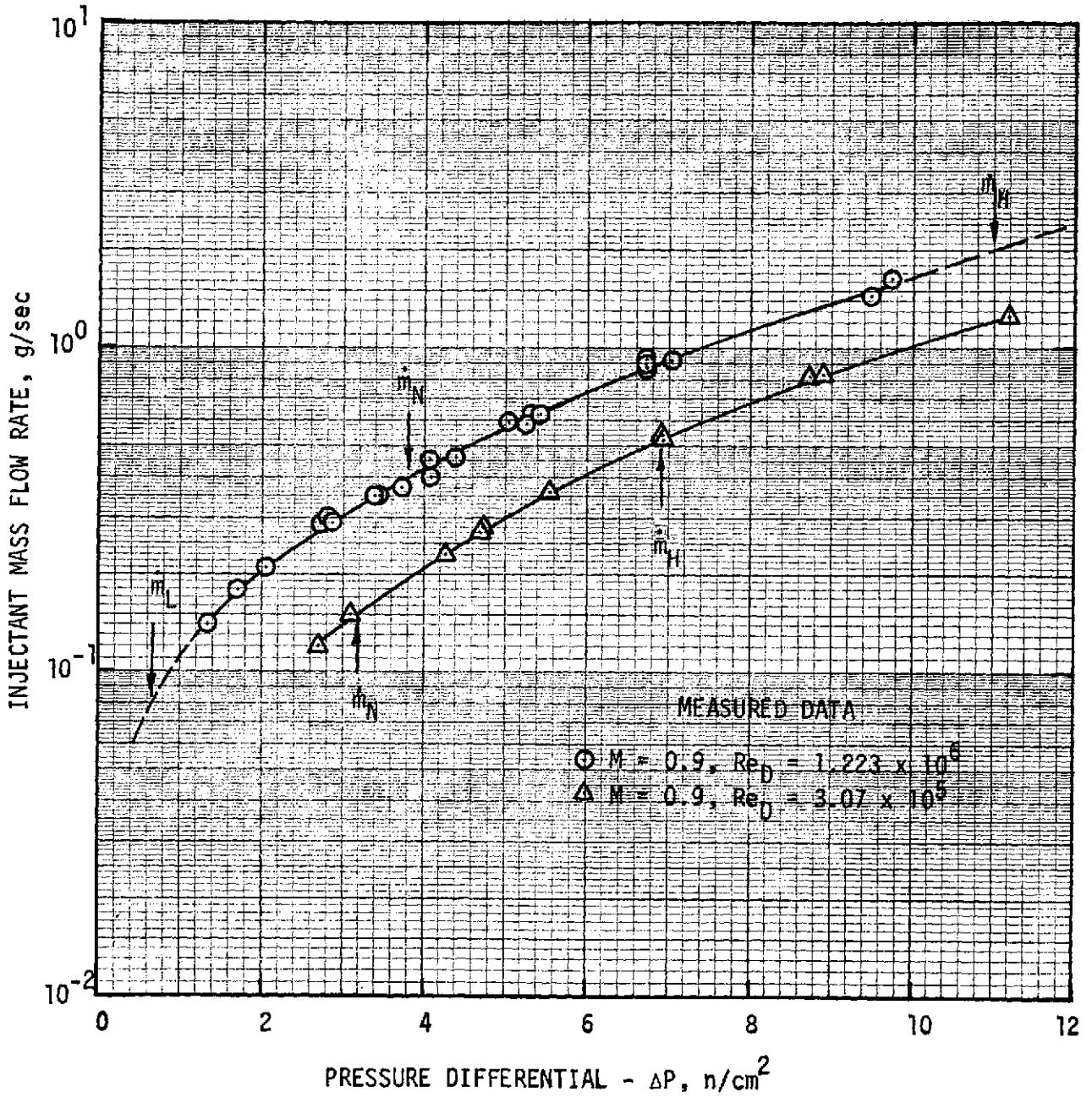


FIGURE 41

METHANE DATA

$M = 0.90$
$Re_D = 1.223 \times 10^6$
$L = 0.0$ cm
$\alpha = 0°$
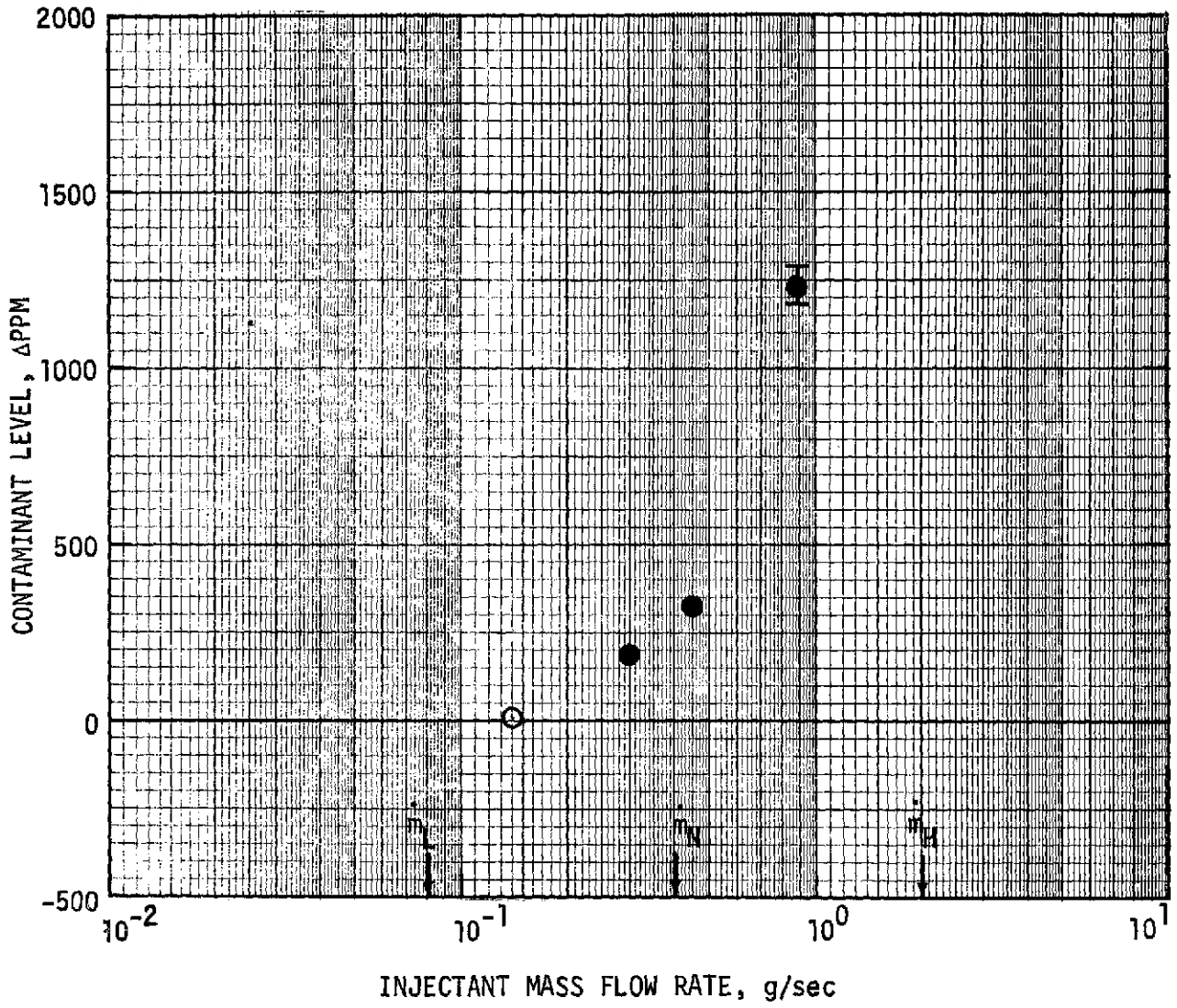
FIGURE 42

METHANE DATA

$M = 0.90$
$Re_D = 1.223 \times 10^6$
$L = 0.0254$ cm (0.01 in)
$\alpha = 0°$

FIGURE 43

57
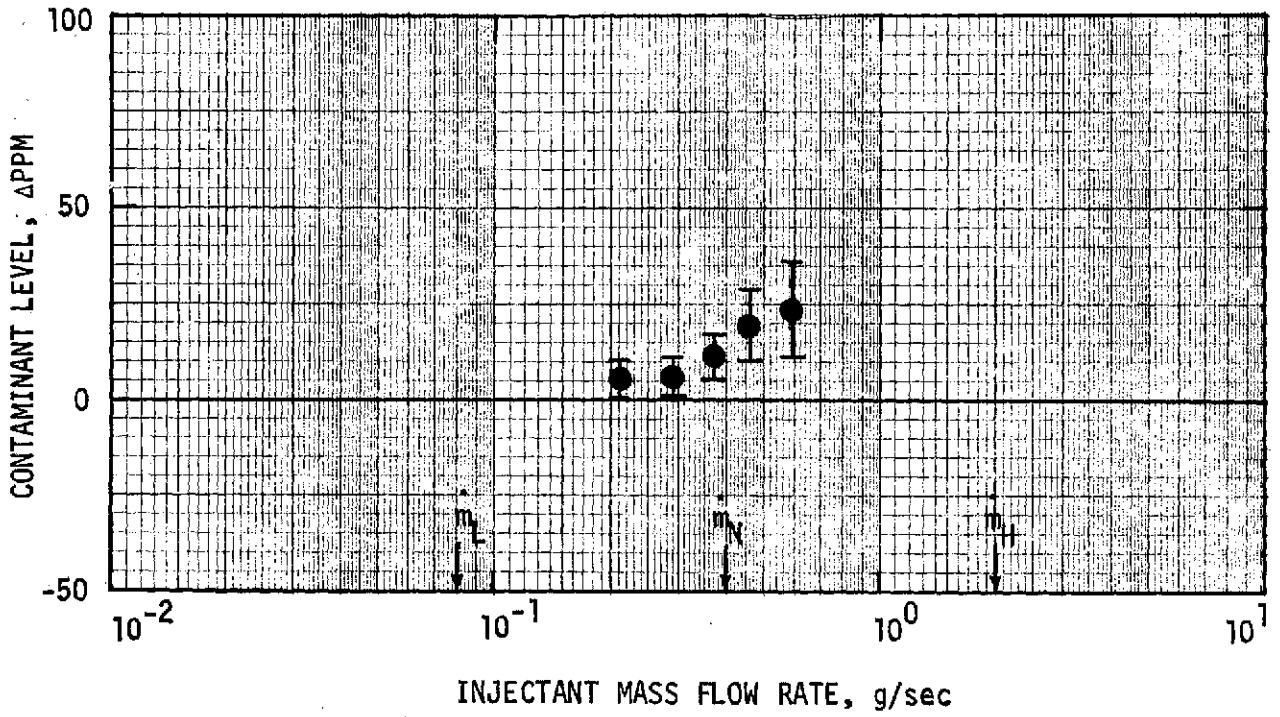
METHANE DATA

$M = 0.90$
$Re_D = 1.223 \times 10^6$
$L = 0.0635$ cm (0.025 in)
$\alpha = 0°$
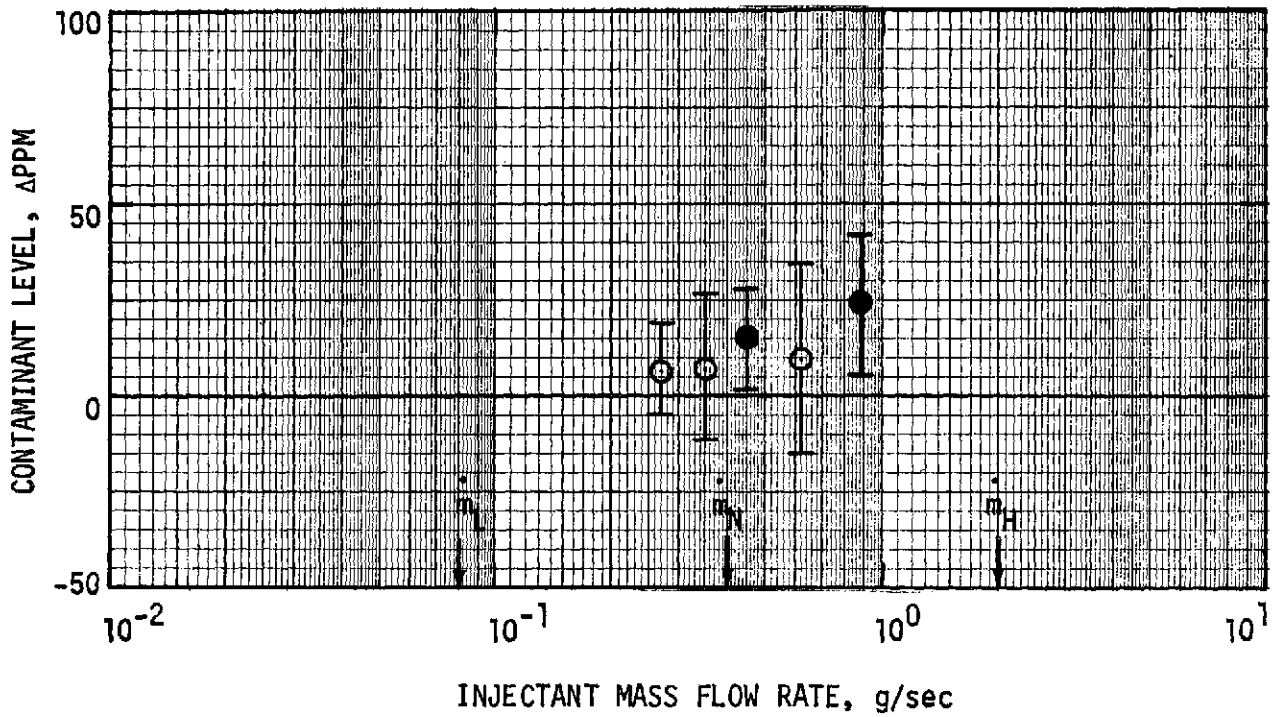
FIGURE 44

METHANE DATA

$M = 0.90$
$Re_D = 1.223 \times 10^6$
$L = 0.127$ cm (0.05 in)
$\alpha = 0°$
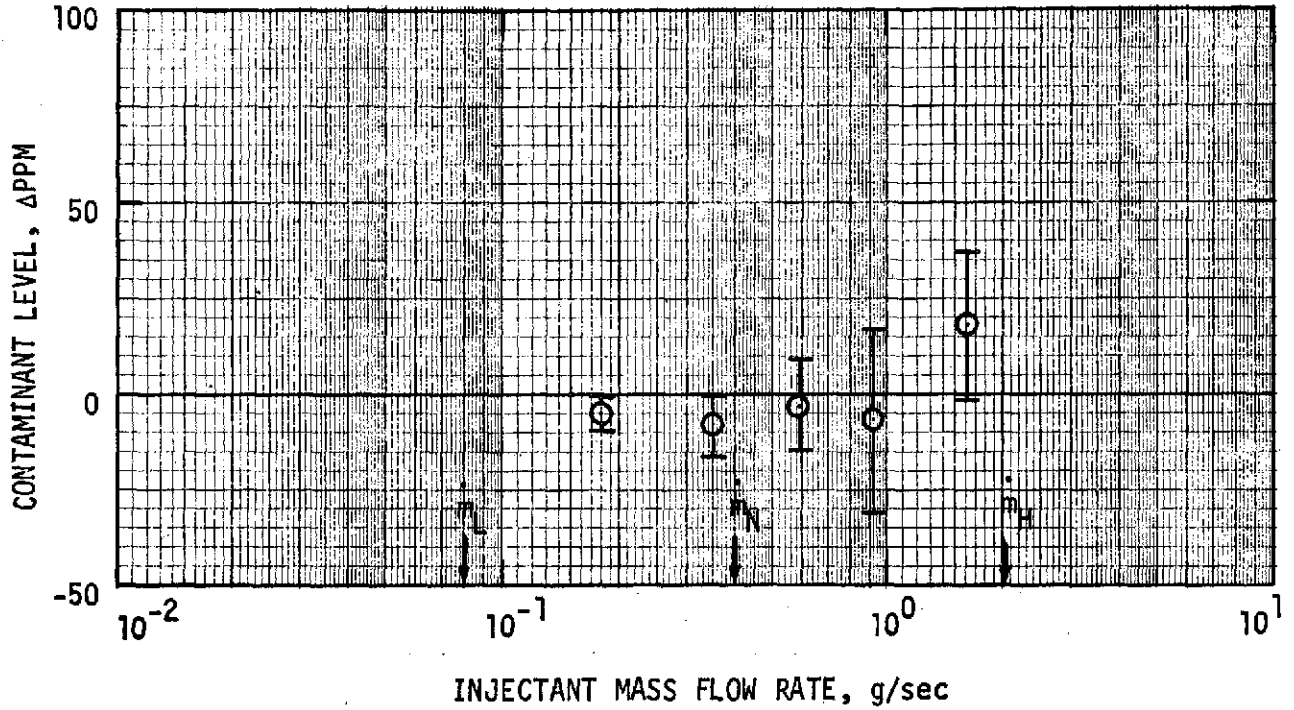


FIGURE 45

METHANE DATA

$M = 0.90$
$Re_D = 1.223 \times 10^6$
$L = 0.508$ cm (0.20 in)
$\alpha = 0°$
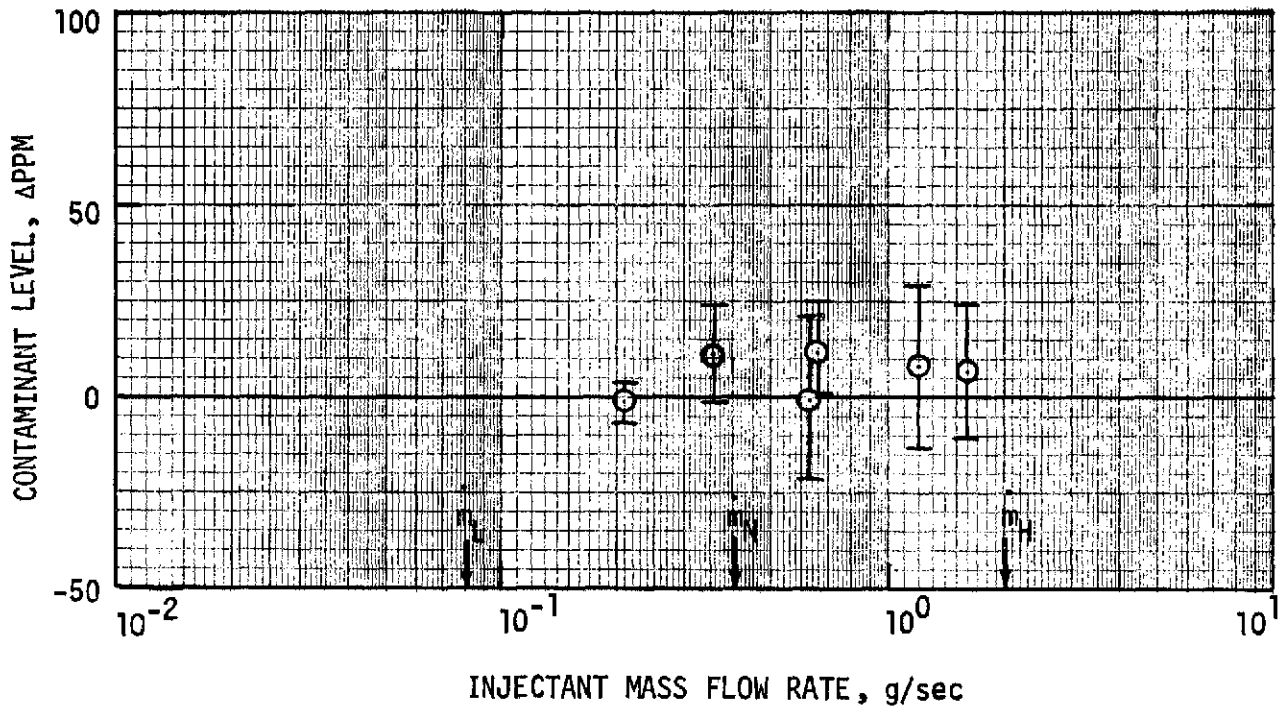


FIGURE 46

level contamination of the atmospheric sample would be unacceptable at flight conditions. A two order of magnitude reduction in the contamination level was achieved by extending the inlet tube to the edge of the velocity boundary layer (Figure 43). Note the scale change on the ordinate between Figures 42 and 43. With the sampling tube in the nondeployed position, the velocity boundary layer was calculated to be $1.5 \times 10^{-2}$ cm ($5.9 \times 10^{-3}$ in) thick in the stagnation region. At the high injectant mass flow rate, the velocity layer thickness was predicted to be nearly $3.0 \times 10^{-2}$ cm ($1.8 \times 10^{-2}$ in). The sampling tube length, for the Figure 43 data, was $2.54 \times 10^{-2}$ cm ($1 \times 10^{-2}$ in). Therefore, the results presented by Figure 43 demonstrate that extending the sampling tube to a length approximately equal to the boundary layer thickness (for a Schmidt number of approximately 1 or greater) reduces the amount of contaminant gas ingested to tens of parts per million. This sampling tube length corresponds to a full scale length in flight of 0.22 cm ($8.75 \times 10^{-2}$ in). The effect of increasing the sampling tube length, relative to the boundary layer thickness is illustrated by Figures 44, 45 and 46.

In Figures 42-46 the open symbols are used to denote that the measured contaminant level is within the experimental uncertainty band for zero contamination. The solid symbol data points note that the data is outside the uncertainty band and that sampling tube contamination is predicted. Except for the 0 and 0.0254 cm sampling tube lengths (Figures 42 and 43), the data trend (Figures 44, 45 and 46) indicates zero contamination within the experimental accuracy.

(b) <u>Methane: Angle of Attack and Off-Nominal Test Results</u> - For a sampling tube length of $2.54 \times 10^{-2}$ cm (0.01 in), the data obtained for the nominal (worst case flight) test conditions resulted in low level contamination detection above the nominal mass injection rate (Figure 43). The contamination was detected when the boundary layer thickness became greater than the sampling tube length at the high mass injection rates. The effect of the boundary layer thickness on the measured contaminant level was further investigated by doubling the boundary layer thickness in the stagnation region through decreasing the nominal tunnel Reynolds number by a factor of four. These off-nominal tunnel conditions resulted in the contaminated boundary layer completely immersing the sampling tube. Figure 47 illustrates the elevated contamination

METHANE DATA

$M = 0.90$
$Re_D = 3.07 \times 10^5$
$L = 0.0254$ cm (0.01 1n)
$\alpha = 0°$

CONTAMINANT LEVEL, $\Delta$PPM

INJECTANT MASS FLOW RATE, g/sec
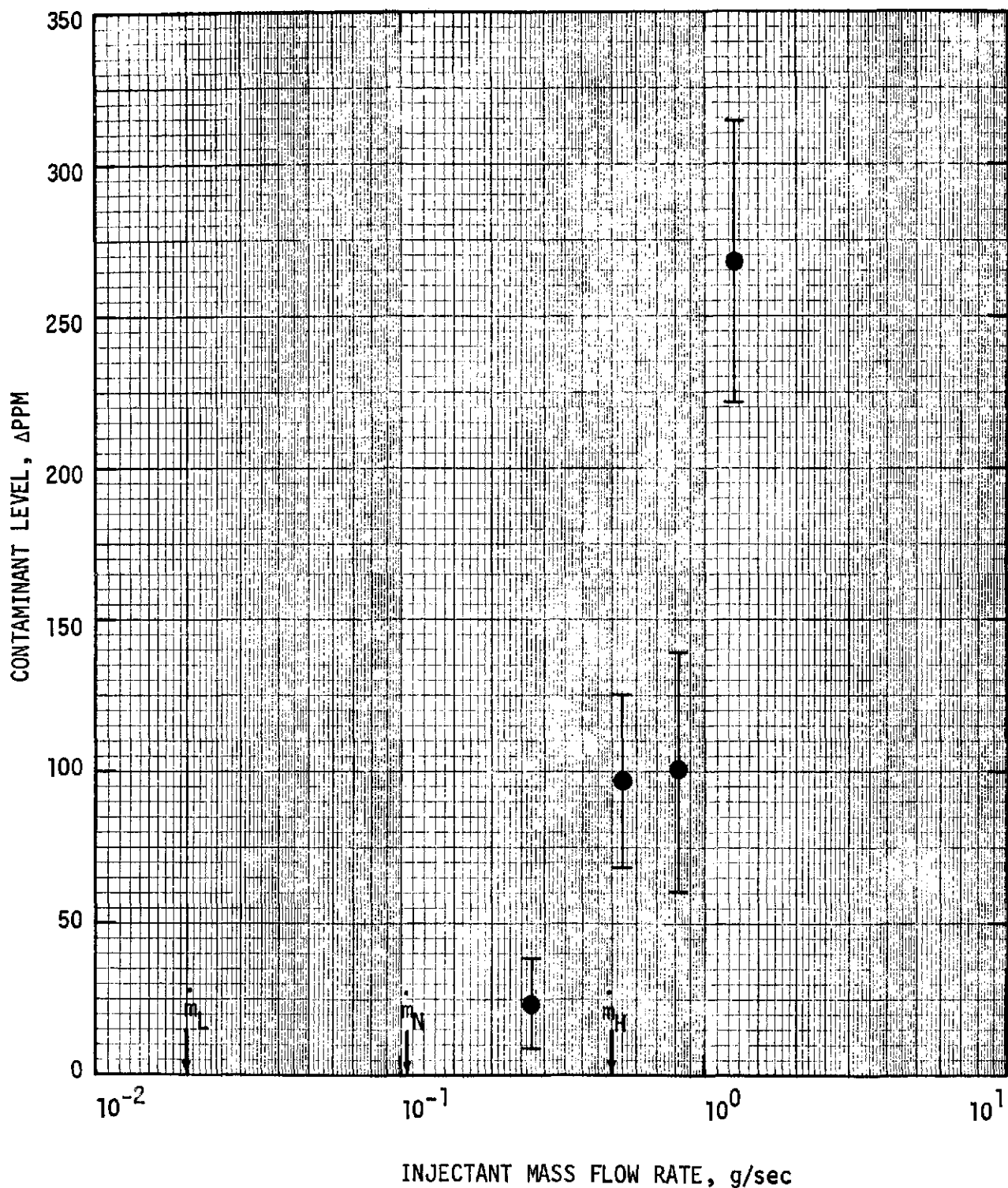
FIGURE 47

detected for the thicker contaminated boundary layer. At the same Reynolds number and sampling tube length, Figure 48 shows the effect of increasing the model angle of attack to 5°. The increase in angle of attack dips the sampling tube even further into the contaminated boundary layer and results in higher levels of contamination even at the low injectant flow rates. The solid triangle symbol on Figure 48 denotes a data point obtained at the nominal test Reynolds number condition. This higher Reynolds number results in a thinner boundary layer but still maintains the sampling tube within the viscous contamination layer. The result is a decrease in the contamination level detected at the sampling tube. Although this data point shows an appreciable decrease in contamination from the low Reynolds number results, the absolute level is still significant. The contamination can be eliminated by increasing the sampling tube length beyond the edge of the contaminant layer for an angle of attack of 5° (illustrated by Figure 49). This figure shows that increasing the sampling tube length to approximately 50% of the baseline design length for flight reduces the potential for contamination to zero, except possibly at the high mass blowing rates. The dramatic reduction in contamination, compared to the $L = 0.0254$ cm results at 5° angle of attack, is attributed to the sampling tube length being greater than the contaminant layer thickness. The importance of the relation between sampling tube length and boundary layer thickness is amplified by Figure 50. These data were obtained at zero angle of attack for the low Reynolds number condition using a sampling tube length of $6.35 \times 10^{-2}$ cm (0.025 in). Unlike the $L = 2.54 \times 10^{-2}$ cm data of Figure 47, the sampling tube length is greater than the boundary layer thickness and the results indicate zero contamination over a wider range of mass injection rates.

(c) Methane: Accuracy of Test Measurements - The methane test series resulted in lower experimental uncertainties than the Freon 114 tests (Appendix B). Due to this improved accuracy, data were obtained to determine the ratio of sampling tube length to boundary layer thickness which resulted in zero contamination. The conclusion was that sampling tube lengths which extend beyond the boundary layer edge ensured that the ingested gas sample was free of the contaminated pyrolysis gases from the heatshield. Figure 51 summarizes the methane test data obtained for sampling tube lengths which extend beyond

METHANE DATA

M = 0.90
$Re_D$ = 3.07 x $10^5$
L = 0.0254 cm (0.01 in)
$\alpha$ = 5°
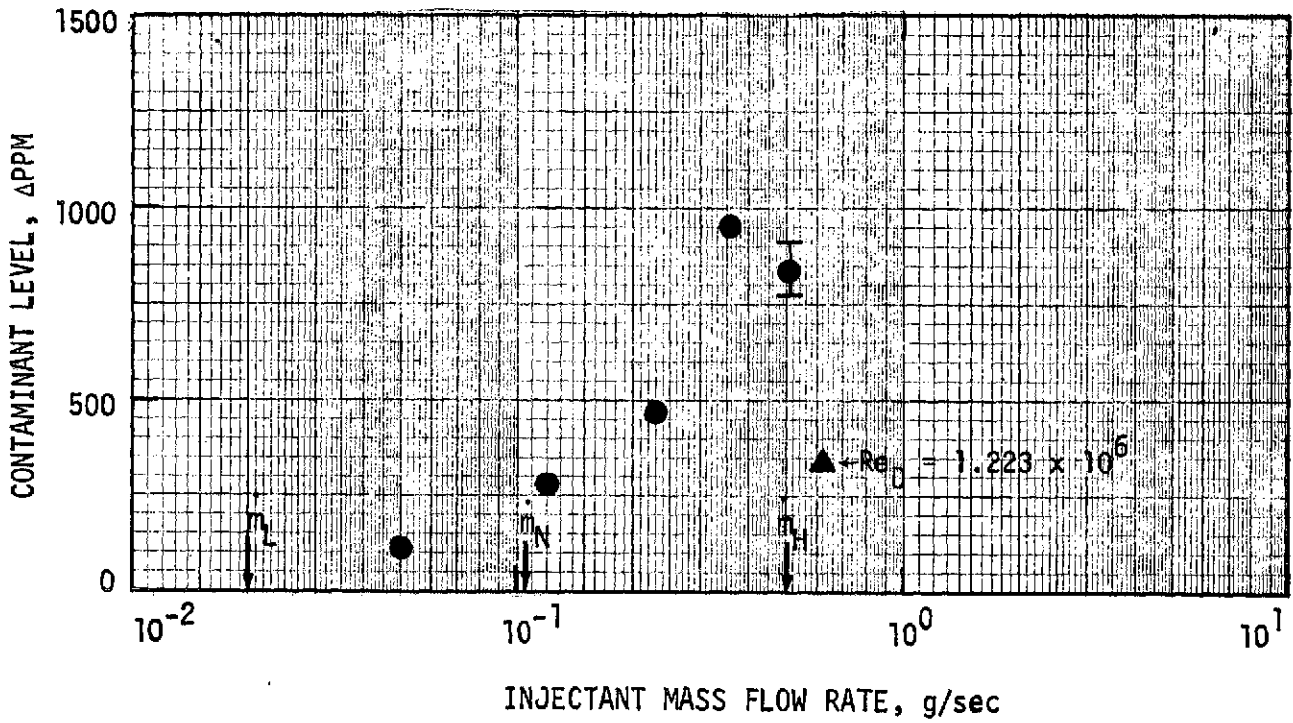


FIGURE 48

METHANE DATA

$$M = 0.90$$
$$Re_D = 1.223 \times 10^6$$
$$L = 0.254 \text{ cm} (0.10 \text{ in})$$
$$\alpha = 5°$$

CONTAMINANT LEVEL, $\Delta$PPM

100

50

0

-50

$\dot{m}_L$      $\dot{m}_N$      $\dot{m}_H$

$10^{-2}$      $10^{-1}$      $10^0$      $10^1$

INJECTANT MASS FLOW RATE, g/sec
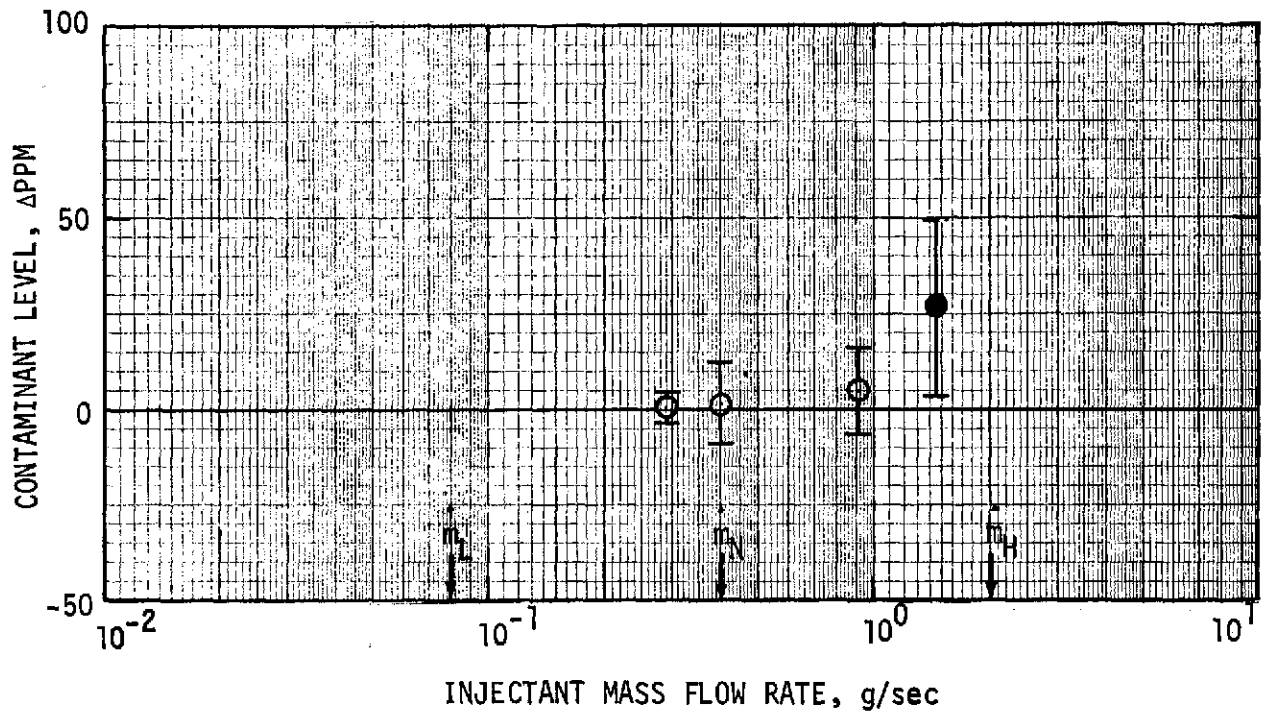
FIGURE 49

METHANE DATA

$M = 0.90$
$Re_D = 3.07 \times 10^5$
$L = 0.0635$ cm (0.025 in)
$\alpha = 0°$
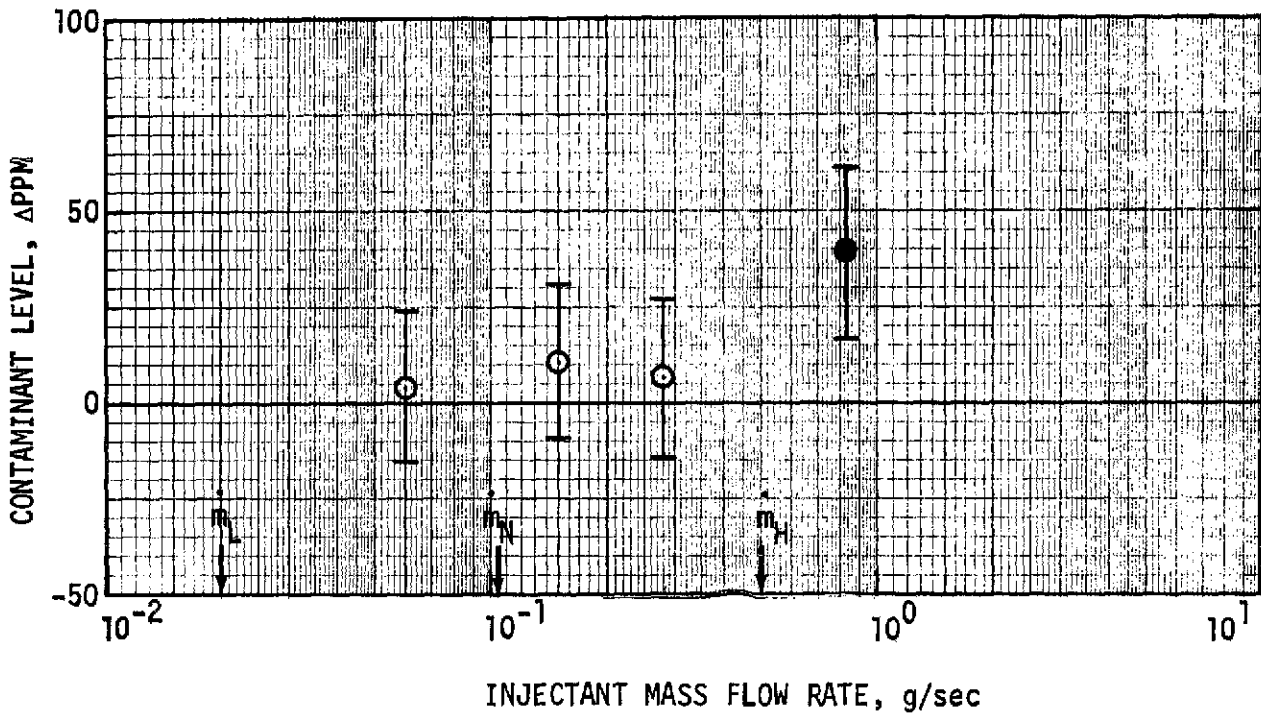
FIGURE 50

METHANE DATA: ERROR ANALYSIS SUMMARY

⊙ L = 0.508 cm
◇ L = 0.127 cm
⊡ L = 0.0635 cm
▷ L = 0.254 cm, α = 5°
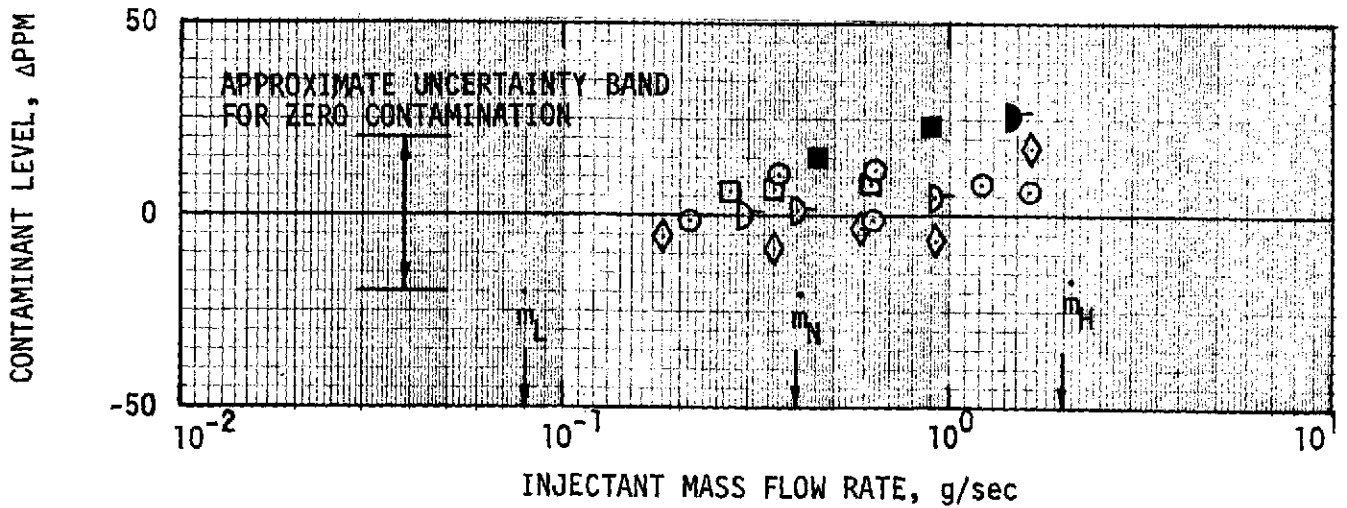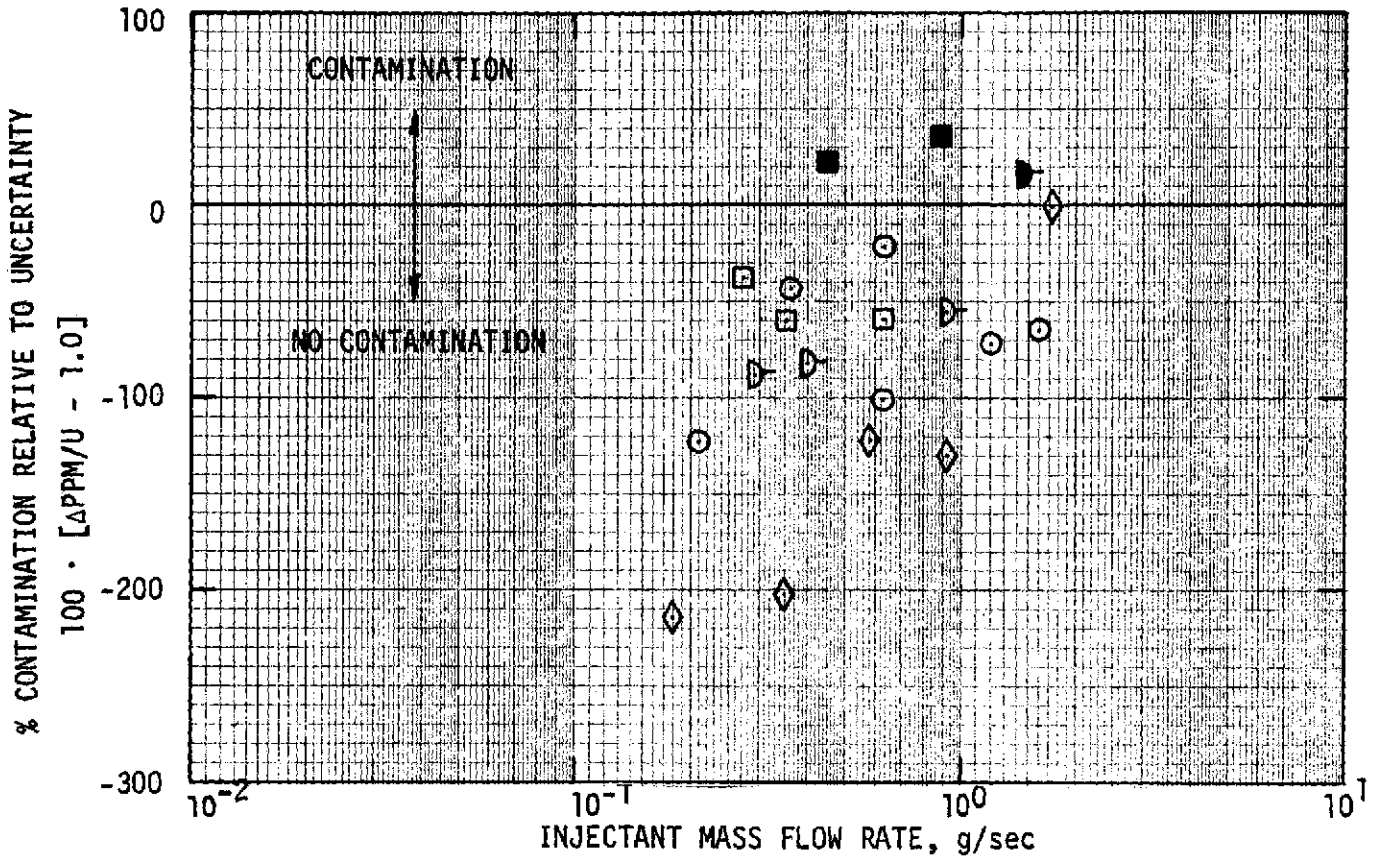
FIGURE 51

the boundary layer edge for the complete range of mass flow rates considered. From Appendix B, the uncertainty in a zero contaminant measurement depends upon the background contaminant level, the chromatogram amplitude accuracy and the uncertainty in the detector calibration as follows:

$$U = \left\{ \pm\, Y(\frac{1}{\lambda_{ST}} + \frac{1}{\lambda_{BP}}) \pm 2X + XY\,(\frac{1}{\lambda_{ST}} - \frac{1}{\lambda_{BP}}) \right\}\ PPM_{BP}$$

where,

$U$ = uncertainty about zero contamination, ppm

$PPM_{BP}$ = background probe contaminant level, ppm

$\lambda_{ST}$ = peak amplitude of sampling tube (ST) chromatogram trace, cm

$\lambda_{BP}$ = peak amplitude of background probe (BP) chromatogram trace, cm

$X$ = calibration factor uncertainty

$Y$ = trace amplitude measurement uncertainty, cm

Thus, the percent contamination relative to the actual uncertainty can be determined from:

$$100 \cdot (\frac{\Delta PPM}{PPM_{BP}} - \frac{U}{PPM_{BP}})/\frac{U}{PPM_{BP}}$$

or

$$100 \cdot (\frac{\Delta PPM}{U} - 1)$$

The solid symbols of Figure 51 denote that the measured contaminate level exceeded the experimental uncertainty and therefore, indicate contamination. The twenty (20) open symbol data points reflect no contamination since their magnitude is within the calculated uncertainty band for zero contamination. From these data it is concluded that the contamination level is zero, within the experimental accuracy, for sampling tube lengths which extend beyond the boundary layer edge. The magnitude of the contaminant level which approximately defines the uncertainty band about zero is $\pm 20$ ppm.

The methane test results indicate that the selected sampling tube length for flight must always be beyond the stagnation region boundary layer edge to avoid heatshield contamination. Furthermore, when compared with the Freon 114 results, these results illustrate the high quality of the methane data in defining potential contamination levels. The experimental uncertainties associated with the methane studies are approximately $\pm 20$ ppm.

# SUMMARY OF RESULTS

The worst case flight conditions, for potential heatshield contamination of atmospheric samples, were scaled in a transonic wind tunnel test program by matching the flight values of Mach number, Reynolds number and ratio of injectant to free stream momentum. The flight trajectory point which corresponded to the greatest potential for an outgassing contaminant being ingested by the atmospheric sampling tube was defined as the worst case. This point was selected from a matrix of trajectory data for steep and shallow entries into the model atmospheres of Saturn, Uranus and Jupiter. The wind tunnel conditions and test injectant properties were scaled from the worst case flight conditions. A 10.16 cm (4 in) diameter scale model was used in the NASA/ARC 2' x 2' transonic test facility to match the flight Reynolds number. A trace, or contaminant, gas was injected through the model forebody to simulate the flight outgassing. Boundary layer calculations were performed to demonstrate that the selected scaling parameters resulted in a match of the contaminant gas mass fraction at the boundary layer edge for flight and test conditions. These calculations illustrated that the criterion (matching the flight and test contaminant gas mass fraction at the boundary layer edge) for scaling the momentum ratio could be met with any molecular weight injectant gas by adjusting its injectant velocity. Therefore, two gases were used in the test program: (1) Freon 114, to approximate the flight ratio of injected gas to free stream gas molecular weight and (2) methane, to provide the lowest experimental uncertainty in determination of the absolute contamination level.

Selected results from the Freon 114 test series are summarized by Figure 52. The experimental error was determined to be $\pm 50$ ppm and measurements exceeding the uncertainty indicate contamination (solid symbols on figure). The magnitude of the uncertainty results from the contaminant level being determined from the difference of two large numbers (sampling tube and tunnel) background contamination) each containing random experimental errors. For the Freon 114 test series conducted at the nominal tunnel conditions (worst case flight conditions), the sampling tube was always extended well beyond the edge of the boundary layer and the resulting contaminant data indicates experimental scatter about zero. It was concluded that within the experimental uncertainty of the test, the absolute contaminant level was

# FREON 114:  DATA SUMMARY

FREON 114 DATA

$M = 0.90$
$Re_D = 1.223 \times 10^6$
$L = 0.508$ cm (0.20 in)
$\alpha = 0°$
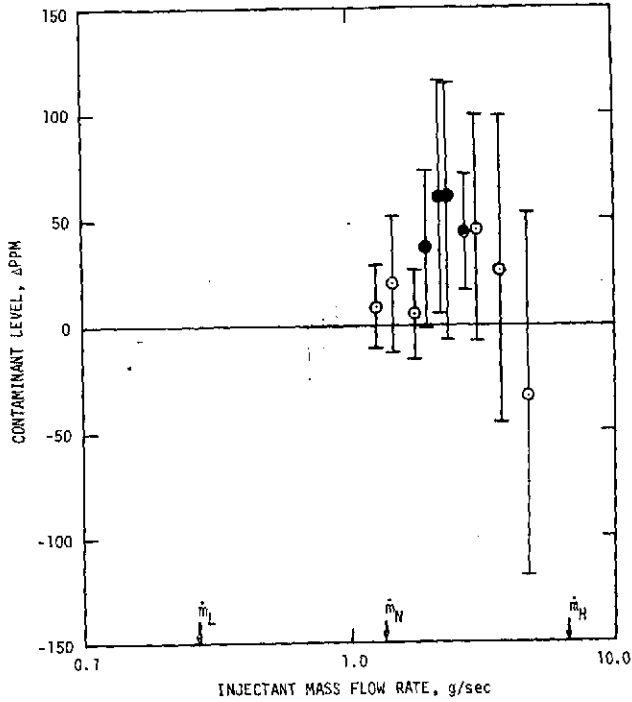
FREON 114 DATA

$M = 0.90$
$Re_D = 1.223 \times 10^6$
$L = 0.762$ cm (0.30 in)
$\alpha = 0°$

(a)  L >> δ

(c)  L >> δ
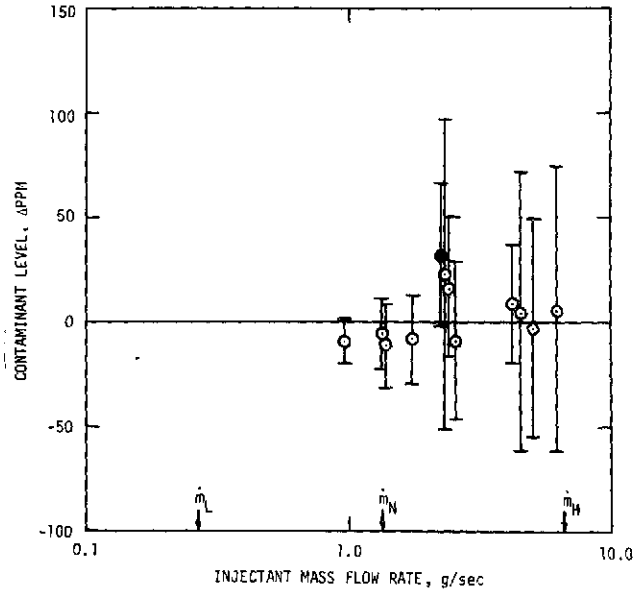
FREON 114 DATA

$M = 0.90$
$Re_D = 1.223 \times 10^6$
$L = 0.635$ cm (0.25 in)
$\alpha = 0°$
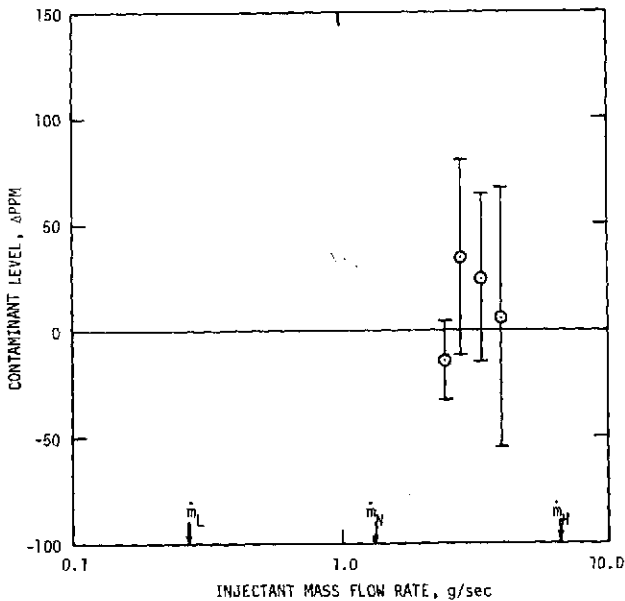
FREON 114 DATA

$M = 0.61$
$Re_D = 2.16 \times 10^6$
$L = 0.508$ cm (0.20 in)
$\alpha = 0°$

(b)  L >> δ
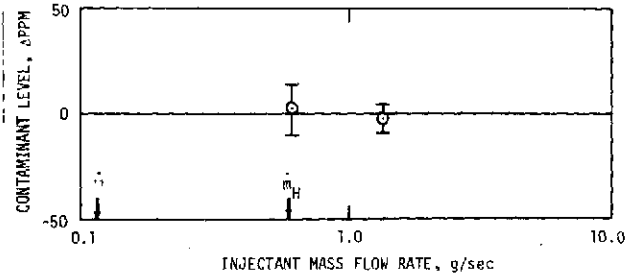
(d) OFF-NOMINAL $Re_D$

FIGURE 52

zero.  The atmospheric models for Saturn, Uranus and Jupiter (References 4, 5 and 6) indicate that the minimum primary trace species abundance is 40 ppm (other undefined species account for 50-650 ppm).  Thus, the experimental data for Freon 114 injection show that the contaminate level is less than 50 ppm while the atmospheric models result in primary trace species concentration of similar value.  The methane results significantly decrease the test uncertainty and result in more definitive conclusions.

The off-nominal Freon 114 data illustrate the effect of delaying the initiation of atmospheric sample acquisition by 75 seconds (Figure 52d).  At these flight conditions, the ablator mass flow rate has decreased by two orders of magnitude from its value at sampling tube deployment.  The combined effect of the decreased outgassing rate (lower test injectant mass flow rates and less contaminant in background) and higher Reynolds number (samples obtained at higher pressures) substantially improve the experimental measurement accuracy.  For these test conditions, the observed contaminant level is $0 \pm 15$ ppm.  Clearly, delaying initial sampling acquisition should be considered as a means of increasing confidence in obtaining a noncontaminated atmospheric sample.

Figure 53 summarizes selected results obtained from the methane injection test series.  These datawere obtained at the nominal test conditions (which simulate the worst case for flight) and zero angle of attack.  Due to the improved measurement sensitivity for the methane tests, data trends were obtained for sampling tube lengths less than, equal to, and greater than the stagnation region boundary layer thickness.  The L=0 results (sampling tube length much less than boundary layer thickness) dramatically illustrate the high level contamination associated with the absence of an extending lip on the sampling tube.  At L = 0.0254 cm (0.01 in.) the theoretical boundary layer thickness is one-half the sampling tube length for no injection and slightly greater than the sampling tube length for the high mass flow rates.  The experimental results, for this sampling tube length, predict increasing contamination with increasing mass flow rate.  The results obtained for cases when the sampling tube length was greater than the boundary layer thickness (L = 0.127 cm and L = 0.608 cm) indicate absolute contaminant levels of $0 \pm 20$ ppm.  The $\pm$ 20 ppm reflects the random errors associated with measuring

# METHANE: DATA SUMMARY

METHANE DATA

M   = 0.90
Re$_0$ = 1.223 x 10$^6$
L   = 0.0 cm
α   = 0°
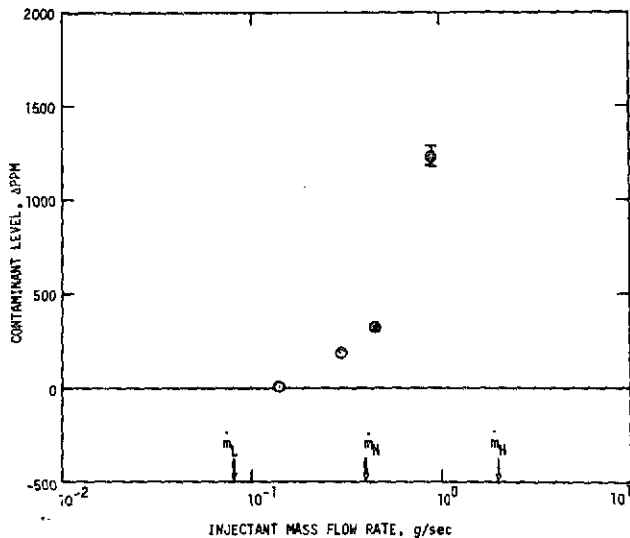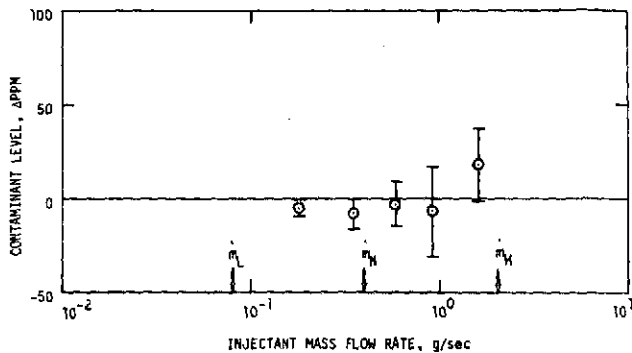
CONTAMINANT LEVEL, ΔPPM

INJECTANT MASS FLOW RATE, g/sec

(a)  L << δ

METHANE DATA

M   = 0.90
Re$_0$ = 1.223 x 10$^6$
L   = 0.127 cm (0.05 in)
α   = 0°

CONTAMINANT LEVEL, ΔPPM

INJECTANT MASS FLOW RATE, g/sec

(c)  L > δ

METHANE DATA

M   = 0.90
Re$_0$ = 1.223 x 10$^6$
L   = 0.0254 cm (0.01 in)
α   = 0°

CONTAMINANT LEVEL, ΔPPM

INJECTANT MASS FLOW RATE, g/sec

(b)  L ≅ δ

METHANE DATA

M   = 0.90
Re$_0$ = 1.223 x 10$^6$
L   = 0.508 cm (0.20 in)
α   = 0°

CONTAMINANT LEVEL, ΔPPM

INJECTANT MASS FLOW RATE, g/sec

(d)  L >> δ

FIGURE 53

72
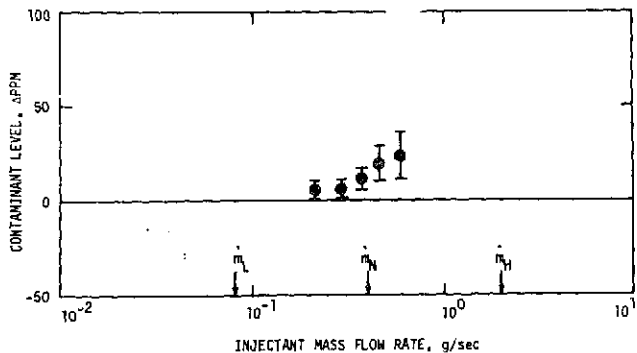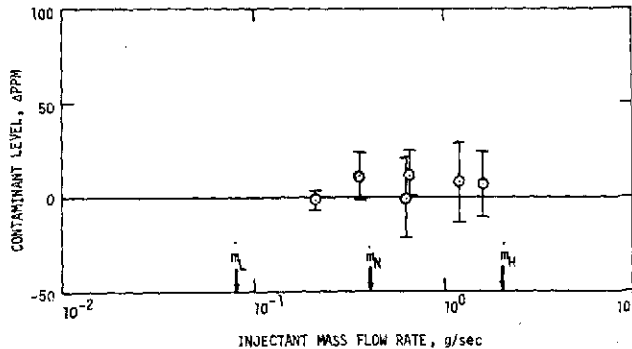
and subtracting the sampling tube and background contamination level.

An off-nominal, low Reynolds number tunnel condition was included in the test matrix to provide contaminant data for a thicker boundary layer. For the off-nominal Reynolds number, the boundary layer thickness is greater than the sampling tube length of 0.025 cm (0.01 in). The data presented by Figure 54a indicate significant contamination at 5° angle of attack for the thick boundary layer (low Reynolds number). An appreciable reduction in contamination is observed at the same sampling tube length and angle of attack for the thinner boundary layer obtained at the nominal Reynolds number (solid symbol data point on Figure 54a). Increasing the sampling tube length to 0.254 cm (0.10 in) at 5° angle of attack eliminates the contamination except possibly at the high mass flow rates. These angle of attack results again demonstrate the importance of ensuring that the atmospheric gas sampling tube is extended beyond the edge of the boundary layer.

Figure 55 pictorially summarizes the results obtained in the experiment. The role of the boundary layer thickness in the inlet region is clear from the observed data trend; the deeper the sampling tube is immersed in the viscous contaminant layer the higher the measured contamination. To avoid contamination of the atmospheric gas sample by outgassing products, the sampling tube must be extended beyond the boundary layer edge. Data obtained for these conditions indicate zero contamination within the experimental uncertainty of 20 ppm. The baseline design for flight (Reference 1) has a sampling tube length which is nominally 10 times the stagnation region boundary layer thickness.

METHANE: DATA SUMMARY FOR $\alpha \neq 0$

$M = 0.90$
$Re_D = 3.07 \times 10^5$
$L = 0.025$ cm (0.01 in)
$\alpha = 5°$

(a) $L < \delta$

$M = 0.90$
$Re_D = 1.223 \times 10^6$
$L = 0.254$ cm (0.10 in)
$\alpha = 5°$

(b) $L > \delta$
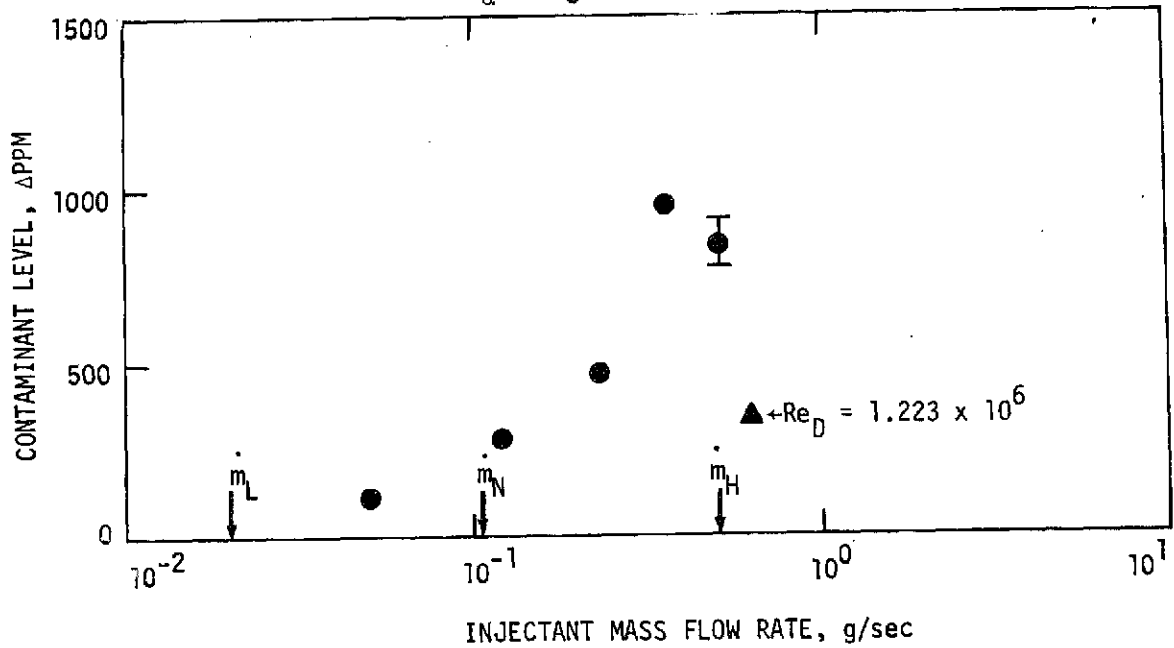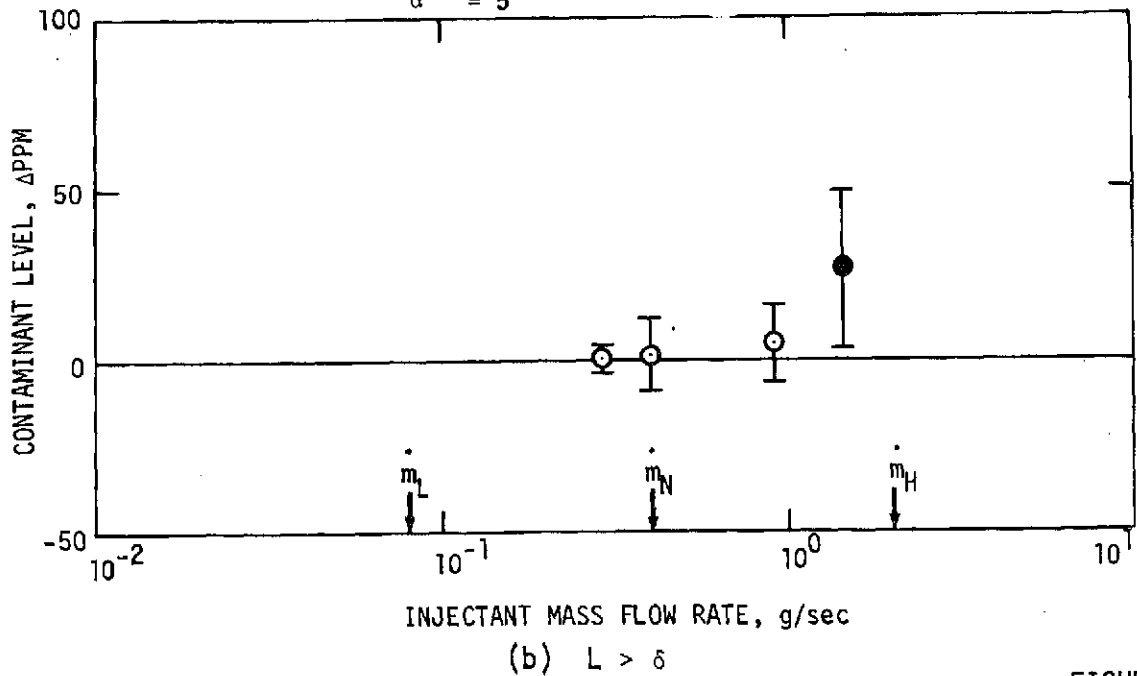
FIGURE 54

# GENERALIZED RESULTS OF EXPERIMENT
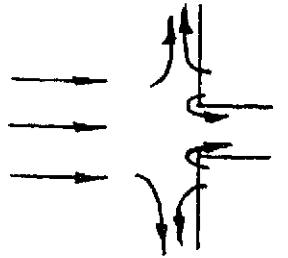
$L << \delta$
HIGH CONTAMINATION
(500 - 1000 PPM)
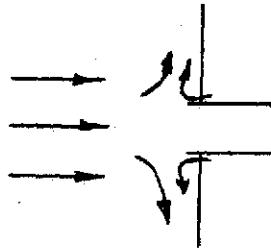
$L \sim \delta$
LOW CONTAMINATION
(0 - 40 PPM)
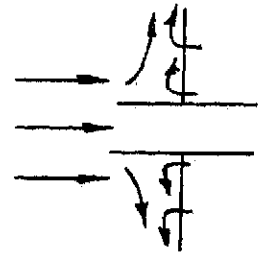
$L >> \delta$
NO CONTAMINATION
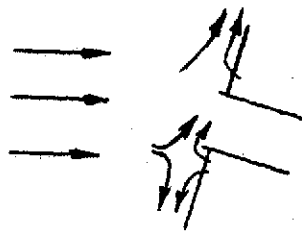
$\alpha \neq 0$
$L \sim \delta$
HIGH CONTAMINATION
($\sim$500 PPM)
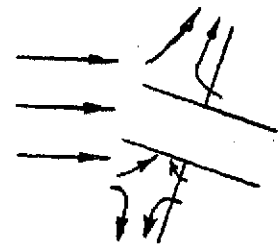
$\alpha \neq 0$
$L >> \delta$
NO CONTAMINATION

FIGURE 55

# CONCLUSIONS

The test evaluation results reveal, in general, that:

1. The retension of the charred heatshield and the baseline atmospheric sampling concept (Reference 1) are compatible with obtaining non-contaminated atmospheric samples. The experimental results indicate that the contaminant level, for the worst case flight conditions for potential contamination, is zero within the experimental uncertainty (20 ppm) of the test.

2. Increasing the sampling tube length so that it extends beyond the viscous boundary layer eliminates within the test uncertainty, contamination of the atmospheric sample. Sampling tube lengths less than the boundary layer thickness clearly result in sample contamination. The flight baseline sampling tube length of approximately 5.0 cm is acceptable based on the current test results.

3. Delaying the initial atmospheric sample acquisition time progressively increases the confidence in obtaining a noncontaminated sample. The potential for heatshield contamination is a maximum at the baseline instrument deployment conditions. Once atmospheric sampling is initiated, the contamination potential continually reduces due to the rapidly decreasing ablator mass flow rate. Test results at tunnel conditions corresponding to the flight trajectory conditions at 75 seconds after instrument deployment indicated that the contaminant level was $0 \pm 15$ ppm.

4. The potential for contamination increases with angle of attack. A six-degree-of-freedom motion analysis for a Jupiter mission indicated that the probe angle of attack at deployment was a minimum when the atmosphere was initially encountered at zero angle of attack.

PRECEDING PAGE BLANK NOT FILMED

# REFERENCES

1. Saturn/Uranus Atmospheric Entry Probe (Contract NAS2-7328), Part II: Technical Discussion, MDC Report E0870, July 1973.

2. DeFrees, R. E., Atmospheric Entry Probes for Outer Planet Exploration - A Technical Review and Summary, NASA CR 137542, August 1974.

3. Pioneer Jupiter Orbiter Probe Mission (1980) - Probe Description, NASA CR 137591, November 1974.

4. The Planet Saturn (1970), NASA SP-8091, June 1972.

5. The Planets Uranus, Neptune and Pluto (1971), NASA SP-8103, November 1972.

6. The Planet Jupiter (1970), NASA SP-8069, December 1971.

7. Fivel, H. J., Analytical Comparison of Hypersonic Flight and Wind Tunnel Viscous/Inviscid Flow Fields - Check Case and Users' Manual, NASA CR-132359, July 1973.

8. Bartlett, E. P., et al, Improved Heat-Shield Design Procedures for Manned Entry Systems, Part II - Application to Apollo, Aerotherm Report No. 70-15, June 1970.

9. Mezines, S. A., and Rusert, E. L., MDAC Multi-Step Carbon Phenolic Verification Tests at NASA-Ames Convective/Radiative ARC Facility, MDAC Design Note: OPP-28, January 1975.

## ACKNOWLEDGEMENTS

## SYMBOLS AND NOTATION

<u>SYMBOLS</u>

| | |
|---|---|
| A | Amplification factor |
| B' | Laminar blowing rate parameter |
| $(CClF_2)_2$ | Freon 114 |
| $C_4F_8$ | Freon C-318 |
| CF | Calibration factor |
| $CH_4$ | Methane |
| D | Diameter of entry probe or model |
| G.C. | Gas chromatograph |
| He | Helium |
| $H_2$ | Hydrogen |
| I | Momentum |
| L | Sampling tube length |
| $\dot{m}$ | Mass injectant rate |
| $\hat{\dot{m}}$ | Mass injectant rate per unit area |
| M | Mach number |
| p | Pressure |
| PPM | Volumetric parts per million |
| Re | Reynolds number |
| $R_o$ | Universal Gas Constant |
| S | Surface distance from stagnation point |
| S* | Nondimensionalized surface distance |
| Sc | Schmidt number |
| T | Temperature |
| U | Measurement uncertainty |
| U or V | Velocity |

# SYMBOLS AND NOTATION

| | |
|---|---|
| $y$ | Distance normal to wall |
| $\alpha$ | Angle of attack |
| $\gamma$ | Specific heat ratio |
| $\delta$ | Boundary or velocity layer thickness |
| $\Delta$ | Differential value |
| $\Theta$ | Momentum thickness |
| $\lambda$ | Amplitude of chromatogram |
| $\mu$ | Viscosity |
| $\bar{\mu}$ | Molecular weight |
| $\rho$ | Density |
| $\sigma$ | Porosity |
| $\chi$ | Mass fraction |
| $\omega$ | Mole fraction |

## SUBSCRIPTS

| | |
|---|---|
| BL | Boundary Layer |
| BP | Background Probe |
| c | Concentration layer |
| c | Chromatograph |
| D | Probe or model diameter |
| e | Edge of boundary layer |
| F | Flight |
| i | Injectant |
| (L,H,N) | Low, high and nominal |
| mix | Mixture |
| PL | Plenum value, with injection |

## SYMBOLS AND NOTATION

| | |
|---|---|
| $PL_o$ | Plenum value, without injection |
| ST | Sampling tube |
| T | Test condition |
| T | Total value |
| W | Wall value |
| $\infty$ | Free stream condition |

# APPENDIX A

## WALL POROSITY

The porosity, $\sigma$, of the charred surface in flight and the sintered metal surface of the model used in the experiment determine the injectant velocity at specified wall conditions and the injectant mass flow rates.

The sintering process used in the experimental model fabrication results in a porous material at a pre-selected porosity. The permeability of the material determines its resistance to the passage of specific injectant gases. In the model fabrication, the particle size of the powdered metal used in the sintering process was selected to provide a specified permeability. The resulting ratio of void volume to total volume within the porous structure, or the porosity of the material, is 0.45.

The porosity of the carbon phenolic heat shield depends on the heat pulse encountered during atmospheric entry. Figure A-1 provides photomicrographs of a charred and uncharred carbon phenolic heatshield specimen. The samples were obtained from a 1/4 scale heatshield which was fabricated to demonstrate the feasibility of the MDAC-E proposed fabrication technique for the full scale Outer Planet Probe's heatshield (Reference 9). Although an accurate measurement of the porosity from the photomicrograph was not made, it is estimated that the void area is approximately 40% of the total area. A theoretical calculation of the in depth char porosity indicated that $\sigma = 0.20$. Near the surface the porosity increased to 0.40 due to surface reactions and sublimation. Based on the available data, it is assumed that the porosities of the charred heatshield and the sintered metal model forebody are approximately equal.

# PHOTOMICROGRAPHS OF VIRGIN AND CHARRED CARBON PHENOLIC
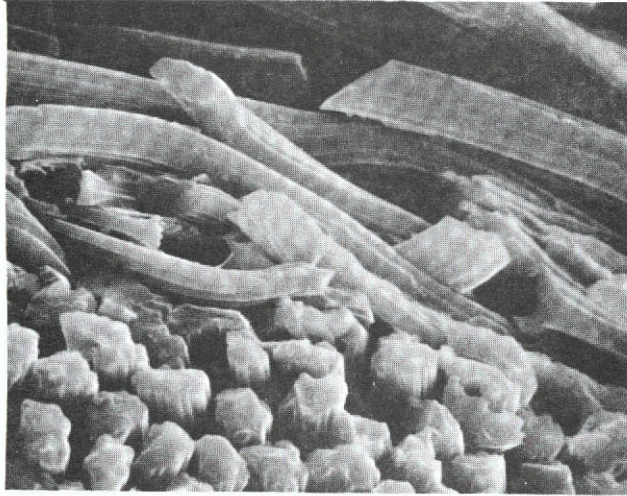


1/4–20 CHARRED LAYER 1000X



1/4–20 UNCHARRED LAYER 1000X

FIGURE A-1

# APPENDIX B

## DATA REDUCTION AND TEST UNCERTAINTIES

A variety of possible systematic and random errors were encountered in the experimental test program. The actual scope of the study and the level of accuracy anticipated,however, preclude an elaborate accounting of all errors in the determination of the experimental uncertainty. Random errors included in the prediction of test uncertainties consist of the uncertainty in the knowledge of the gas chromatograph detector calibration factor and the uncertainty in reading the amplitude peak of the chromatogram. Systematic errors, such as the accuracy of the absolute contamination introduced in preparing the standards for detector calibration and the difference in volume of the twin sampling loops, are shown to be much smaller than the random errors and are not included in the reported test uncertainties. The following paragraphs discuss the primary sources of error and the data reduction equations.

The absolute concentration of the reference standards used in detector calibration was expressed in volumetric parts per million and the standards were prepared by repeated volumetric dilution. Experience indicates that, with proper precautions and care, the uncertainty in the specified trace concentration is less than 2% of value. Since this is a systematic error which affects both of the gas chromatograph channels in the same direction, any resulting uncertainty in the measurement of the difference between the sampling tube and background contamination would be relatively small. Although a 2% uncertainty may be present in the specified value of the standard, the effect is an insignificant value, compared to random error affects, in the absolute differential in contamination. The systematic errors due to the volume differences in the sampling loops are also small. The remaining paragraphs describe the experimental uncertainties encountered for the Freon 114 and methane test series due to random errors.

Freon 114 - The peak-top noise in the Freon peaks broadened the peak making it difficult to read the amplitude of the chromatogram with high confidence. The uncertainty in reading the trace amplitudes was different for each channel of the gas chromatograph as illustrated by the actual chromatograms shown by

Figure B-1. The chromatogram for the contamination detection at the sampling tube is clearly of lower quality than the chromatogram for the background contamination. Apparently the separation column used in the sampling tube contaminant detection suffered a packing void during fabrication.

## SAMPLE FREON 114 CHROMATOGRAM
### ( Run No. 135)

CHROMATOGRAM FOR SAMPLING TUBE



CHROMATOGRAM FOR BACKGROUND PROBE
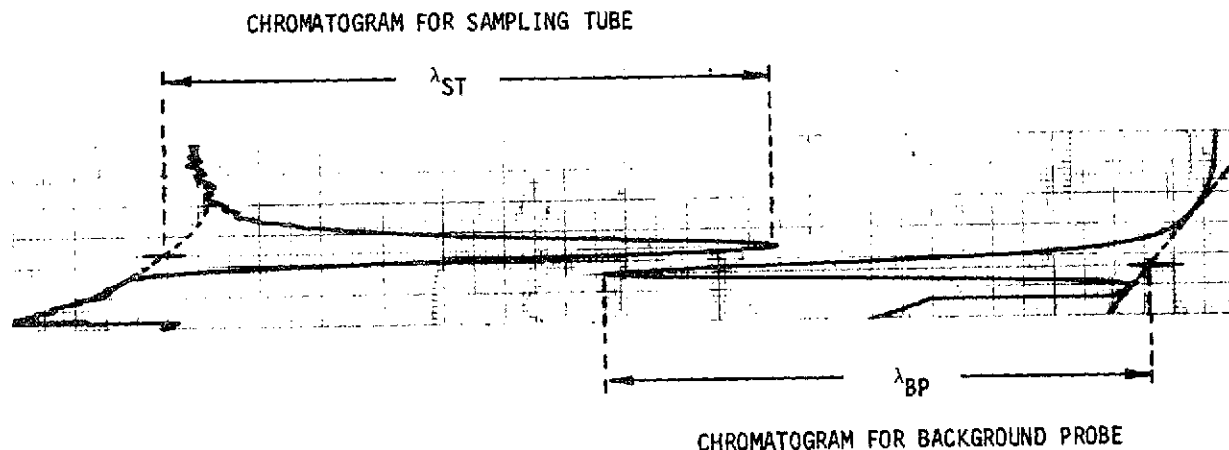
FIGURE B-1

The relationship between the contaminant level and the measured experimental parameters (used for data reduction) is:

$$PPM = (CF)(A)(\lambda)(p_c/p_T)$$

where,

PPM = Volumetric concentration of trace species in ppm

CF = Recorder calibration factor, ppm/cm

A = Amplification factor

$\lambda$ = Measured amplitude of chromatogram, cm

$p_c$ = Gas chromatograph sample pressure required to obtain $10^6$ molecules for analysis, atm

$p_T$ = Pressure of sample as supplied to gas chromatograph, atm

There are measurement uncertainties associated with the calibration factor (CF), the measured amplitude ($\lambda$) and the sample pressure ($p_T$).

Appendix C presents the Freon 114 calibration time history taken during the 40 hours of testing. The calibration factors during the Freon test series have the following values and uncertainties:

$$CF_{ST} = 39.33 \pm 0.71 \text{ ppm/cm, (1.8\% uncertainty)}$$

$$CF_{BP} = 20.43 \pm 0.20 \text{ ppm/cm, (1.0\% uncertainty)}$$

All Freon calibrations were performed at an attenuation of two and with a 500 ppm standard. The uncertainty in reading the peak amplitude from the traces was determined in terms of a percentage for the Freon test. A series of eight calibration traces, which had been averaged to define a single calibration factor were reviewed to determine the repeatability of the peak measurements. The resulting uncertainty in the measured amplitude is:

$$\lambda_{ST}: \pm 5\%$$

$$\lambda_{BP}: \pm 2\%$$

Systematic errors associated with the measurement of the sample pressure are expected to be less than 2%. Since this error is systematic and will affect both the sampling tube and background probe contaminate level in the same numerical direction, the actual uncertainty will be 2% of the difference in the contaminate measurements. Such an uncertainty level is negligible, within the scope of this study, when compared to the random errors. The absolute contaminant level may now be written in terms of the uncertainties:

$$\Delta PPM = PPM_{ST} - PPM_{BP} = \frac{P_c}{P_T} \left\{ CF_{ST} (1.00 \pm 0.018) \lambda_{ST} (1.00 \pm 0.05) A_{ST} \right.$$

$$\left. - CF_{BP} (1.00 \pm 0.01) \lambda_{BP} (1.00 \pm 0.02) A_{BP} \right\}$$

Let $\Delta PPM_0$, $\Delta PPM_{max}$ and $\Delta PPM_{min}$ represent the nominal, maximum and minimum of the absolute contamination. The nominal contamination and the extremes become:

$$\left. \begin{array}{l} \Delta PPM_0 = PPM_{ST} - PPM_{BP} \\[6pt] \Delta PPM_{max} = 1.069 \, PPM_{ST} - 0.970 \, PPM_{BP} \\[6pt] \Delta PPM_{min} = 0.933 \, PPM_{ST} - 1.030 \, PPM_{BP} \end{array} \right\} \quad (B-1)$$

where,

$$PPM_{ST} = \frac{P_c}{P_T} \cdot CF_{ST} \cdot \lambda_{ST} \cdot A_{ST}$$

$$PPM_{BP} = \frac{P_c}{P_T} \cdot CF_{BP} \cdot \lambda_{BP} \cdot A_{BP}$$

Equation (B-1) may be used to define the uncertainty band for an absolute zero contaminant level by letting $PPM_{ST} = PPM_{BP}$. The result follows:

$$\left.\begin{array}{l} \Delta PPM_0 = 0 \\[4pt] \Delta PPM_{max} = 0.099\ PPM_{BP} \\[4pt] \Delta PPM_{min} = -0.097\ PPM_{BP} \end{array}\right\} \qquad (B-2)$$

The relations presented by equation (B-1) were used in calculating the contaminant level and uncertainty band for the Freon 114 test series. Equation (B-2) was used in defining the uncertainty band about a zero contaminant level at specified background contamination levels. For the Freon 114 test series, Equation (B-2) relates the accuracy of any absolute data measurement ($\Delta PPM$) directly to the background contamination level ($PPM_{BP}$). Note that $P_c = 1$ atm and values for $P_T$ are given in Figure 32.

Methane - The quality of the methane chromatograms was significantly higher than those obtained for the Freon tests. For the methane test series, both channels of the gas chromatograph provided well defined and repeatable chromatograms (Figure B-2) and only the random errors were considered in determining the measurement uncertainty. For the early methane tests (Run numbers 174-182) a calibration factor uncertainty of $\pm 1\%$, on both channels was assumed due to slight calibration drifts. Data from Run numbers 184-214 were not analyzed due to problems in calibration drift. Numerous calibrations were taken during the final test phase (Run numbers 215-253) to provide an extremely accurate calibration factor time history. During this phase of testing, the only uncertainty in the calibration factor was the uncertainty in reading the trace amplitudes. Repeated reading of chromatograms demonstrate that the methane trace amplitudes may be consistently measured to within 1.0 mm. These error sources were included in an error analysis for methane.

## SAMPLE METHANE CHROMATOGRAM
### (Run No. 204)

CHROMATOGRAM FOR BACKGROUND PROBE



CHROMATOGRAM FOR SAMPLING TUBE
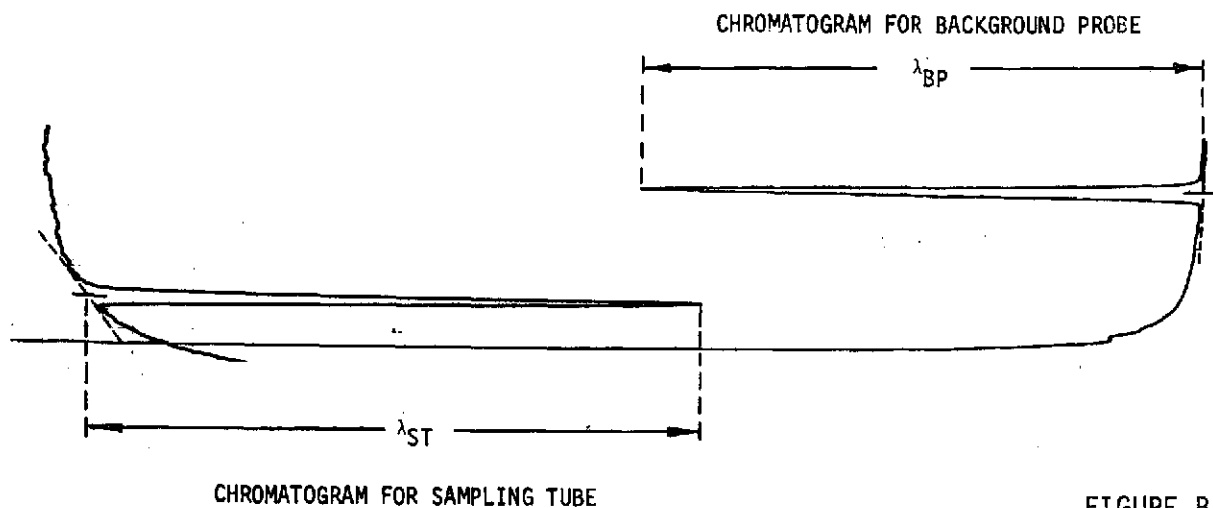
FIGURE B-2

The absolute contaminant level may be written in terms of the uncertainties:

$$\Delta PPM = PPM_{ST} - PPM_{BP} = \frac{P_c}{P_T} \left\{ CF_{ST}(1 \pm X)\,(\lambda_{ST} \pm Y)\,A_{ST} - CF_{BP}\,(1 \pm X)\,(\lambda_{BP} \pm Y)\,A_{BP} \right\} \tag{B-3}$$

where, X = assigned calibration factor error

Y = assigned accuracy in reading chromatogram, cm

For Run numbers 174-182, X = 0.01 and Y = 0.1 cm were used to determine the uncertainty bands about a measured data point. For the remaining runs, X = 0.001 and Y = 0.1 cm was used to define the uncertainty. The improvement in knowledge of the calibration factors from 1% to 0.1% was due to the continual monitoring of the calibration after Run number 182. Note that in the Freon 114 error analysis the uncertainty in reading the peak amplitude ($\lambda$) was represented as a percent of the value while for the methane test series the amplitude uncertainty is always a magnitude value of 0.01 cm. The improvement reflects the better repeatability in the chromatograms during the methane tests. The uncertainty band in an absolute zero contaminant measurement is determined to be a function of the background contamination level and the two trace peak amplitudes:

$$\left.\frac{\Delta PPM}{PPM_{BP}}\right|_{\Delta PPM_o = 0} = \pm Y\left(\frac{1}{\lambda_{ST}} + \frac{1}{\lambda_{BP}}\right) \pm 2X + XY\left(\frac{1}{\lambda_{ST}} - \frac{1}{\lambda_{BP}}\right) \tag{B-4}$$

Equation (B-3) was used to define the contaminant level magnitude and uncertainty band for the data obtained during the methane test series. Equation (B-4) defines the uncertainty band about zero contamination and hence, determines the experimental accuracy of the experiment.

# APPENDIX C

## DETECTOR CALIBRATION

The twin detector calibration factors are required to convert the chromatogram peak amplitudes from a distance measurement to volumetric parts per million. Calibration factors were obtained at various times throughout the test program to determine if calibration drifting occurred.

The Freon 114 tests were conducted over a time span of 40 hours. During this period, only random deviations from the average calibration factor occurred (Figure C-1). Deviations in the sampling tube calibration factor were less than 2% and an uncertainty of 1% was observed in the background probe calibration factor. Thus, a single calibration factor was assigned for each channel of the sampling system and the uncertainty incorporated in the error analysis.

During the methane test series a significant calibration drift was noted and some contamination level data was lost due to the high uncertainty in the calibration factors. The drift was attributed to the combined effect of the local environment changes and operating the sampling system at too high a sensitivity. The Freon columns were wrapped with heat tape to maintain a constant temperature of 80°C while the methane columns were nude. The effect was a loss in sensitivity and increased thermal stability during the Freon tests and an overall drift in sensitivity for the methane tests. Once the drift was identified, the sensitivity was decreased by increasing the current to the thermistors. From this point on, the calibration factors for both gas chromatograph channels were monitored frequently to provide an accurate time history. Figures C-2 and C-3 illustrate the calibration factor time histories for run numbers 215-253. Even though an "early morning" drift and some slight variations from the average (possibly due to temperature surges in the tunnel control room) were still present, this experimental technique results in an accurate knowledge of the calibration factors for each run.

# DETECTOR CALIBRATION: FREON 114
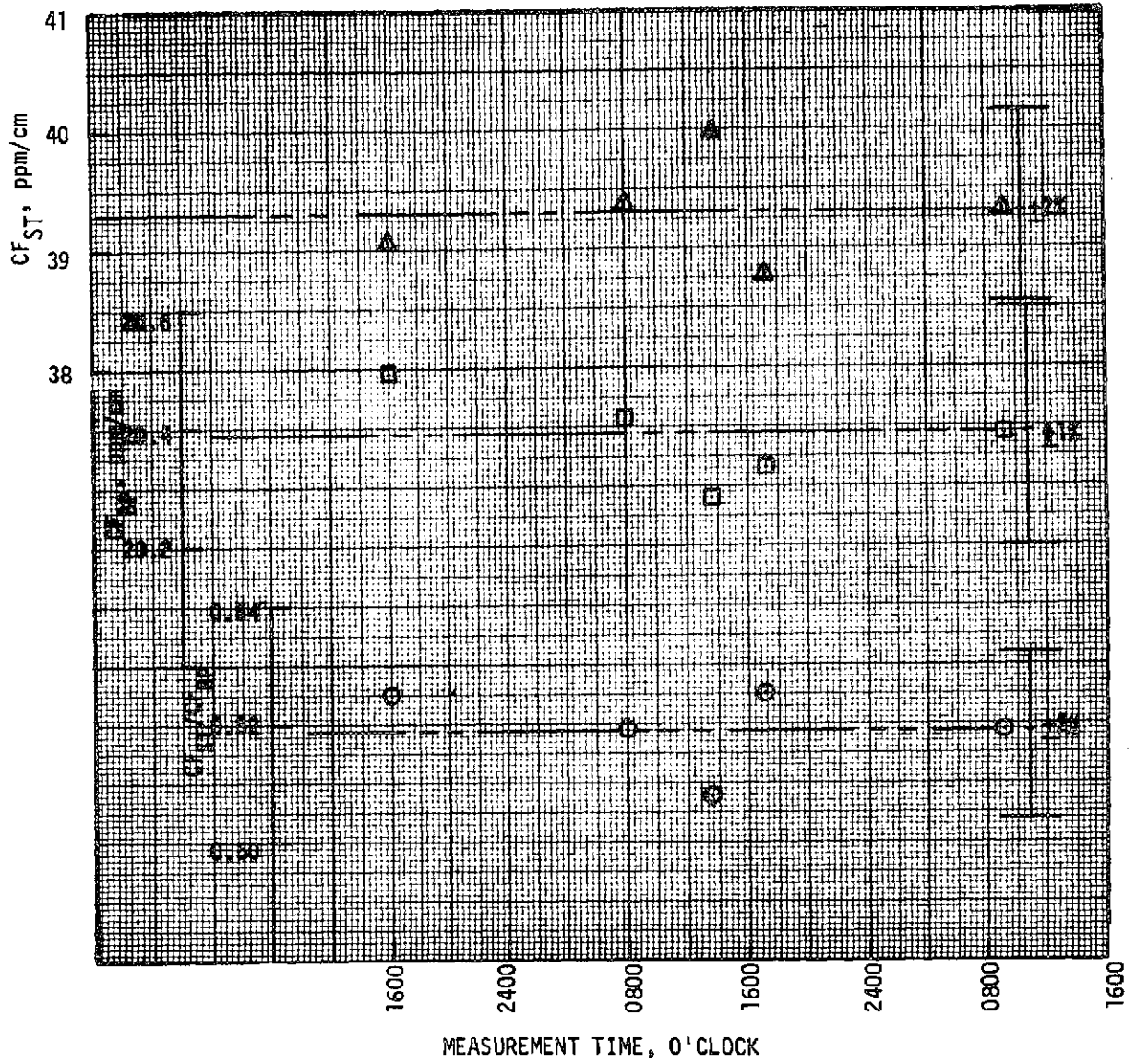


FIGURE C-1

# DETECTOR CALIBRATION: METHANE
## (Run Nos. 215–238)
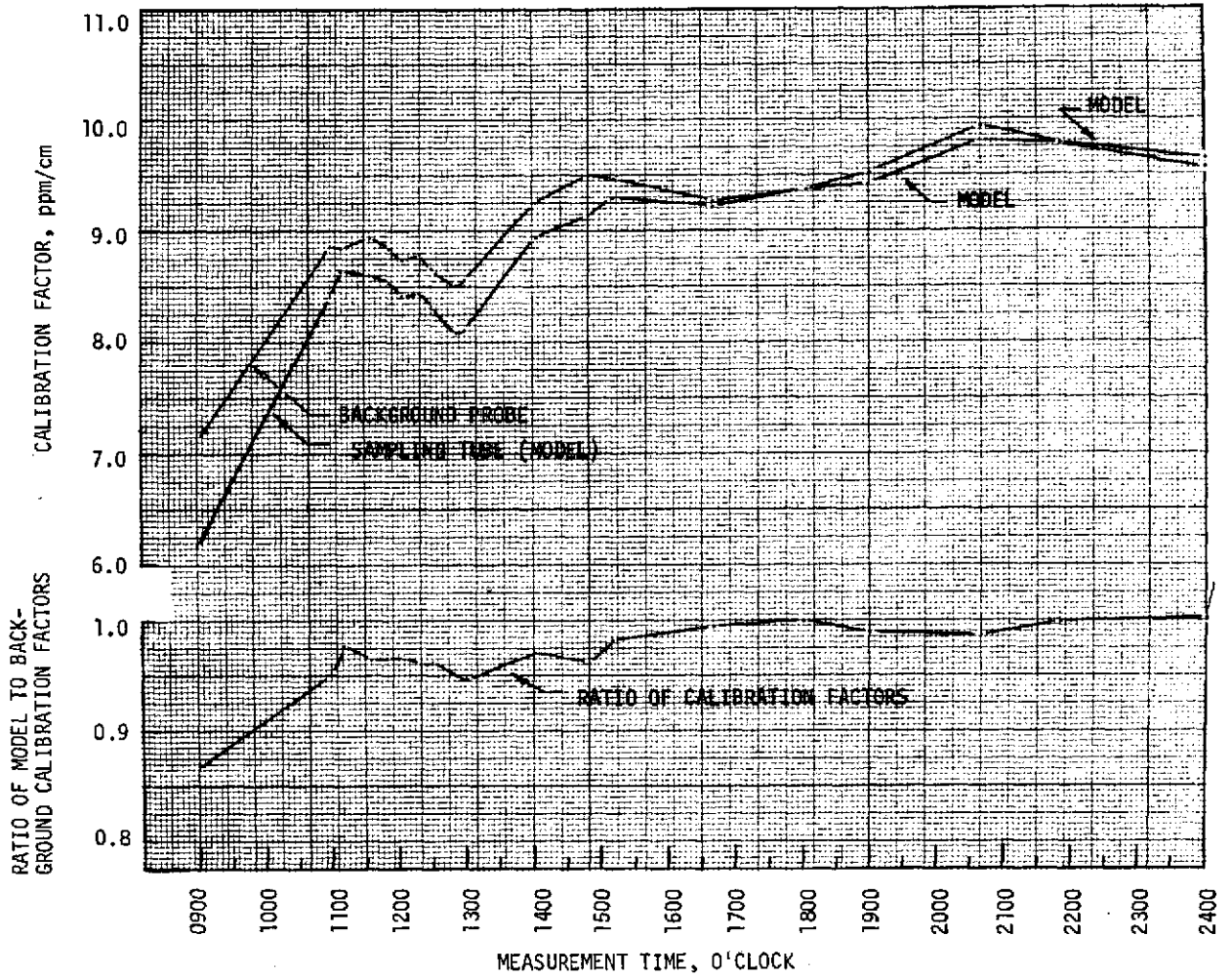


FIGURE C-2

C-2

DETECTOR CALIBRATION: METHANE
(Run Nos. 239-253)

FIGURE C-3